WORLD ATLAS

of

Typhoons and Hurricanes

1951-1995

Wind Research Laboratory Paper 250

by

Tetsuya T. Fujita

James W. Partacz

Duane J. Stiegler

September 1999

WORLD ATLAS

of

Typhoons and Hurricanes

1951-1995

WRL Research Paper 250

by

Tetsuya T. Fujita

James W. Partacz

Duane J. Stiegler

Wind Research Laboratory
Department of Geophysical Sciences
The University of Chicago

September 1999

Not to be sold

In Memory of

Professor Tetsuya Theodore Fujita

1920 - 1998

PREFACE

It is with much sadness and joy that I write the preface to the "World Atlas of Typhoons and Hurricanes." *Sadness* because it is the last contribution made by Dr. Tetsuya Theodore Fujita in increasing our understanding of natural phenomena leading to improvements in the quality of life throughout the world. This work is being published posthumously by his staff and colleagues as Ted died in his sleep on 19 November 1998. It was not his desire that this be his last publication, but he recognized that it might be and, as such, he devoted the last two years of his life to make certain that it was a significant contribution to the advancement of knowledge as well as a fitting tribute to a long and distinguished scientific career.

Joy because it is not too often that one has the privilege of both knowing and observing the research of such magnitude and importance as that developed by Dr. Fujita. Even though I had known him for the past 25 years and had the opportunity to work closely with him for the past 23 years, he continued to impress not only me, but the international scientific community as well, by his dedication, insights, and seemingly endless energy in the pursuit of knowledge. From mesoscale analysis, to tornadoes and the discovering of suction vortices, to the development of the Fujita scale for assessing and classifying damage resulting from tornadoes (F-scale), to the discovery of downbursts, to his most recent devotion to improving our understanding of tropical cyclones and their relationship to El Nino and La Nina phenomena, he always seemed to drive the field, rather than be driven by it; always working at the leading edge and having the ability to extract deep insights hitherto not seen.

Never one to shrink from controversy, Dr. Fujita developed his F-scale which led to the ability to assess tornado risk and hazard threat probabilities for the insurance and nuclear industries, as well as other critical facilities needing advanced wind design such as schools and hospitals. Through his advancements in our understanding the phenomena known as downbursts (a discovery made by him), the airline industry has been able to reduce significantly the loss of aircraft and reduce the number of airline fatalities. In this last publication he demonstrates a new and novel way of understanding the phenomena of El Nino, ocean circulations, and the resulting impact on tropical cyclone behavior; these results promise to affect the way naval operations are conducted as a result of increased ability to predict tropical cyclone paths, sizes, and their intensities.

While enduring much intense physical pain, he continued to work each day, all day, with his never-ceasing belief that "research is my life!" He was incapable of just simply resting and could not wait until he had the strength to write down his thoughts and direct his associates Jim Partacz and Duane Stiegler to follow-through on his ideas and carry out his missions. This atlas is the culmination of that effort.

Truly an individual of remarkable spirit, he set goals that only he could meet and standards that only he could achieve. His scientific accomplishments reflect the genius and wisdom that he possessed. The scientific community has been blessed to have had such an individual and the world is much the better for the contributions made by my friend, Dr. Tetsuya Fujita. Ted often remarked to me that he would "do research until the last breath of his physical life." Somehow I know he did. But to those of us whom he touched in so many different ways, Ted will always be an inspiration, and his spirit and legacy will live forever.

Dr. Robert F. Abbey, Jr.
Friend

ACKNOWLEDGMENTS

This research was supported by the Office of Naval Research (ONR) under Grant N00014-91-J1136. A debt of gratitude is owed to Dr. Robert F. Abbey, Jr. of ONR for not only initiating this support, but also extending it to allow for the publication of this research in the wake of the principal author's passing.

All SST data used in this atlas were supplied by the Japan Meteorological Agency (JMA). Storm path data was supplied by both the JMA and National Climatic Data Center, to which the authors are also grateful.

Dedication photo provided by the University of Chicago News Office.

TABLE OF CONTENTS

Chapter One

Calendar Year and Storm Year

Introduction to Chapter One

One year is the time between one vernal equinox to the next. During one year, the earth rotates 365.2422 times or one mean solar year is 365 days, 5 hours, 48 minutes, and 46 seconds. Gregorian calendar days in an ordinary year is 365 days and 366 days in leap year, which occurs once every 4^{th} year.

Although one calendar year, January 1 through December 31 is divided into 12 months of 28 to 31 days each, arbitrary 12-month periods are used for different purposes. Examples are: GROWER'S YEAR, November 6 through next November 5 in Great Britain; WATER YEAR, October 1 through next September 30 in the United States.

Presented in this book is STORM YEAR, defined as March through next February in Northern Hemisphere and September through next August in Southern Hemisphere. Here, the term storm refers to worldwide cyclones of tropical origin that meet or exceed the windspeed criteria of tropical storm status. Storm-season months are the six consecutive months in the center of a STORM YEAR. Under this definition, most of the storm activity in a storm year occurs in the storm-season months.

Seven areas of aggregate storm activity over oceans around the world were identified. No storm has been reported from South Atlantic Ocean, the 7^{th} area, however as the Atlantic Ocean widens due to Continental Drift, storms in the North Atlantic Ocean will increase and it is likely that storms will begin to form in the South Atlantic Ocean after 200 million years. Both daily and monthly counts of storms in each of the areas 1 through 6 were computed and presented in graphical form. They clearly show the difference in storm activity in northern and southern hemispheres.

1.1 Number of Storms Around the World by Month

Over the Oceans around the world, 3600 tropical storms occurred in 45 years, 1951-95. In other words, an average of 80 storms per year occurred in the world, of which 56 (70%) were in the Northern Hemisphere and 24 (30%), in the Southern Hemisphere. Their occurrences by month are tabulated below:

Month	1	2	3	4	5	6	7	8	9	10	11	12
N. Hemisphere	28	11	23	43	104	211	368	537	539	375	211	88
S. Hemisphere	243	265	205	95	24	5	9	0	4	19	52	139
Total in 45 yrs	271	276	228	138	128	216	377	537	543	394	263	227
Total per Year	**6**	**6**	**5**	**3**	**3**	**5**	**8**	**12**	**12**	**9**	**6**	**5**

Table 1.1 Worldwide storm occurrences in 45 years, 1951-95, by month.

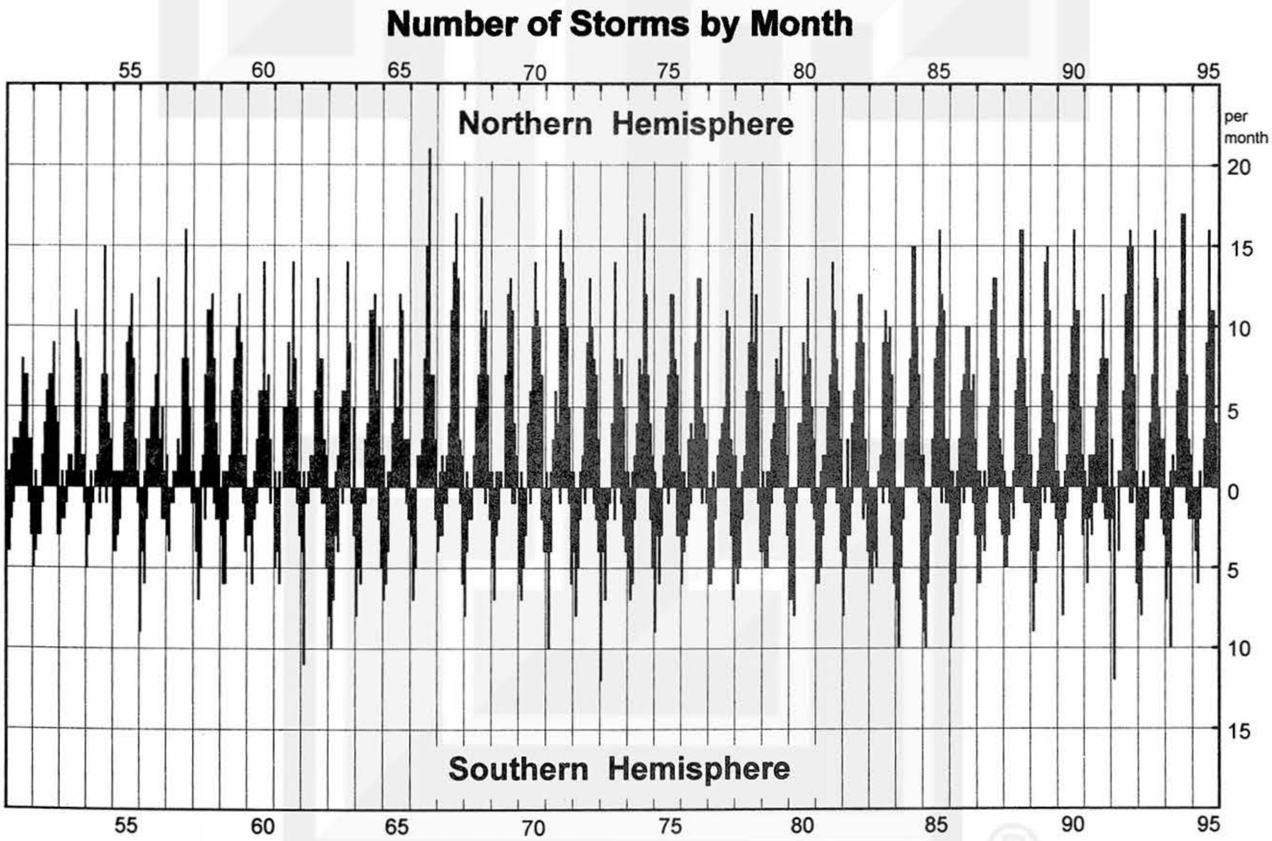

Fig. 1.1 Number of storms by month originating in Northern and Southern Hemispheres. No relationship was found between the number of storms in both hemispheres

1.1 Number of Storms Around the World by Month

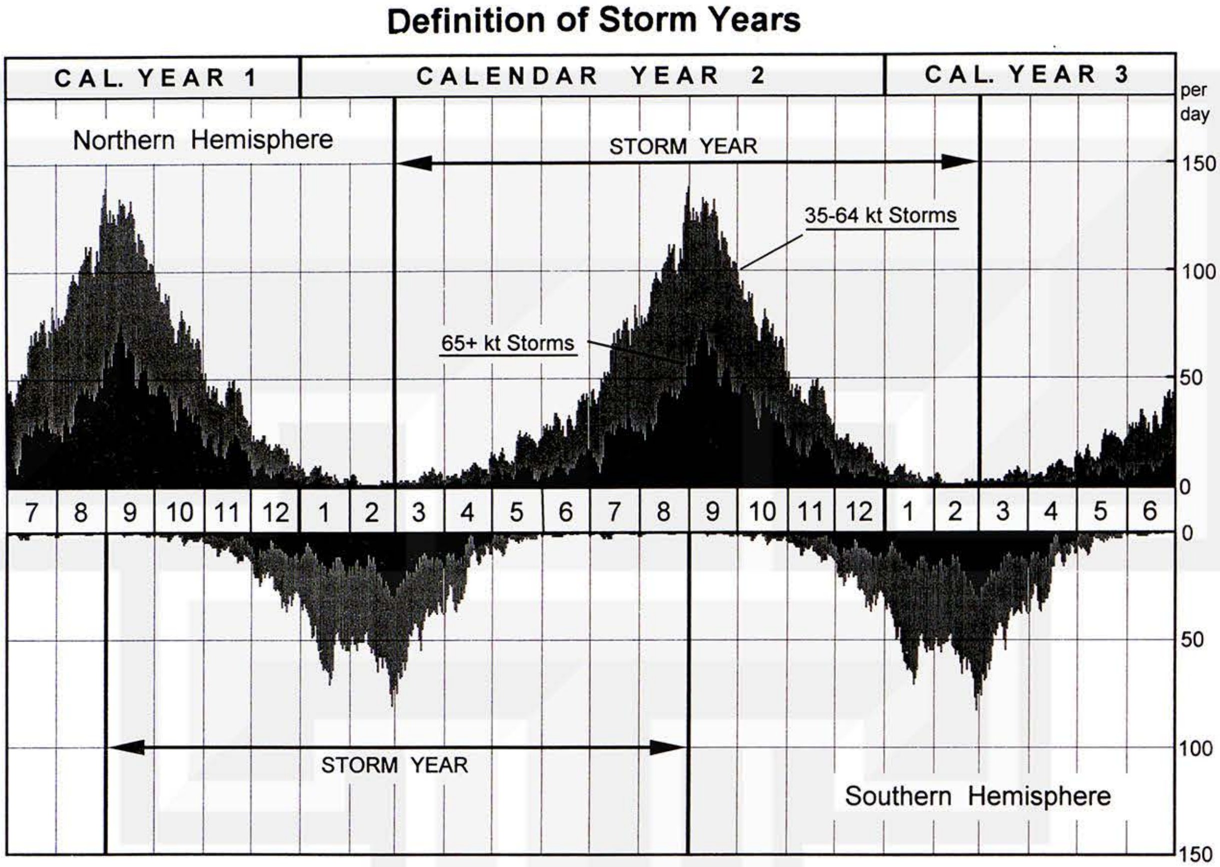

Fig. 1.2 Daily count of Northern and Southern Hemisphere storms. Painted areas denote hurricanes.

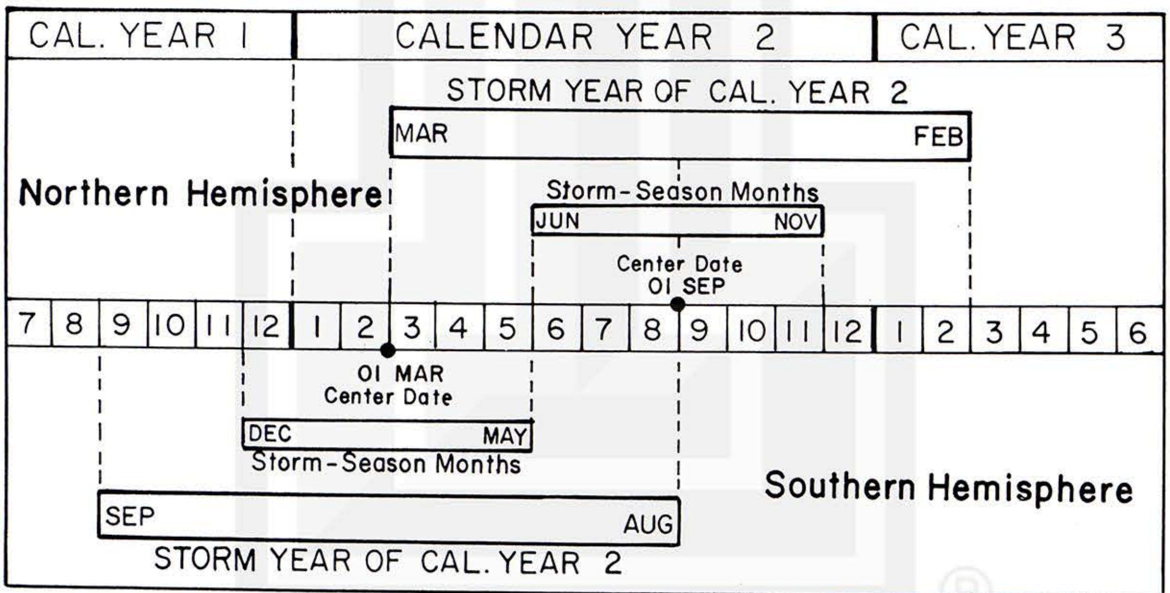

Fig. 1.3 Definition of Storm Year, Storm-season Months, and Center Date. Refer to the Glossary, pages 100-101.

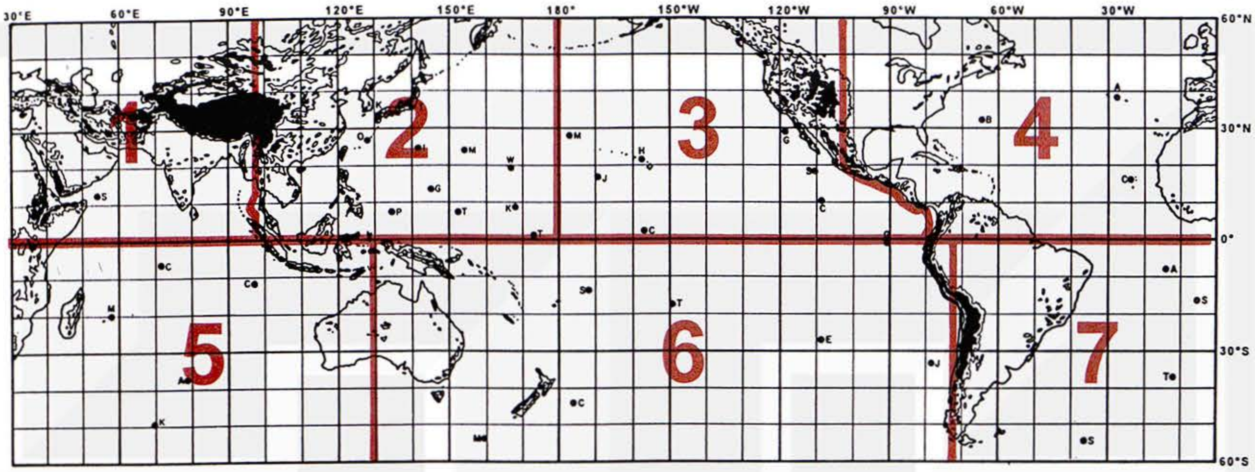

Fig. 1.4 Seven areas of storm activity are identified in this map. They are: 1. North Indian Ocean, 2. West Pacific Ocean, 3. East Pacific Ocean, 4. North Atlantic Ocean, 5. South Indian Ocean, 6. South Pacific Ocean, and 7. South Atlantic Ocean. So far, no tropical storm has been reported to have occurred in Area 7.

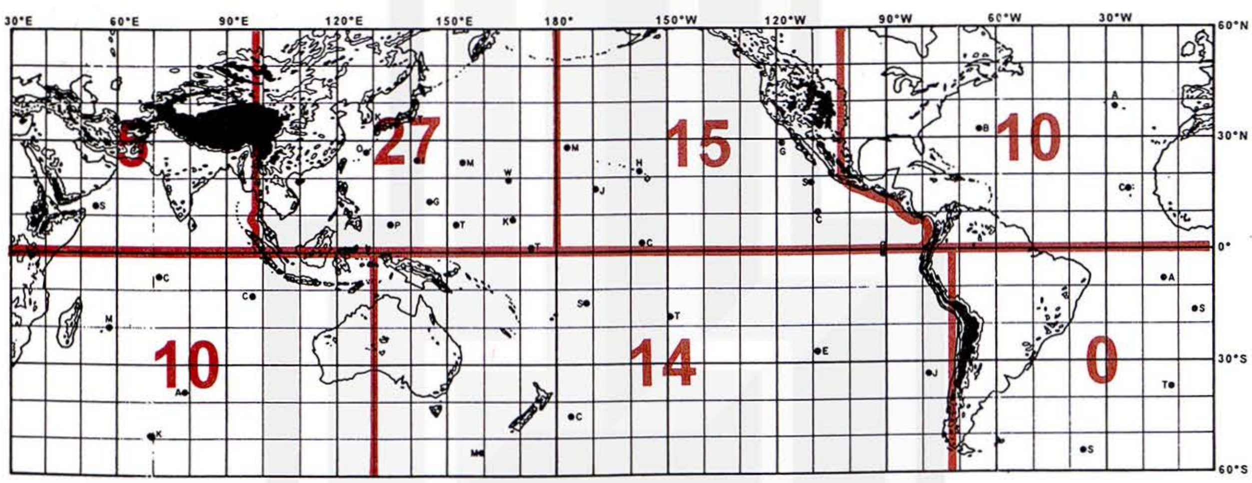

Fig. 1.5 Annual number of storms (tropical storms and hurricanes) in seven areas. Annual numbers are computed by dividing the total storms within each area during the 45-year statistical period, 1951-95, by 45. The largest number, 27 is seen in Area 2, and no storm has been reported from Area 7 dominated by the cold Benguela current.

1.3 Monthly Count and Daily Count of Storms

A count of storms is commonly used in assessing the storm activity within an area during a specific period. Used in this chapter are Monthly Count and Daily Count.

Monthly Count is the count of storm formations in consecutive months within a storm-activity area during the statistical period of 45 years (1951-95 storm years). The count can be prorated to per 100 year count by multiplying the factor, 100/45.

Daily Count is the count of storms in progress within a specific area on consecutive days in a statistical period. In other words, Daily Count is the number of storms in progress on consecutive calendar days.

Both counts are presented in bar graphs. Open bars denote the counts of storms which include tropical storms and hurricanes by definition. Counts of hurricanes are shown by painted bars.

The total monthly counts are the number of storms within the statistical period, while total daily counts vary with the total monthly counts and the life of individual storms. For example, a storm with a 15-day life leaves behind 15 daily counts during its lifetime.

1. North Indian Ocean Monthly Count

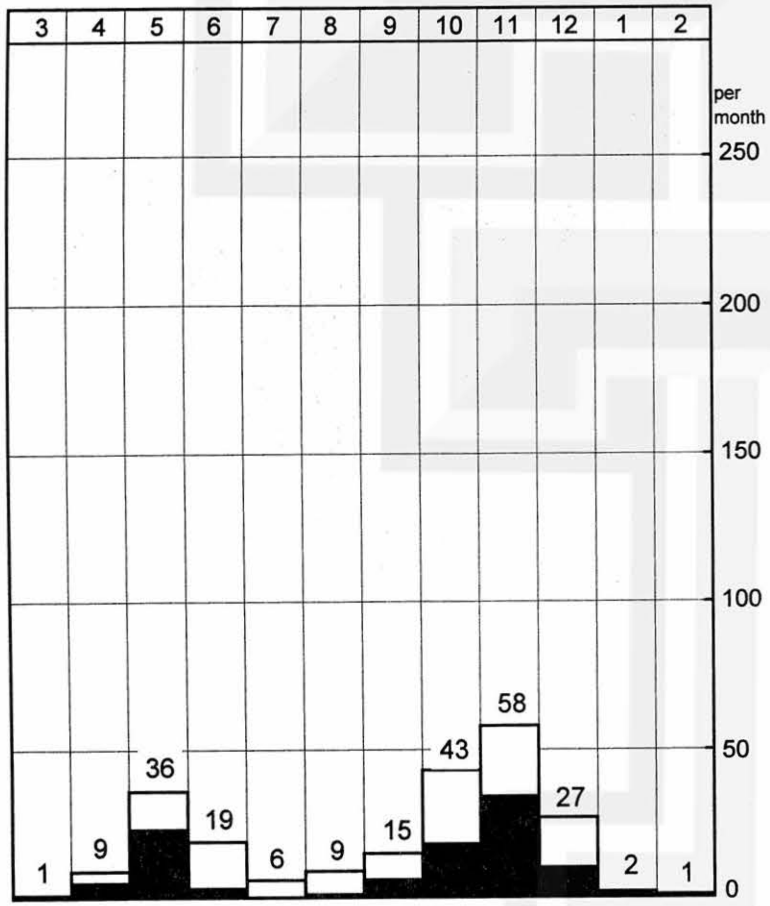

Fig. 1.6 Monthly count of storms in the North Indian Ocean. Total count is 226 in 45 years.

1. North Indian Ocean Daily Count

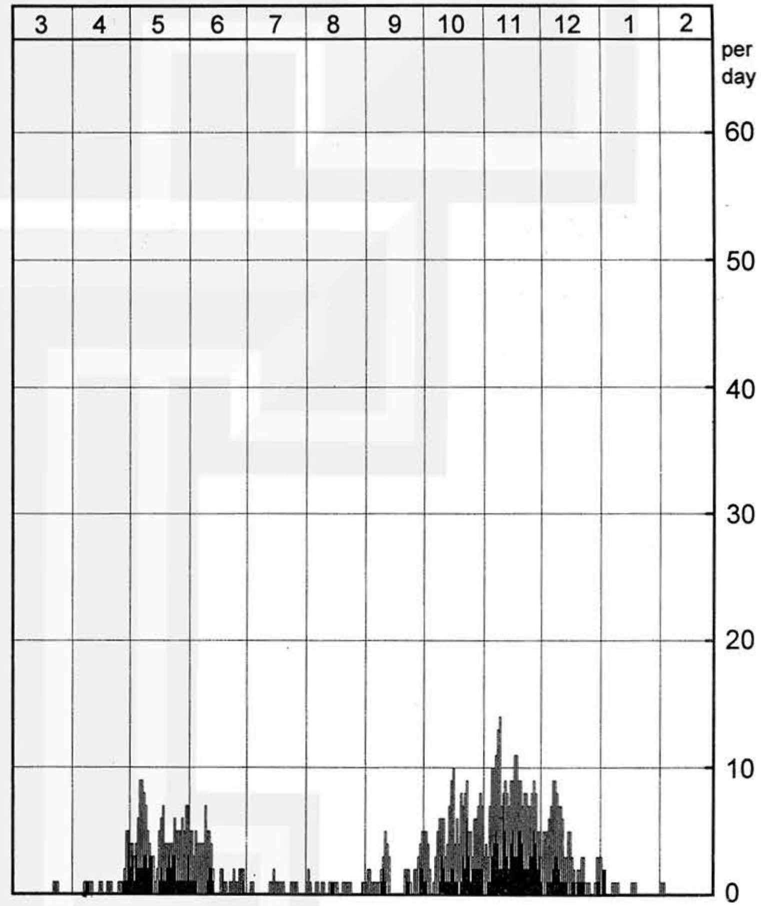

Fig. 1.7 Daily count of storms in North Indian Ocean.

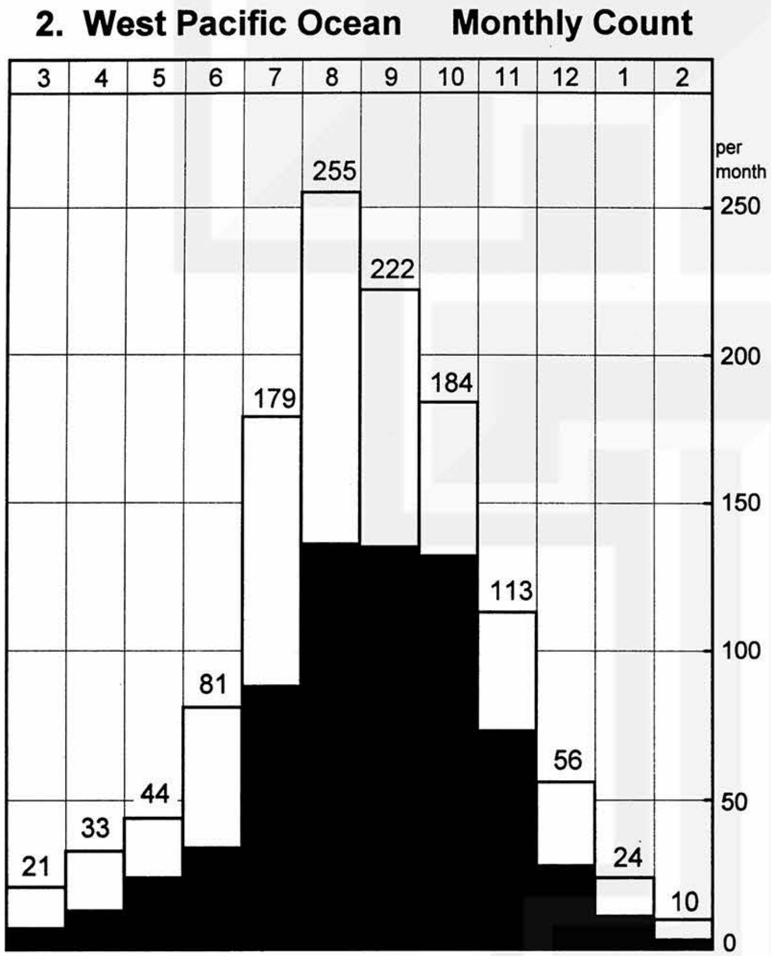

Fig. 1.8 Monthly count of storms in the West Pacific Ocean. Total count is 1222 in 45 years.

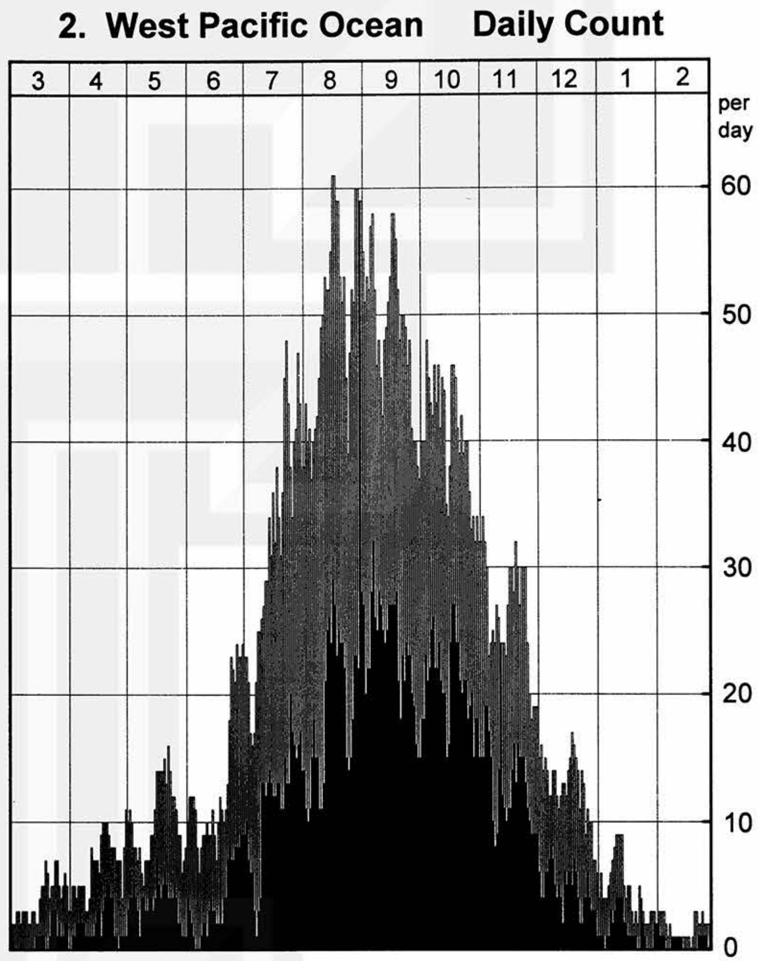

Fig. 1.9 Daily count of storms in West Pacific Ocean.

3. East Pacific Ocean Monthly Count

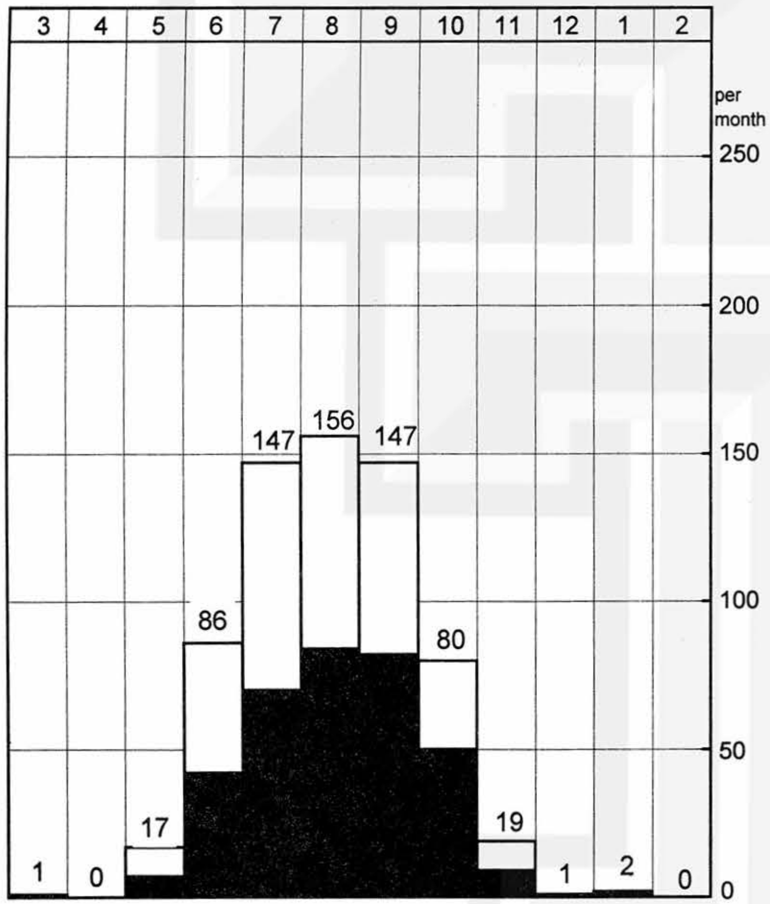

Fig. 1.10 Monthly count of storms in the East Pacific Ocean. Total count is 656 in 45 years.

3. East Pacific Ocean Daily Count

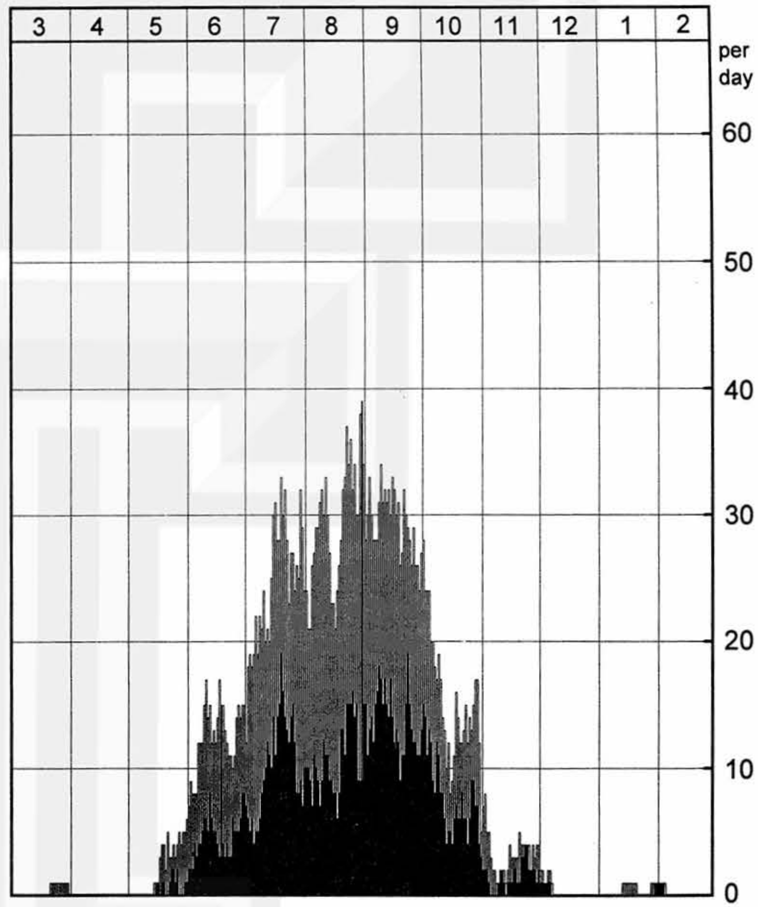

Fig. 1.11 Daily count of storms in East Pacific Ocean.

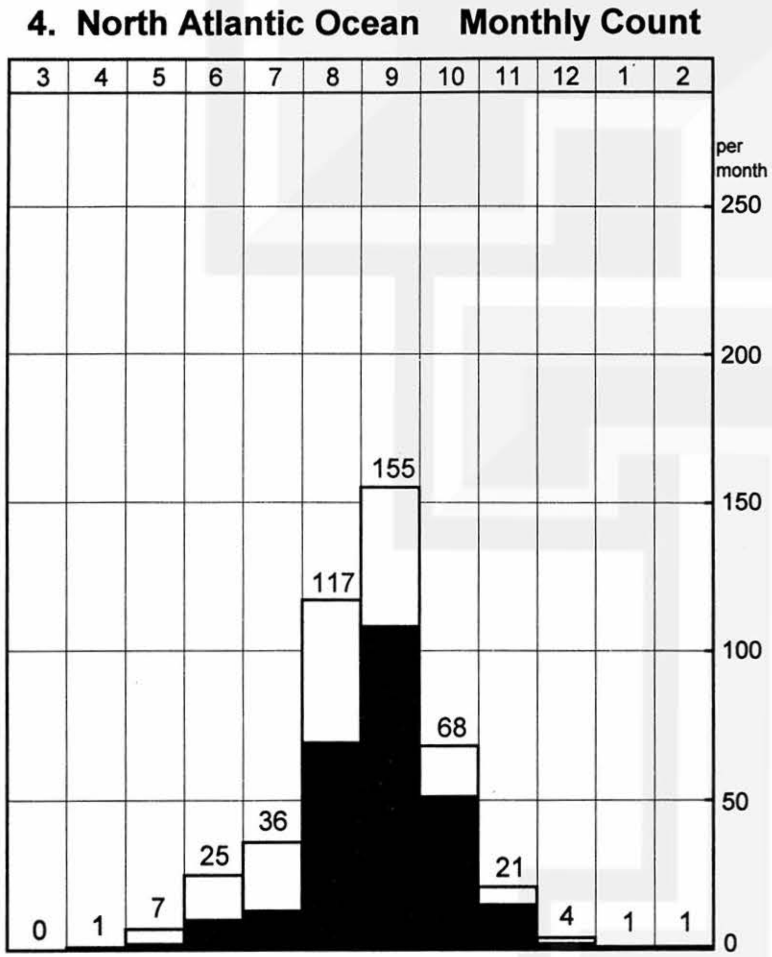

Fig. 1.12 Monthly count of storms in the North Atlantic Ocean. Total count is 436 in 45 years.

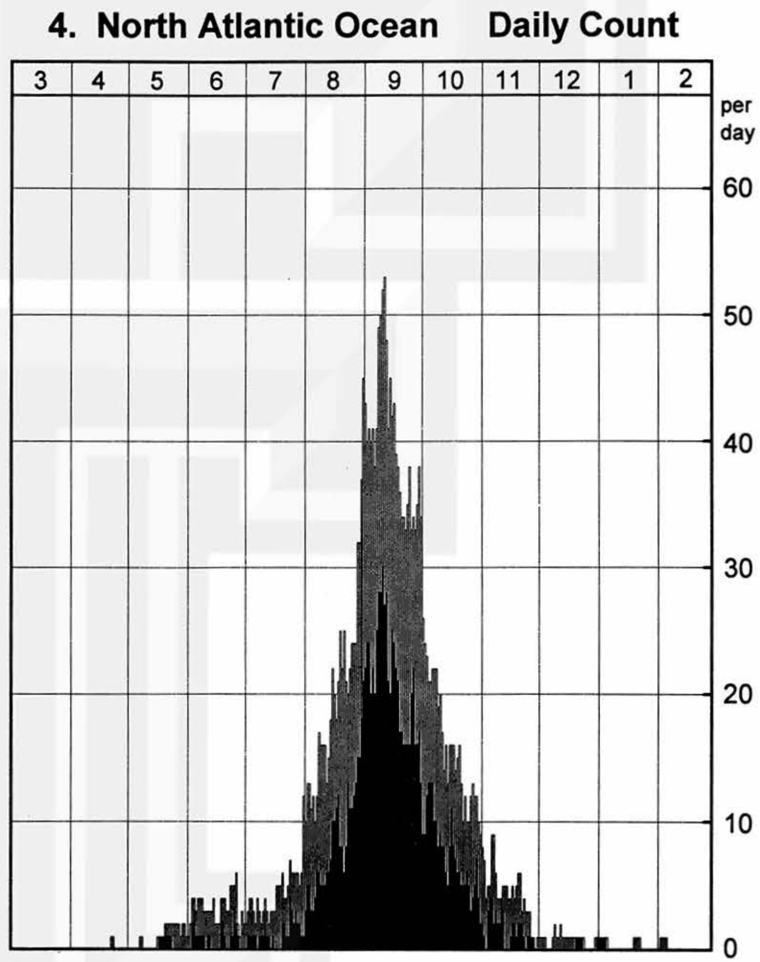

Fig. 1.13 Daily count of storms in North Atlantic Ocean.

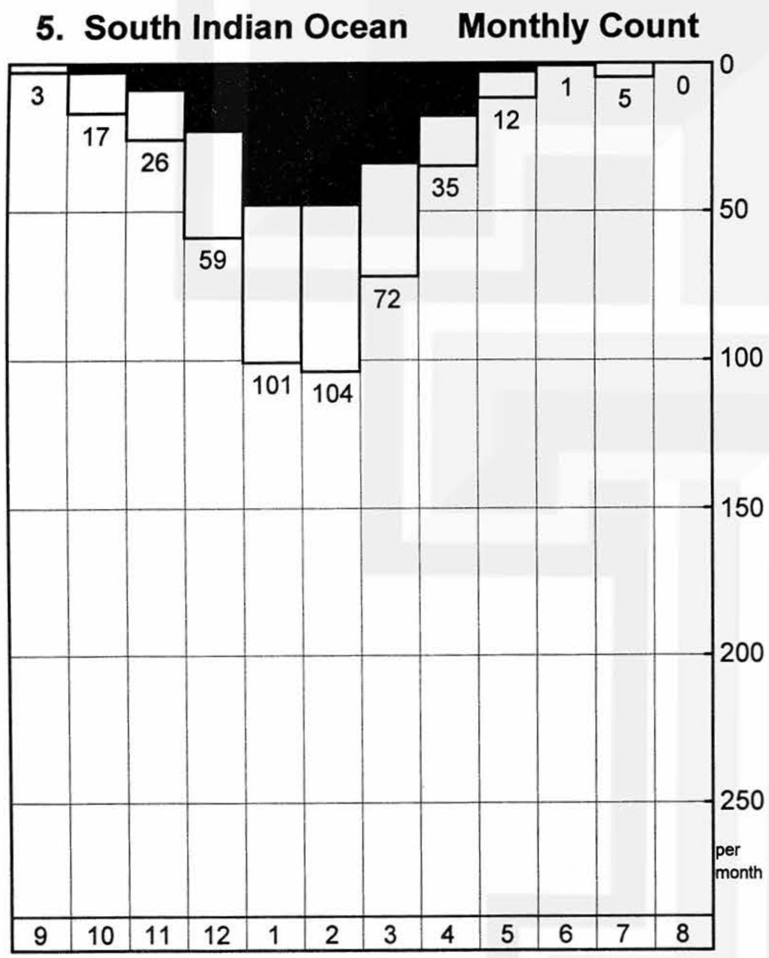

Fig. 1.14 Monthly count of storms in the South Indian Ocean. Total count is 435 in 45 years.

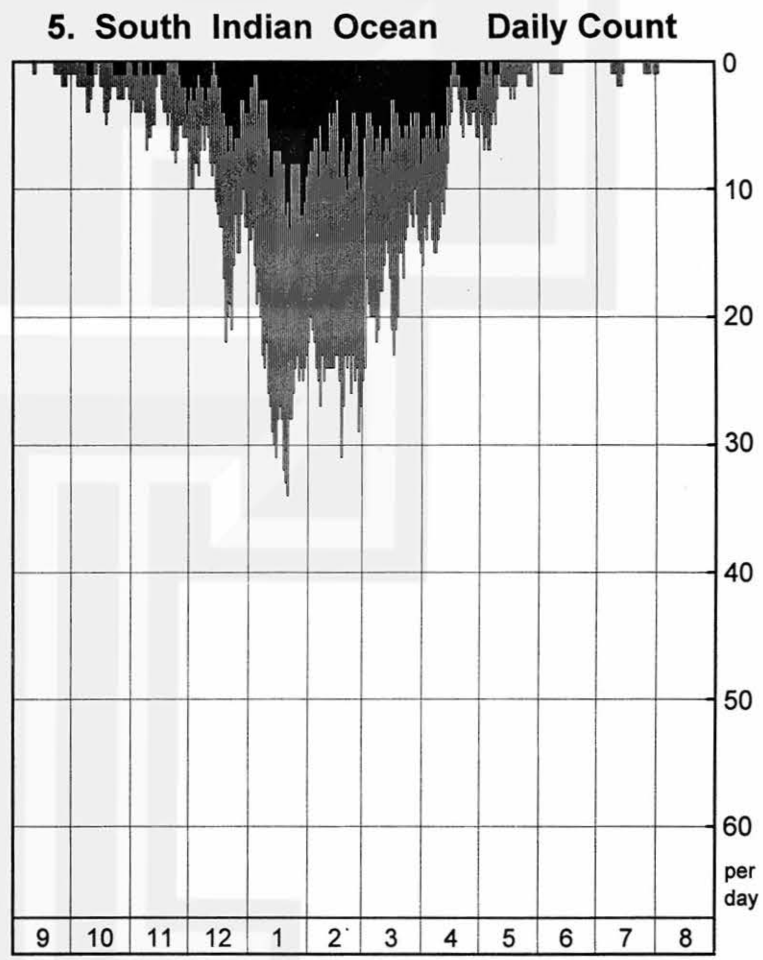

Fig. 1.15 Daily count of storms in South Indian Ocean.

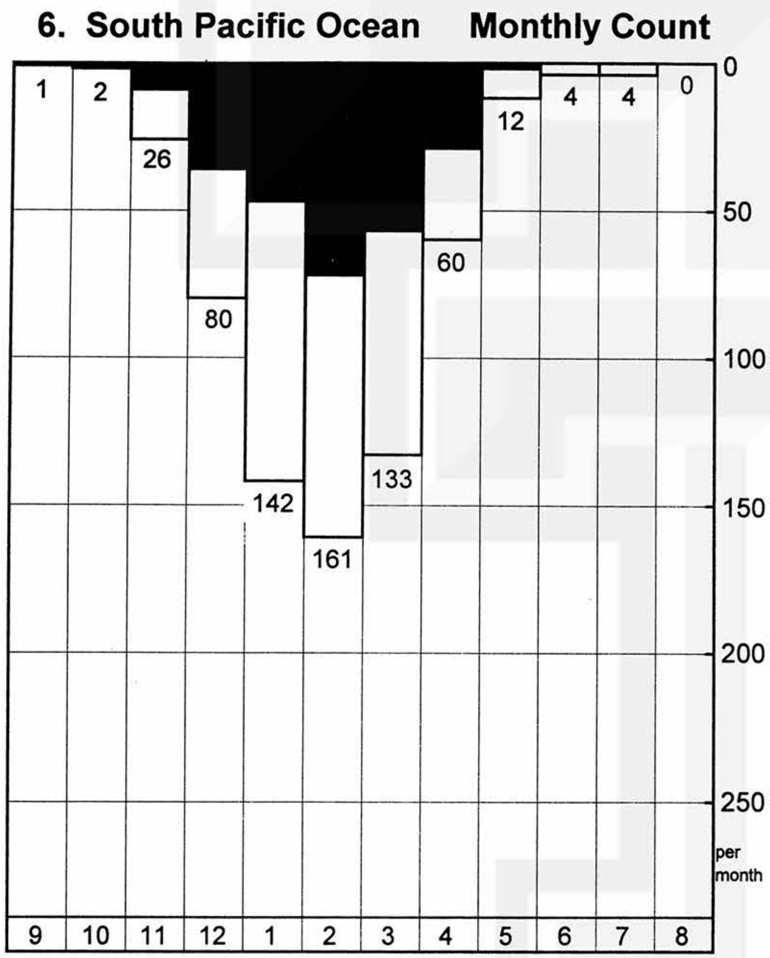

Fig. 1.16 Monthly count of storms in the South Pacific Ocean. Total count is 625 in 45 years.

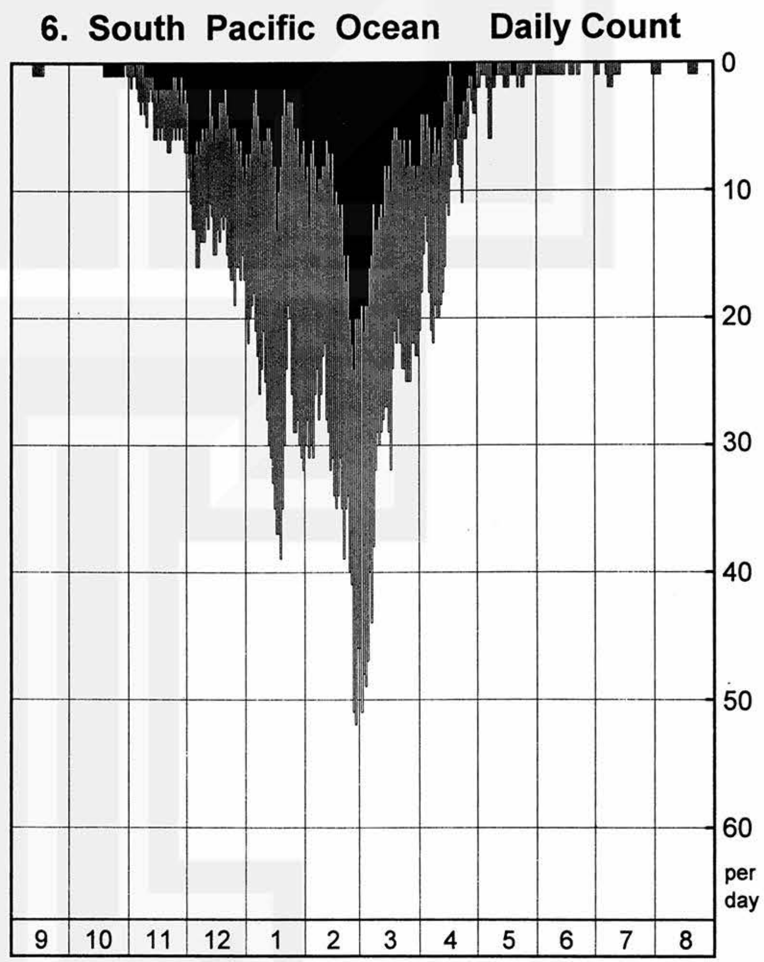

Fig. 1.17 Daily count of storms in South Pacific Ocean.

Chapter Two

Mapping of Global Storms

Introduction to Chapter Two

It is customary to map paths of storms (tropical storms and hurricanes) by connecting their positions from the initiation point to the end point. In view of the fact that the storm path from initiation to recurving and from recurving to end are affected by steering easterlies and westerlies, respectively, storm paths were divided into initial paths and recurved paths and mapped together or as initial paths only. Initial paths are useful in studying the initiation of storms.

In mapping the storms around the world by specific period, by year, by month, etc., storms in North Indian Ocean, West Pacific Ocean, East Pacific Ocean, North Atlantic Ocean, South Indian Ocean, and South Pacific Ocean were mapped individually. Thereafter, they were joined into large-area maps as desired.

Paths of storms around the world revealed the feature of the Intertropical Irrotational Zone (ITIZ) with well-defined North and South boundaries. It was found that these boundaries vary by season of the year in relation to the location of the Intertropical Convergence Zone (ITCZ).

Finally, initial paths of storms and surface isobars at 5-mb intervals relating mean pressure fields were superimposed upon 12 monthly maps for use in determining the interannual variation of storms around the world.

2.1 Definition of Initial and Recurved Paths

In mapping the paths of storms around the world, individual paths were divided into **initial path** and **recurved path** segments, corresponding to the respective steering Easterlies and Westerlies. The initial path is defined as being the segment between the initial and recurving points, while the recurved path is that between the recurving and end points (Fig, 2.1).

Expressing the east longitude of the center of a storm by θ, the initial path is defined as $d\theta/dt < \theta$ and the recurved path as $d\theta/dt > \theta$, because most storms move either toward the south or north as they recurve.

Initial and Recurved Path

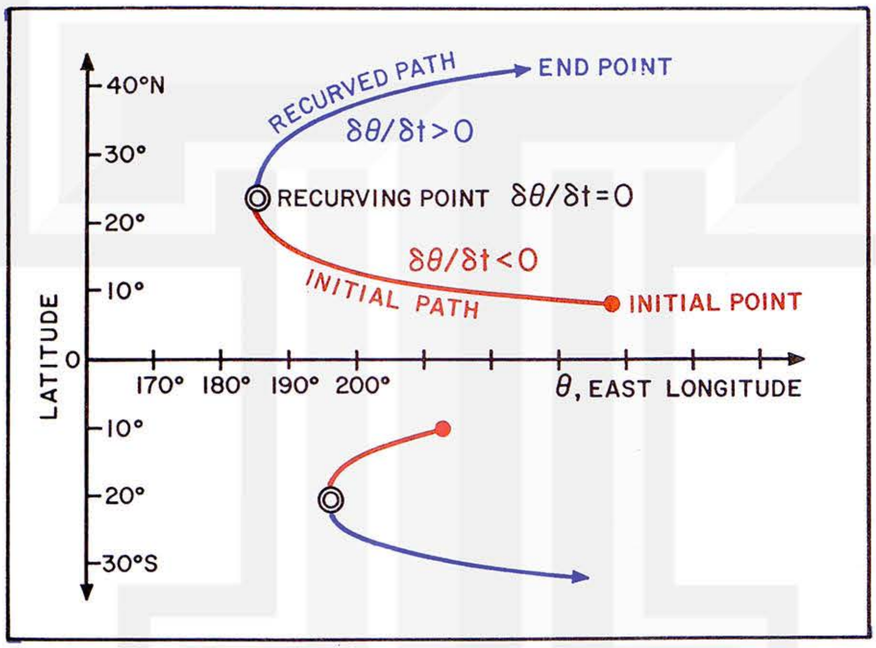

Fig. 2.1 Schematic diagram showing initial and recurved paths.

In a general sense, this separation into initial and recurved paths allows us to examine distributions of the initiation and intensification stages of storms by plotting maps of only initial paths. A global map of 45 years of initial paths only is presented in Fig. 2.3 (page 17) for comparison with the total paths for the same period shown in Fig. 2.2 (page 16). Also, monthly maps of initial paths and mean surface pressure are shown in Figs. 2.10 through 2.21 (pages 22 through 25) begining with March, the first month of the Northern Hemisphere storm year.

STORM PATHS (45 yr Period)

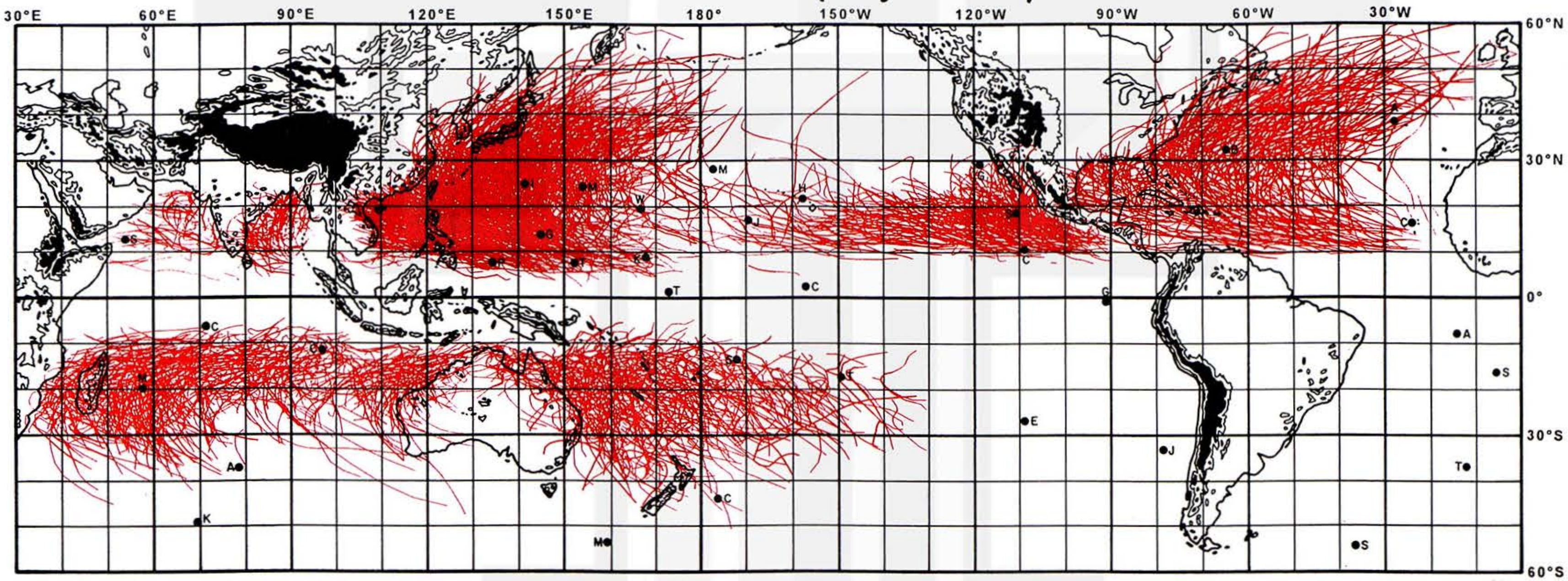

Fig. 2.2

1951-95

INITIAL PATHS (45 yr Period)

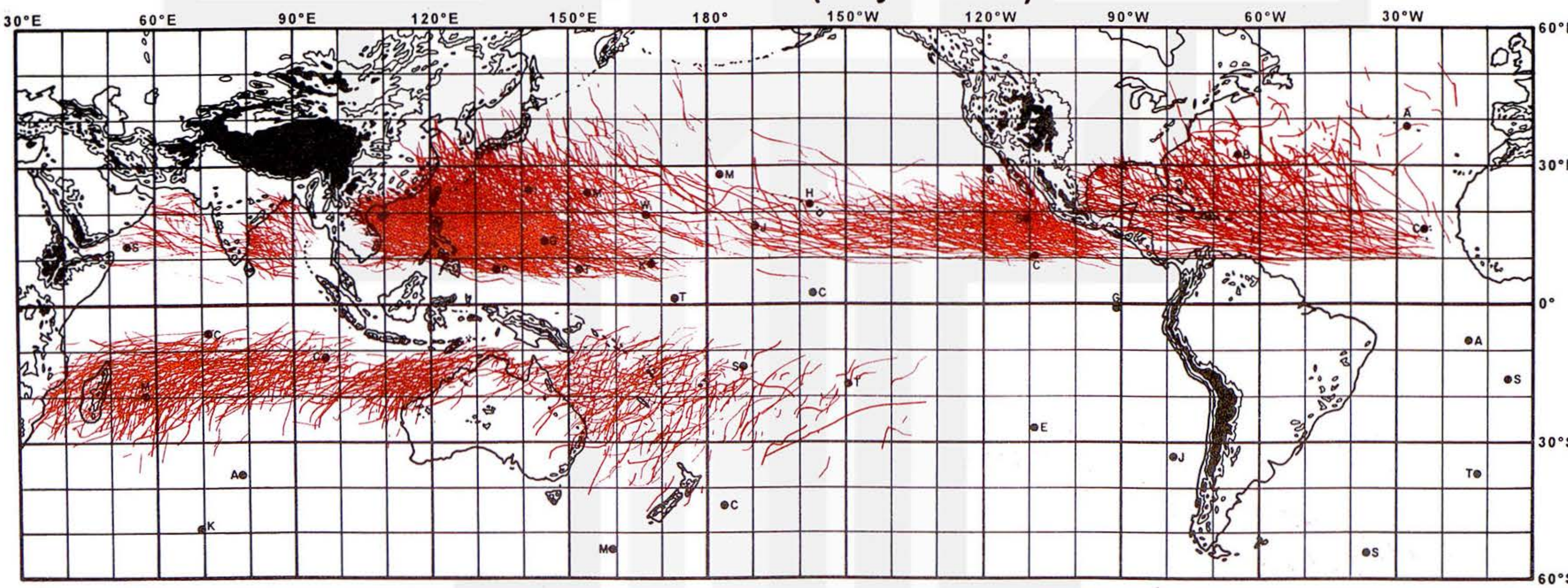

Fig. 2.3

1951-95

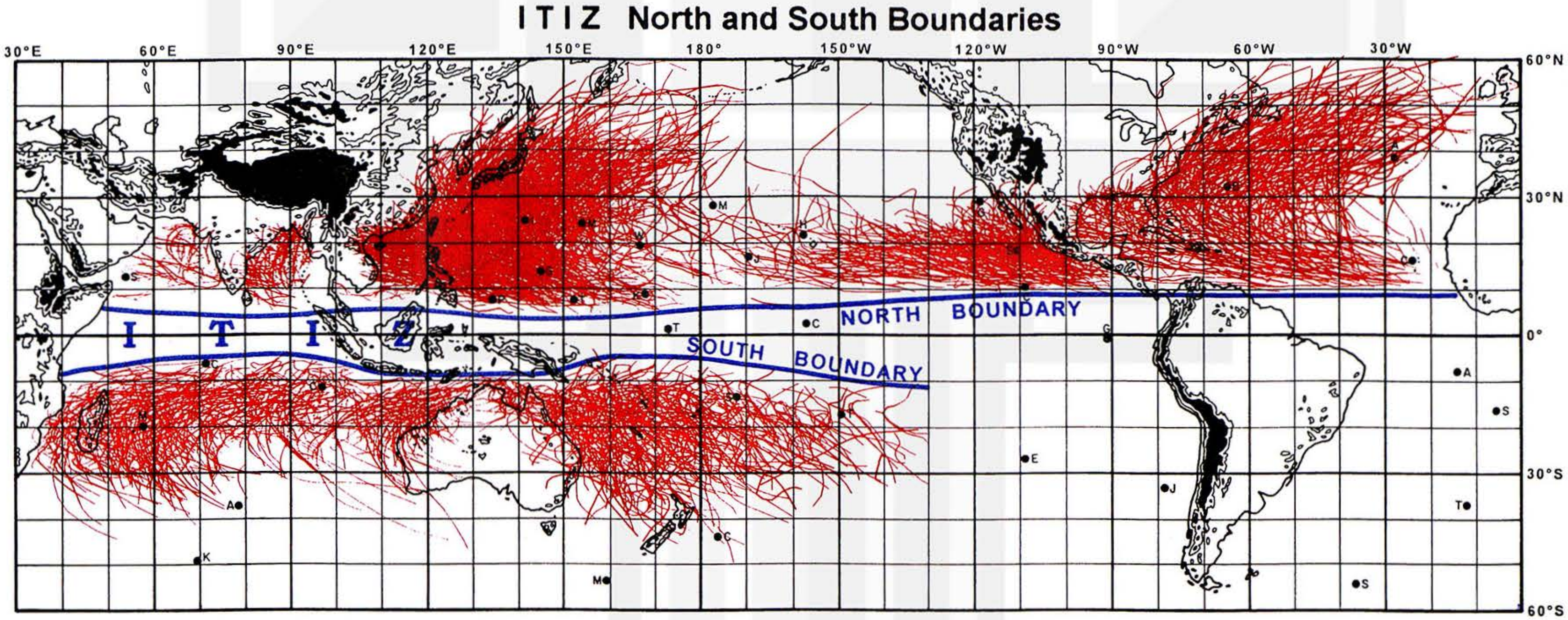

Fig. 2.4 The ITIZ (Intertropical Irrotational Zone) and its north and south boundaries superimposed upon the storm paths during the 45-yr period 1951-95 storm years. The boundaries shown approximate their positions closest to the equator during the statistical storm year.

2.3 Intertropical Irrotational Zone (ITIZ)

It is known that the vertical component of the rotation of the earth is the most important condition to the initiation of tropical storms. Due to this component, storms rotate counterclockwise to the north of the equator and clockwise to the south of the equator. Since this component approaches zero near the equator - equaling zero at the equator - there exists a band of irrotation along and extending to either side the equator known here as the Intertropical Irrotational Zone (ITIZ) where convective systems cannot organize to the extent of becoming storms (see Fig. 2.4).

It is also known that the Intertropical Convergence Zone (ITCZ) is critical to the formation of convective systems near the equator. If we define the North and South boundaries of the ITIZ as being the northernmost and southernmost limits, respectively, beyond which storms initiate, then the location of these boundaries will vary with the position of the ITCZ (Fig. 2.5). This variance was found to be greatest, from 4° to 22°N, in Area 1, the North Indian Ocean.

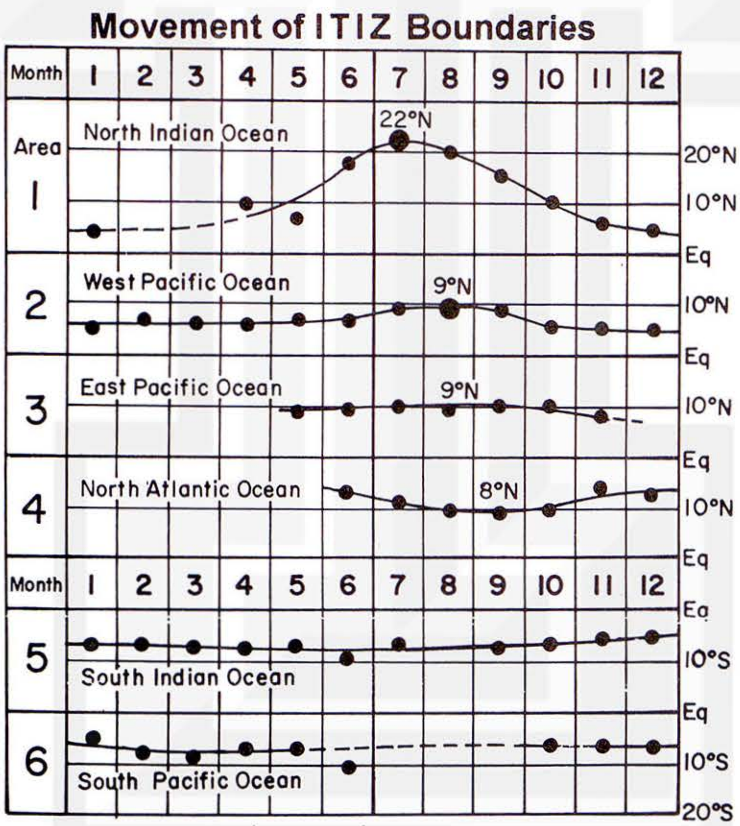

Fig. 2.5 North-south movement of the ITIZ boundaries on both sides of the equator. It is likely that the movement is related to the variation of the ITCZ. The northernmost movement in Area 1 coincides with the warming of India south of the Himalayan Mountains.

2.4 Seasonal Variation of Storms Around the World

Storm paths are mapped here by three-month meteorological season beginning with **MAR APR MAY,** Northern Hemisphere spring. March 1st is the start of the Northern Hemisphere storm year when storm activity is weakest in the Northern Hemisphere but strongest in the Southern Hemisphere.

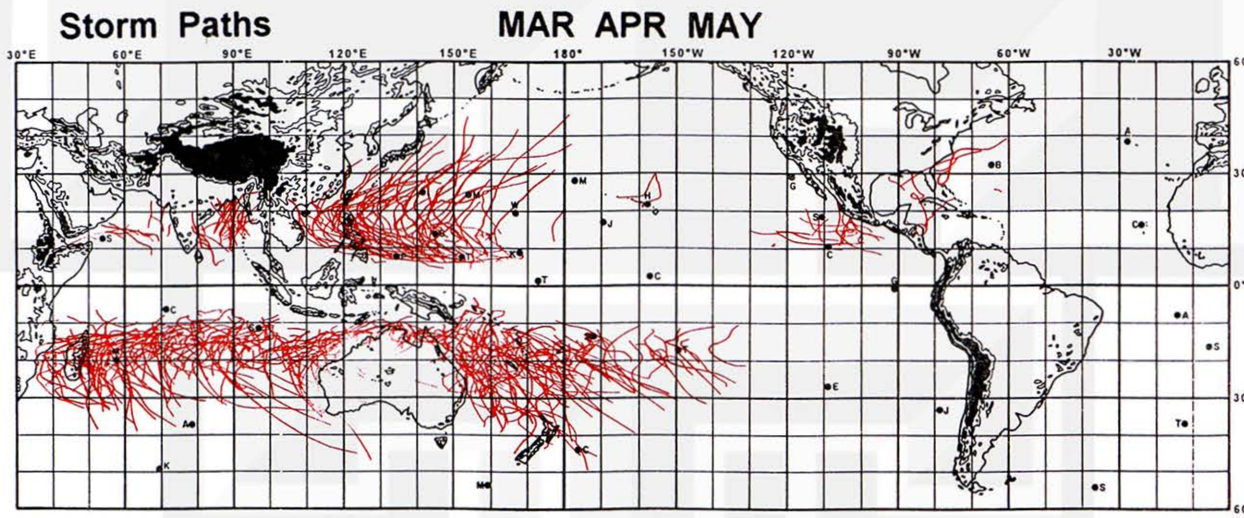

Fig. 2.6 Northern Hemisphere spring, Southern Hemisphere autumn. 1951-95

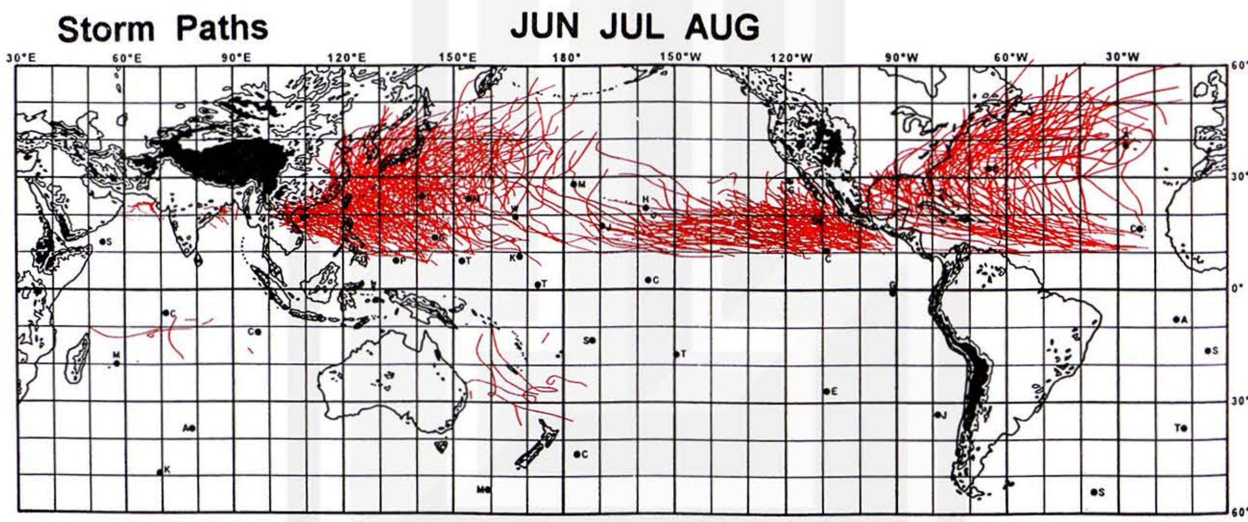

Fig. 2.7 Northern Hemisphere summer, Southern Hemisphere winter. 1951-95

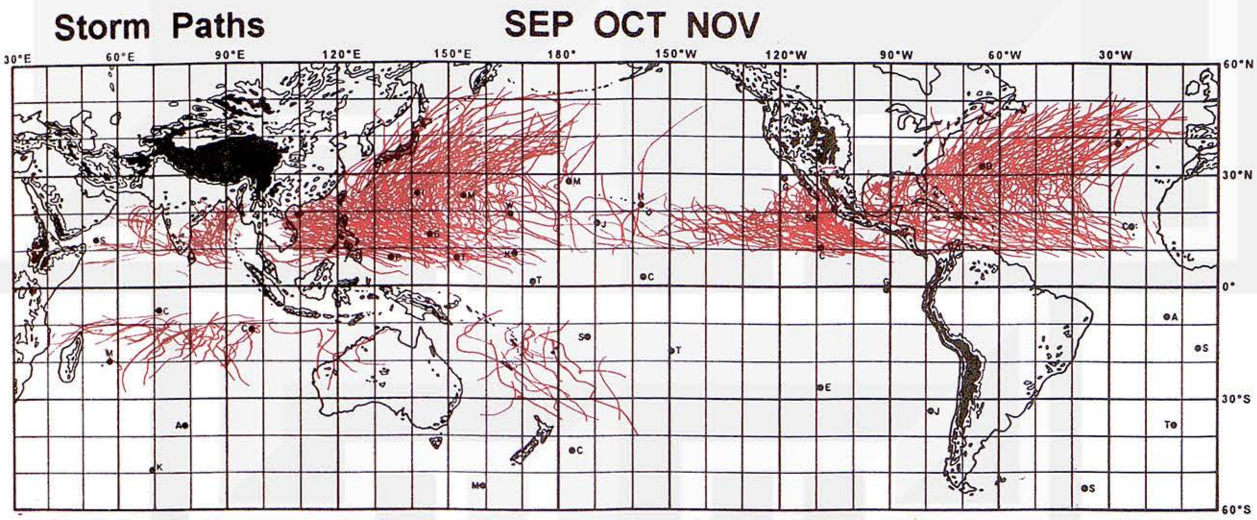

Fig. 2.8 Northern Hemisphere autumn, Southern Hemisphere spring. 1951-95

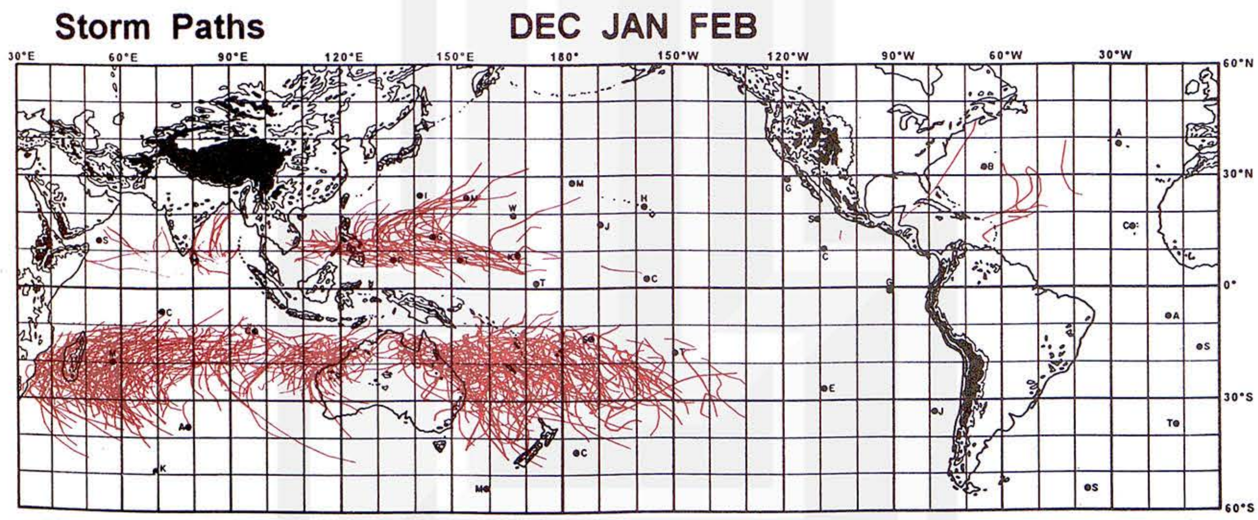

Fig. 2.9 Northern Hemisphere winter, Southern Hemisphere summer. 1951-95

2.5 Initial Paths and Surface Isobars by Month

Initial Paths **MARCH**

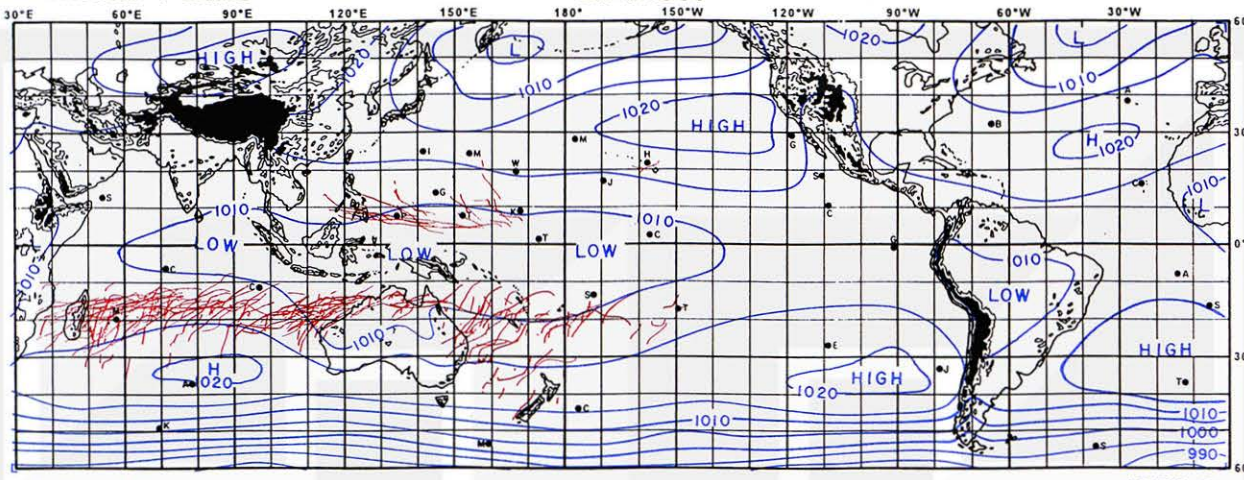

Fig. 2.10 1951-95

Initial Paths **APRIL**

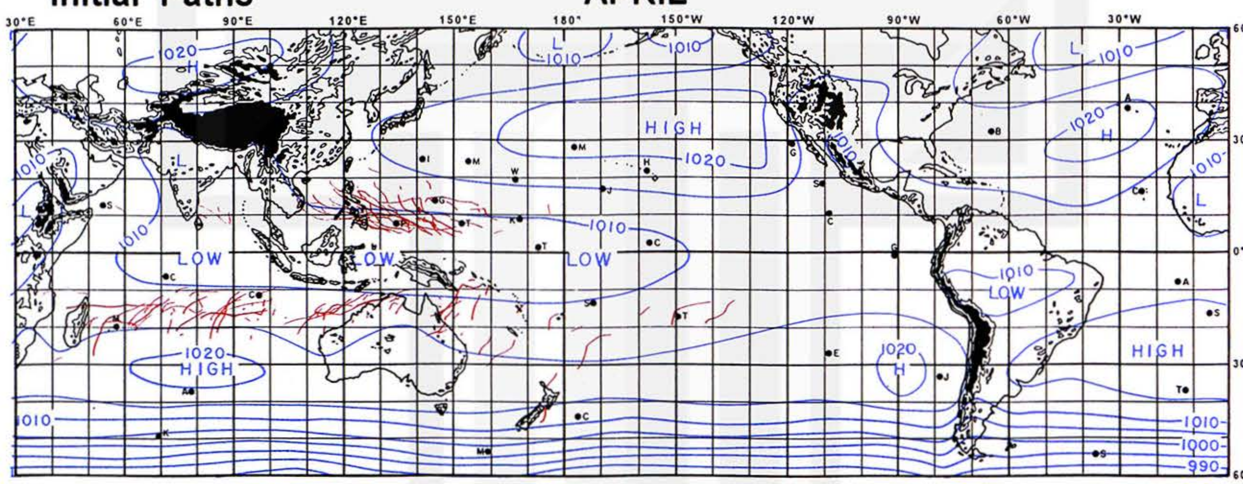

Fig. 2.11 1951-95

Initial Paths **MAY**

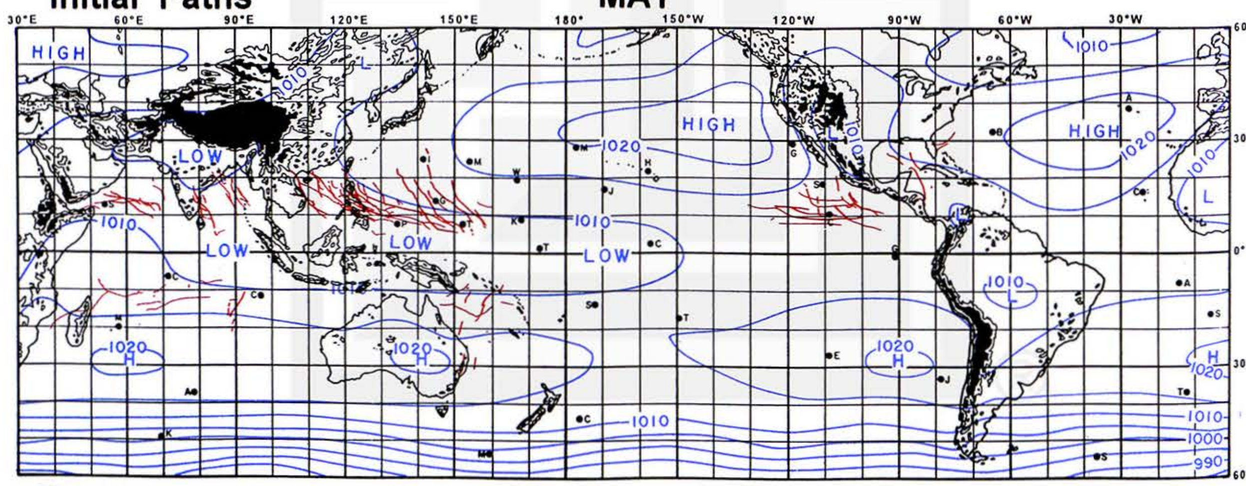

Fig. 2.12 1951-95

Initial Paths **JUNE**

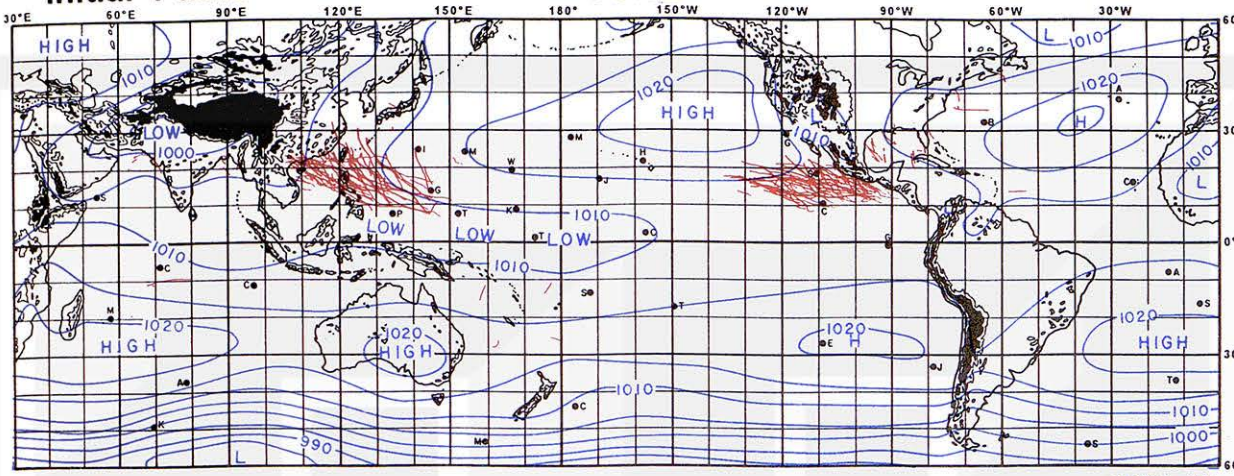

Fig. 2.13 1951-95

Initial Paths **JULY**

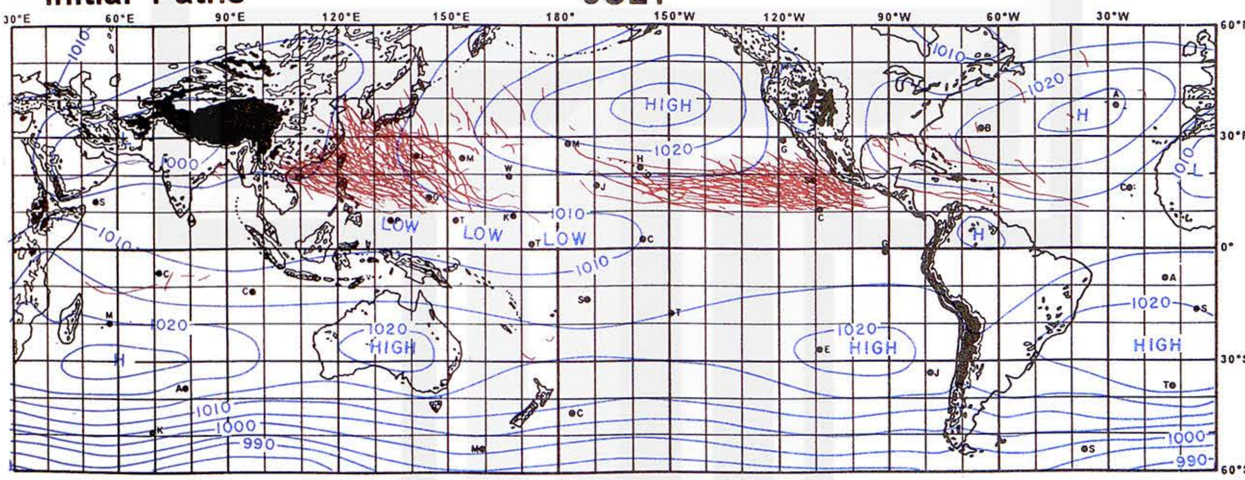

Fig. 2.14 1951-95

Initial Paths **AUGUST**

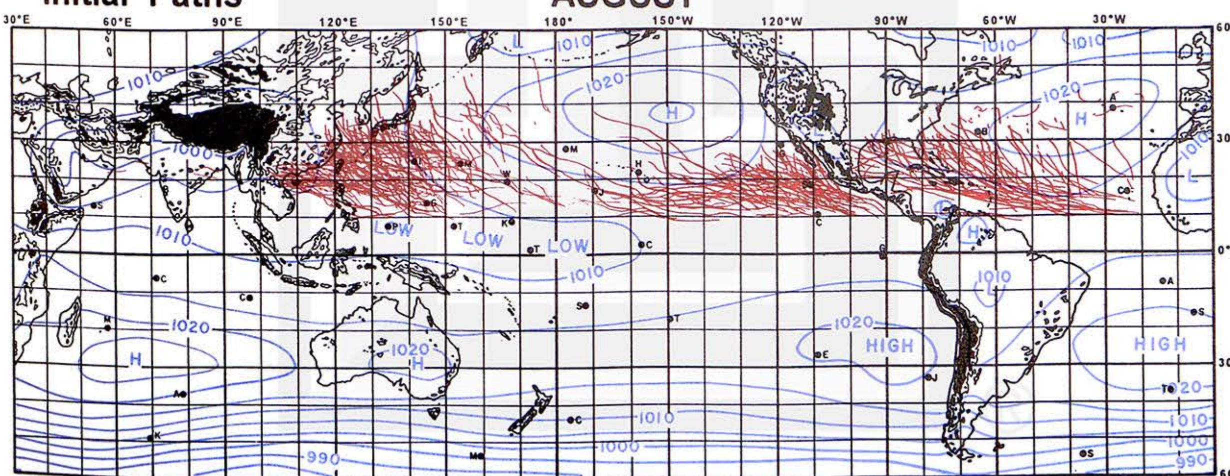

Fig. 2.15 1951-95

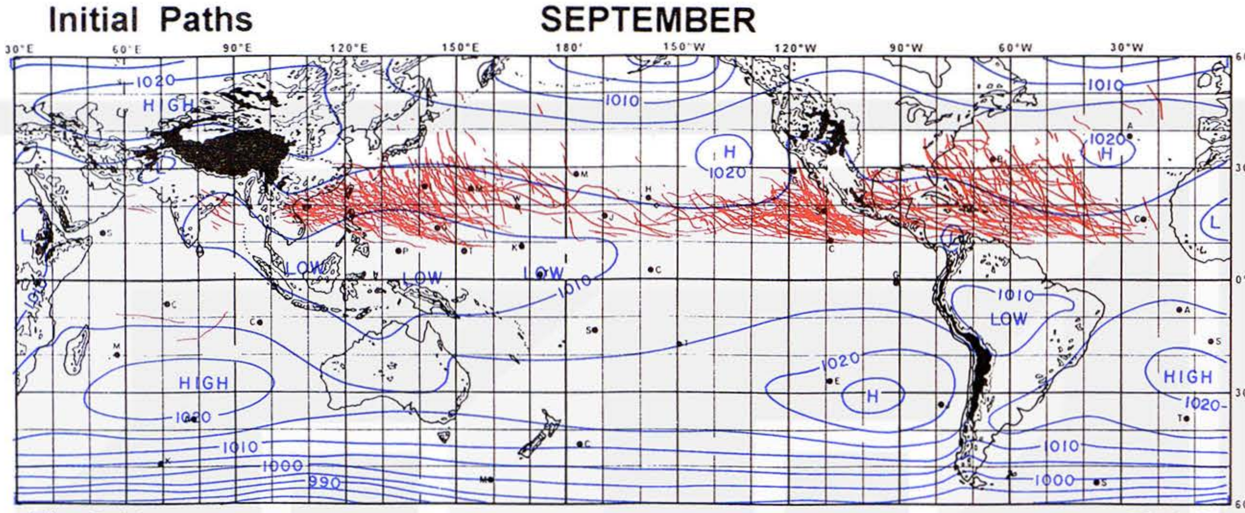

Fig. 2.16 1951-95

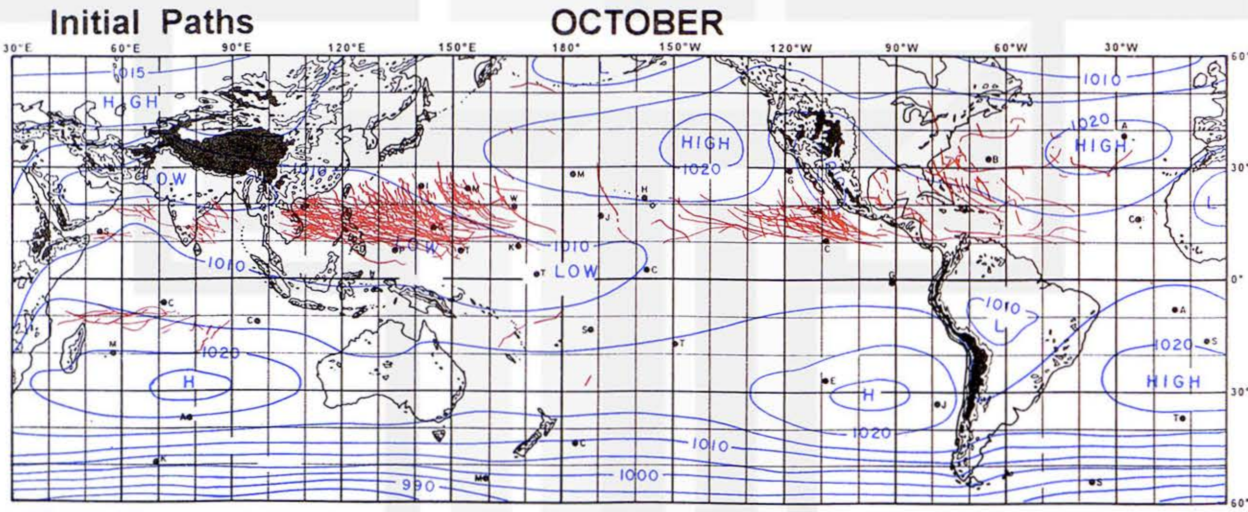

Fig. 2.17 1951-95

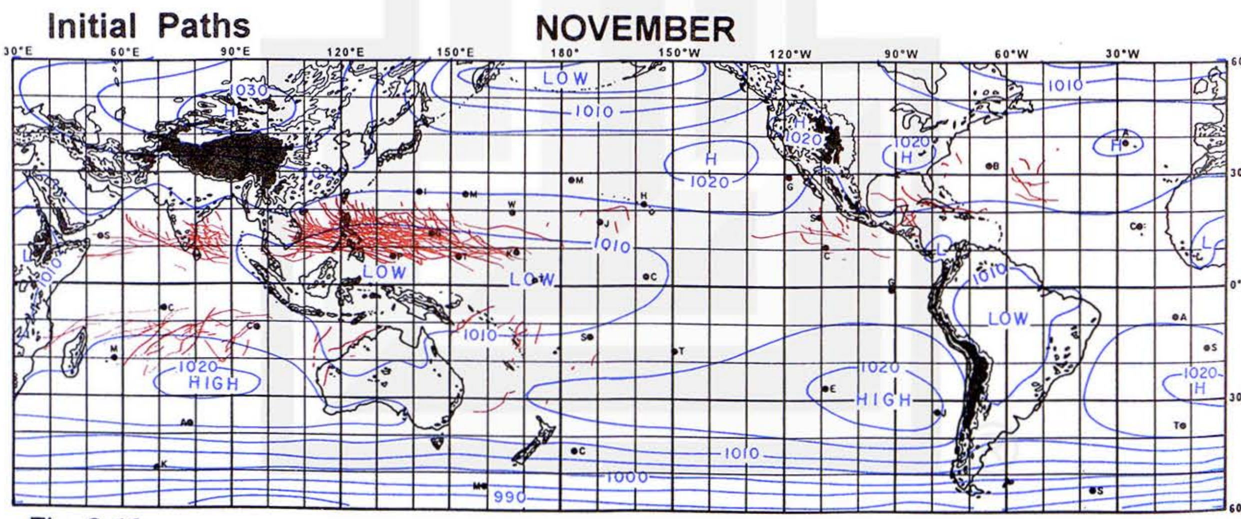

Fig. 2.18 1951-95

2.5 Initial Paths and Surface Isobars by Month

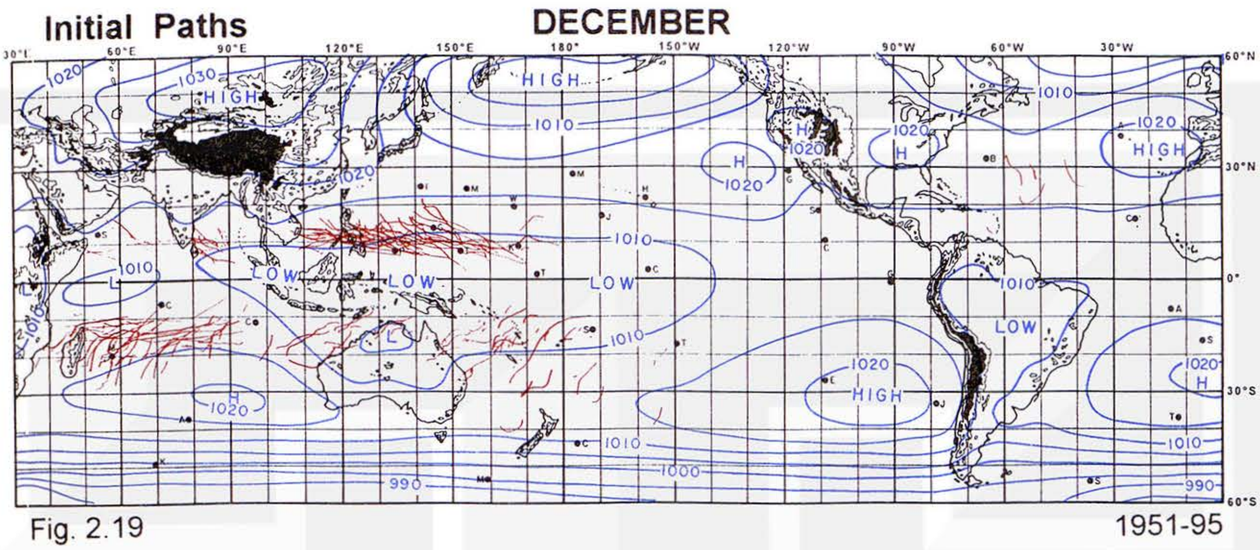

Fig. 2.19

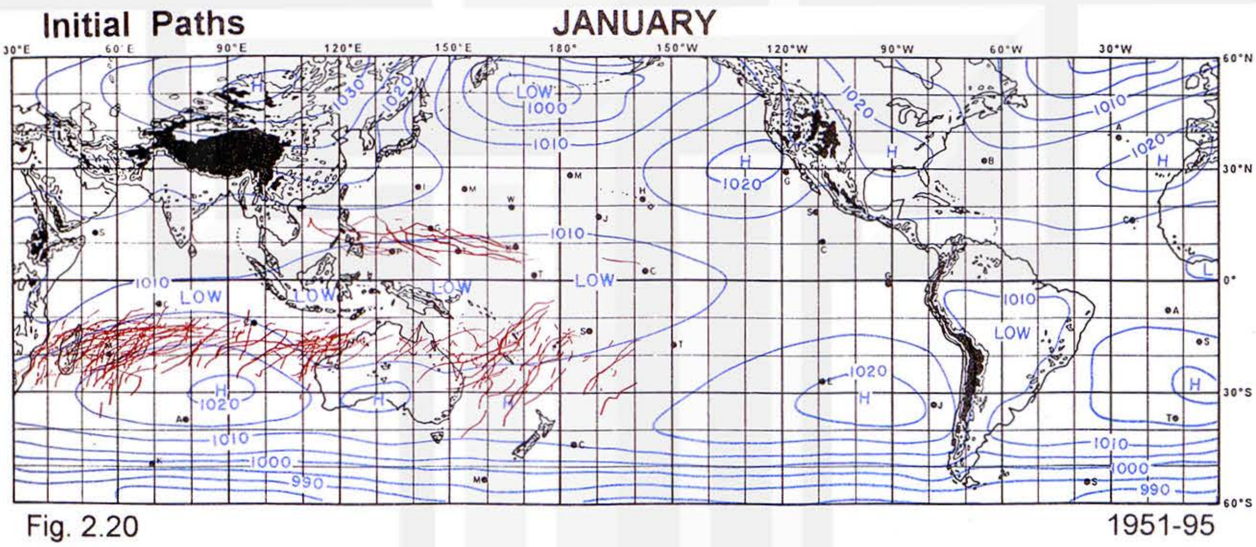

Fig. 2.20

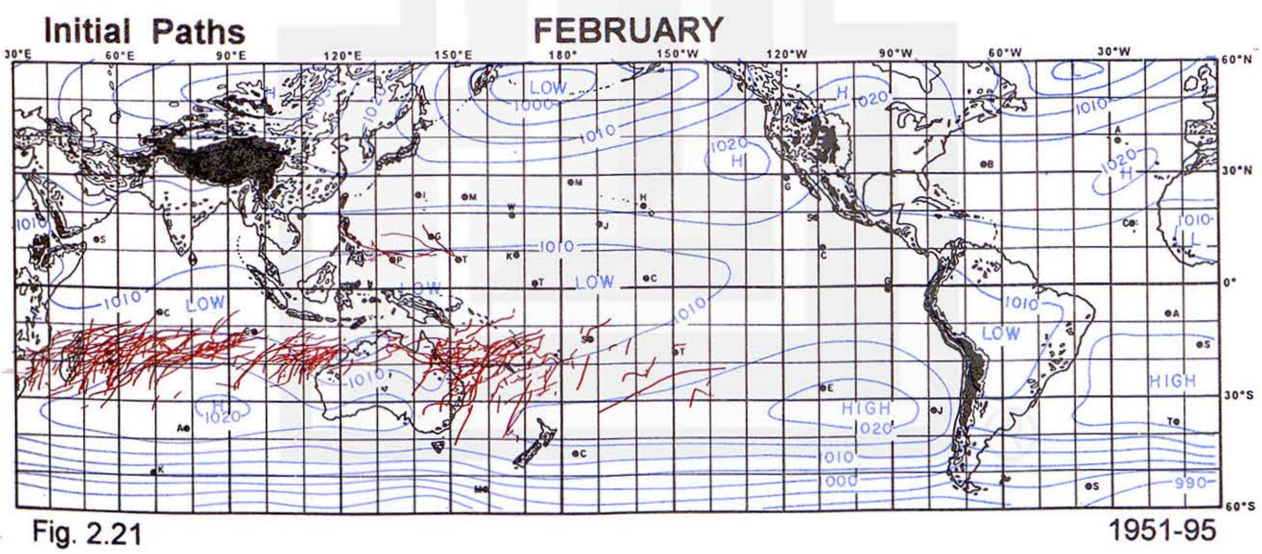

Fig. 2.21

Chapter Three

Maps of Prorated Position Counts

Introduction to Chapter Three

It is not practical to geographically assess density of storms by merely counting the number of storm paths passing through a location or small area, because a storm will affect a much larger area than the locations that lie in the path of its center. In other words, storms with centers passing near but outside of a location are also affecting that location. Also, such a count does not take into account the period of time each storm affects a small area. On the other hand, taking a count of storm center positions of a specified time interval and occurring within a larger sampling area, and prorating that count to the smaller given area is a better measure of the storm density inside that given area.

Utilized in this Atlas is the count of 6-hourly storm positions inside a latitude-longitude square area anywhere in the world. The count is identified as Position Count (PC) with unit, count per square area per statistical years. In order to determine the normalized density, the position count is prorated to a 1° equatorial square area and 100-year period. The prorated PC is called the Prorated Position Count (PPC). This parameter is used widely in this book in computing the storm density anywhere in the world. Various PPC maps in global and local areas are presented.

By virtue of the compatible nature of the PPC computed from any period and square area, PPC is useful in comparing storm densities from different data sources. In addition, PPC values integrated inside a storm-activity area can be compared with those of other areas and periods for the purpose of assessing the variation due to period and El Niño / La Niña situations.

3.1 Concepts of Storm Count and Position Count (PC)

A storm count is the number of storm paths which pass through a specific area within a specific period. Position count (PC) is the number of storm center positions of a chosen time interval occurring within a specific area and specific period. Consequently, position count is significantly larger than storm count. Figure 4.1 provides an example where a storm count of 3 yields a position count of 16. The figure also demonstrates that position count factors in time; storm path No. 2 yields 7 position counts while No. 3, a shorter-lived storm, yields only 4 position counts. By virtue of its temporal contribution and larger data base, it is clear that PC is a far greater statistical tool than a simple storm count. As dictated by data availability, a 6-hourly position count is utilized as the raw data base for statistical analysis in this atlas. This means that each storm renders 4 position counts per full day of existence.

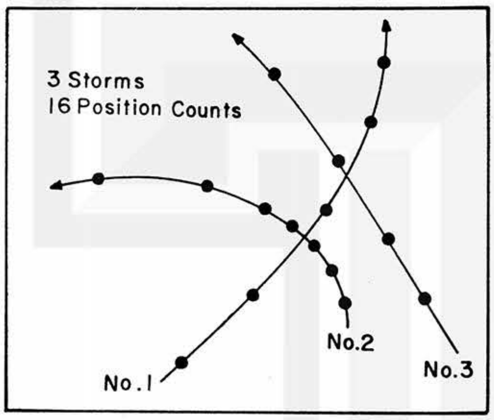

Fig. 3.1 The difference between Storm Count and Position Count (PC).

3.2 Principal of Prorated Position Count

To create the normalized data base used in the analyses of this atlas, 6-hourly position counts were made for 4° latitude and longitude square areas and specified statistical periods (see Figure 4.2). Each resulting PC was then assigned to the center latitude and longitude of its area, ϕ+2° and θ+2° respectively. However, the area of 4° latitude-longitude squares on the earth varies with latitude, making values of PC non-comparable for analysis across locations of different latitude without normalization. The same non-comparability would apply for data sets with periods of different length. For this reason, all position count data is prorated to an area of 1° equatorial square (see Figure 4.3) and a 100-year period. This prorated value achieves the normalized storm density necessary for analysis and is called the Prorated Position Count (PPC).

3.2 Principal of Prorated Position Count

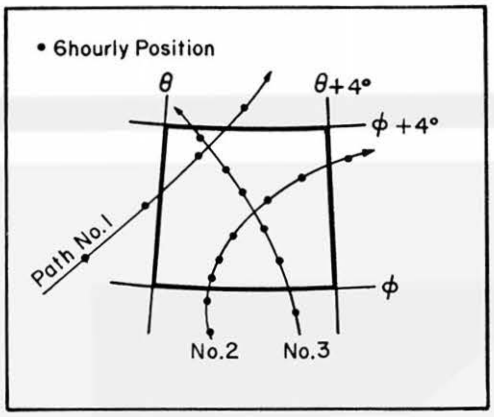

Fig. 3.2 6-hourly positions inside a 4° latitude by 4° longitude square. The center latitude and longitude are $\phi + 2°$ and $\theta + 2°$, respectively.

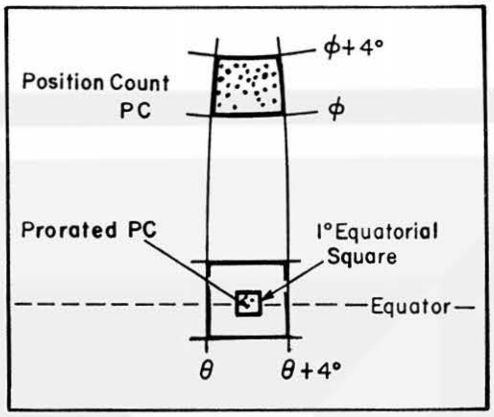

Fig. 3.3 Position counts inside a 4° latitude by 4° longitude square, prorated to the area of a 1° square box centered at the equator.

3.3 Statistical Periods of Analysis

Based on the availability of reliable data, the total period of the data base used is 45 statistical years, 1951-95 storm years for each of the northern and southern hemispheres (refer to section 1.1, page 4). Additionally, three 15-year periods, sequential divisions of the 45-year period, are also analyzed for inter-comparison. These 15-year periods approximately reflect phases of improving data collection methods: 1951-65 — ship, buoy, land-based and aircraft monitoring only, 1965-80 — early satellite monitoring added, and 1981-95 — modern geostationary satellite monitoring and computerization.

Three Periods of 45 Statistical Years

First 15 Years	(Period **A**)	1951-65
Second 15 Years	(Period **B**)	1966-80
Third 15 Years	(Period **C**)	1981-95
Total 45 Years	(Period **ABC**)	1951-95

The PPC distributions for these 45-year and 15-year periods are presented and analyzed on a global scale and for six local areas in the following two sections: **3.4** Global PPC Maps and **3.5** Local PPC Maps. They can be compared with storm path distributions, which are also shown.

STORM PATHS (First 15 years) Period A

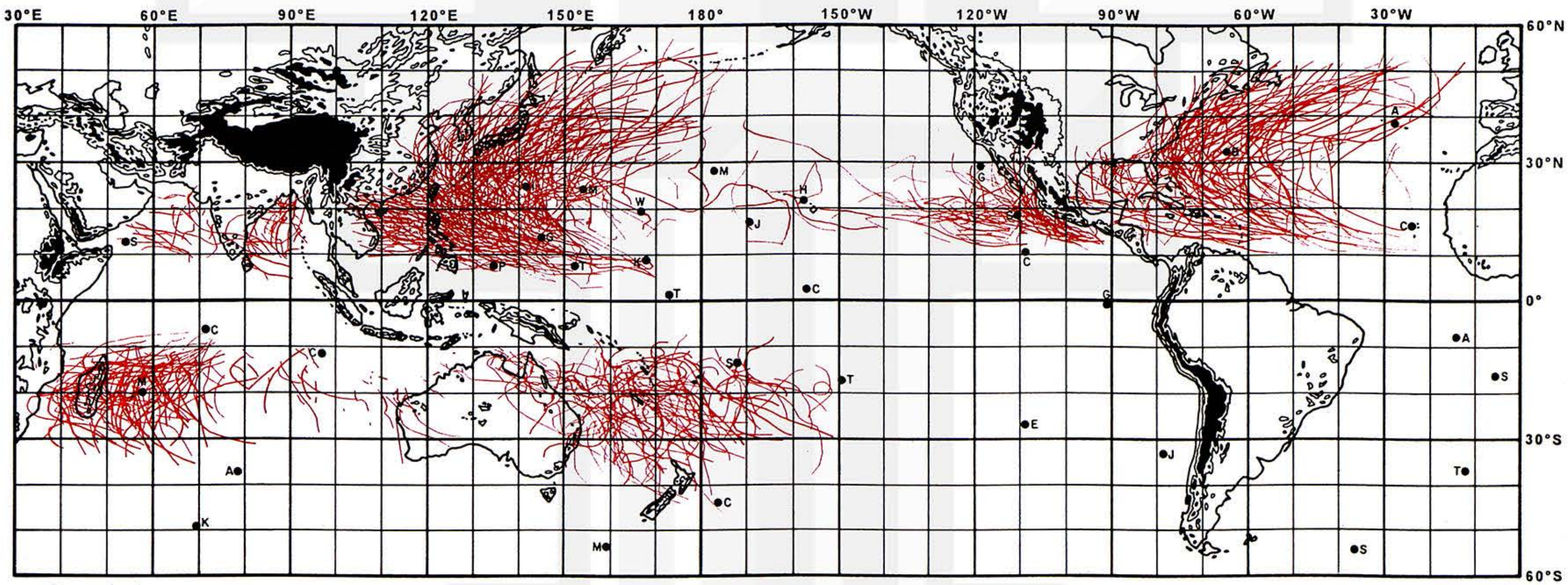

Fig. 3.4

1951-65

PPC (First 15 years) Period A

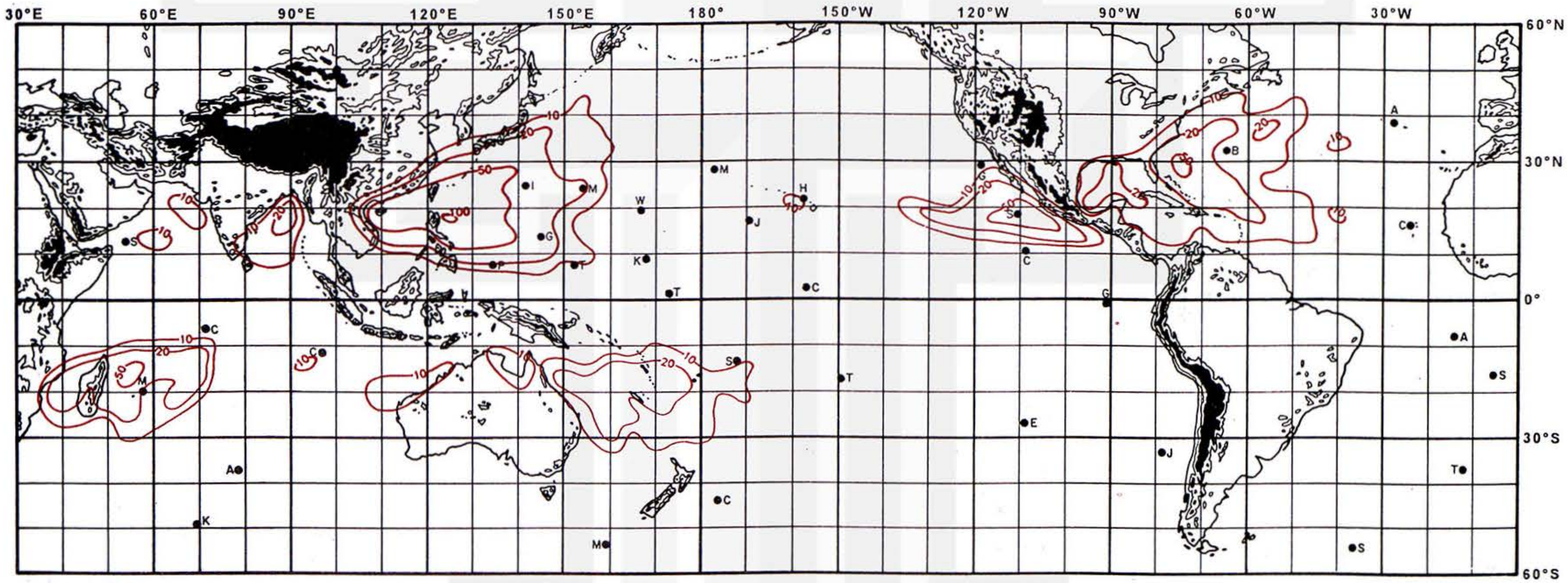

Fig. 3.5

1951-65

STORM PATHS (Second 15 years) Period B

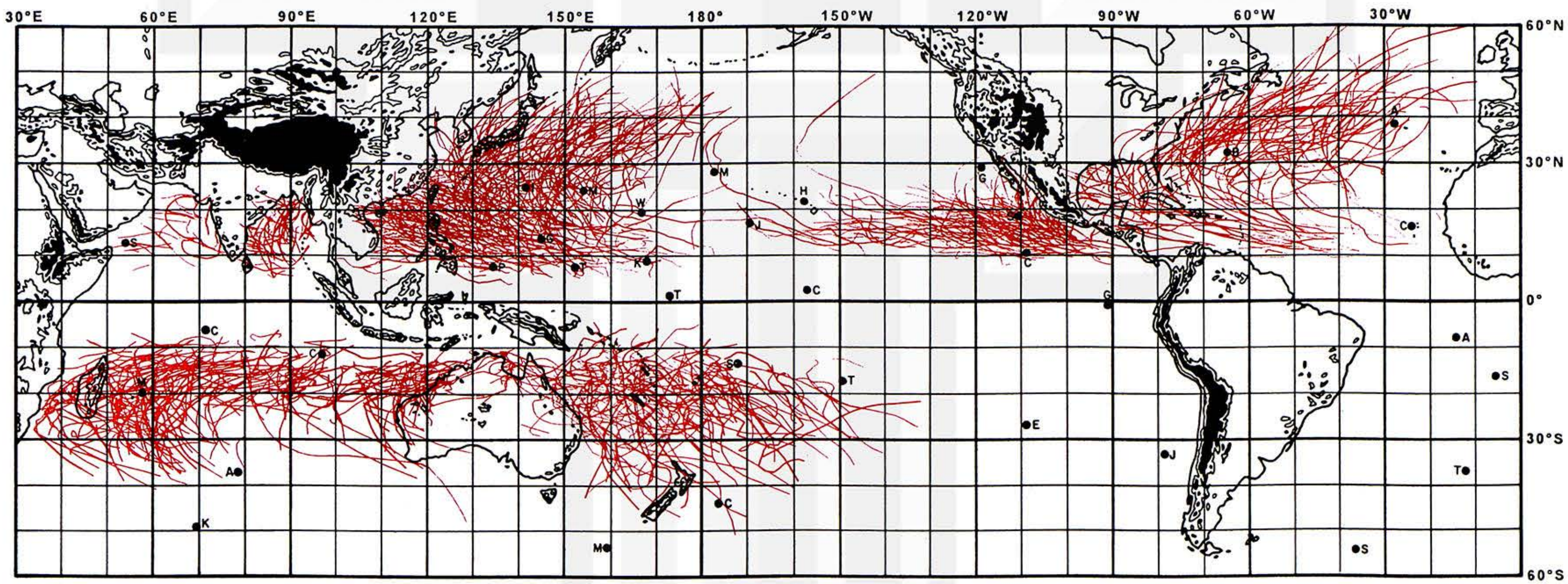

Fig. 3.6

1966-80

PPC (Second 15 years) Period B

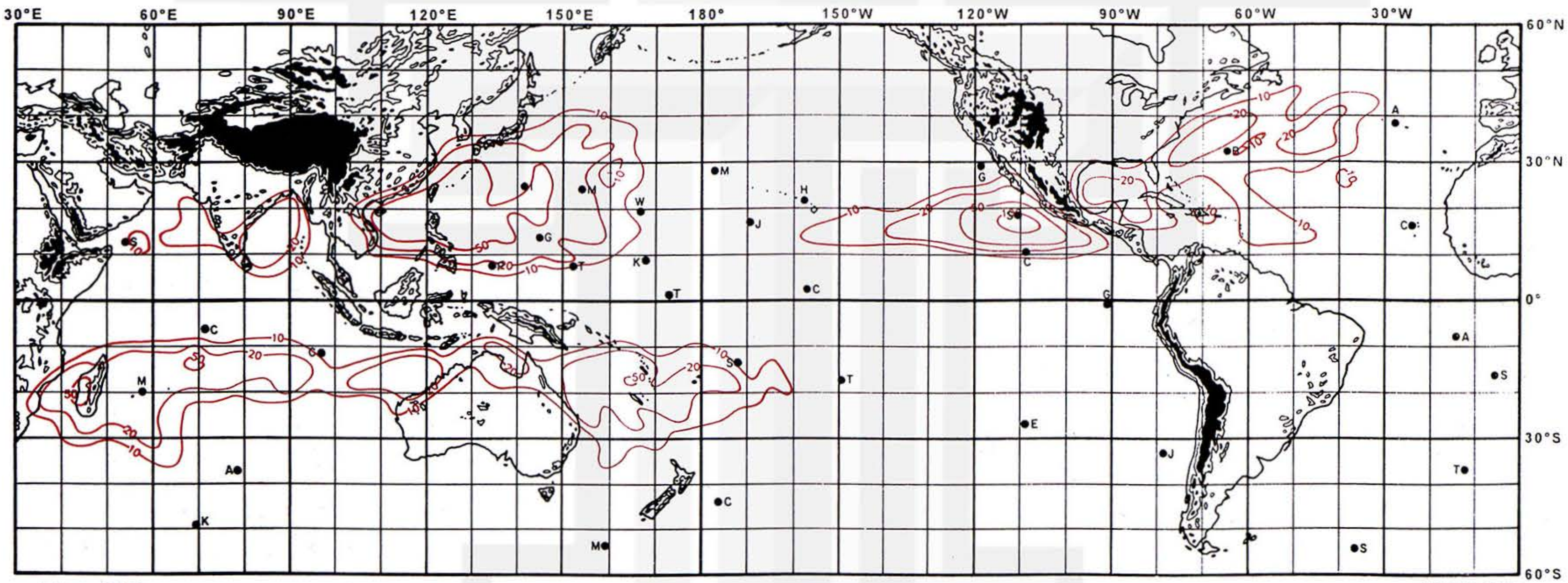

Fig. 3.7

1966-80

STORM PATHS (Third 15 years) Period C

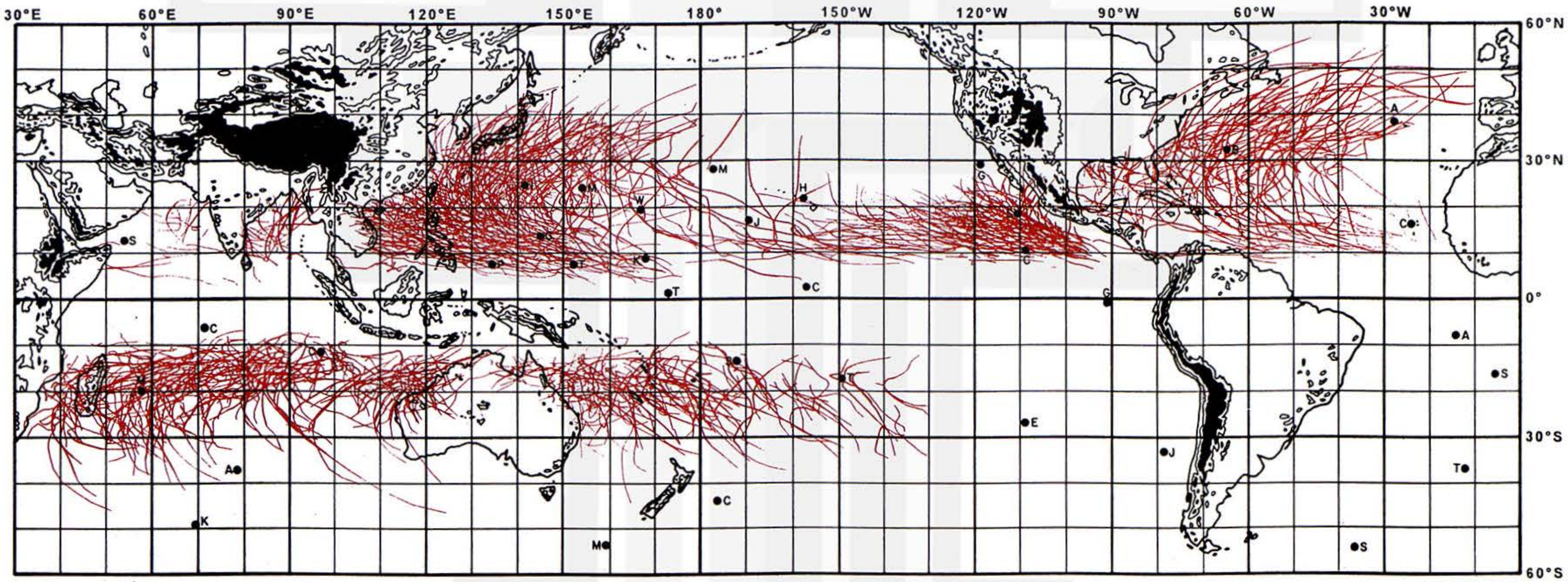

Fig. 3.8 1981-95

PPC (Third 15 years) Period C

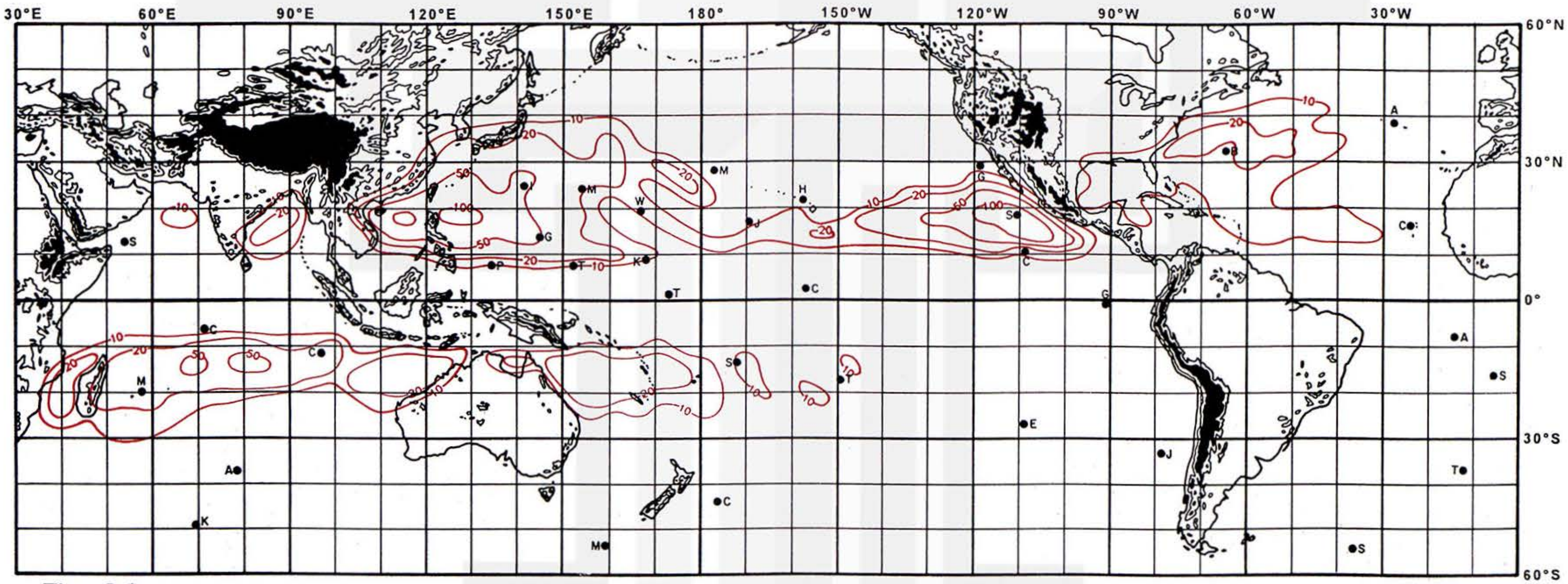

Fig. 3.9

1981-95

STORM PATHS (Total 45 years) Period ABC

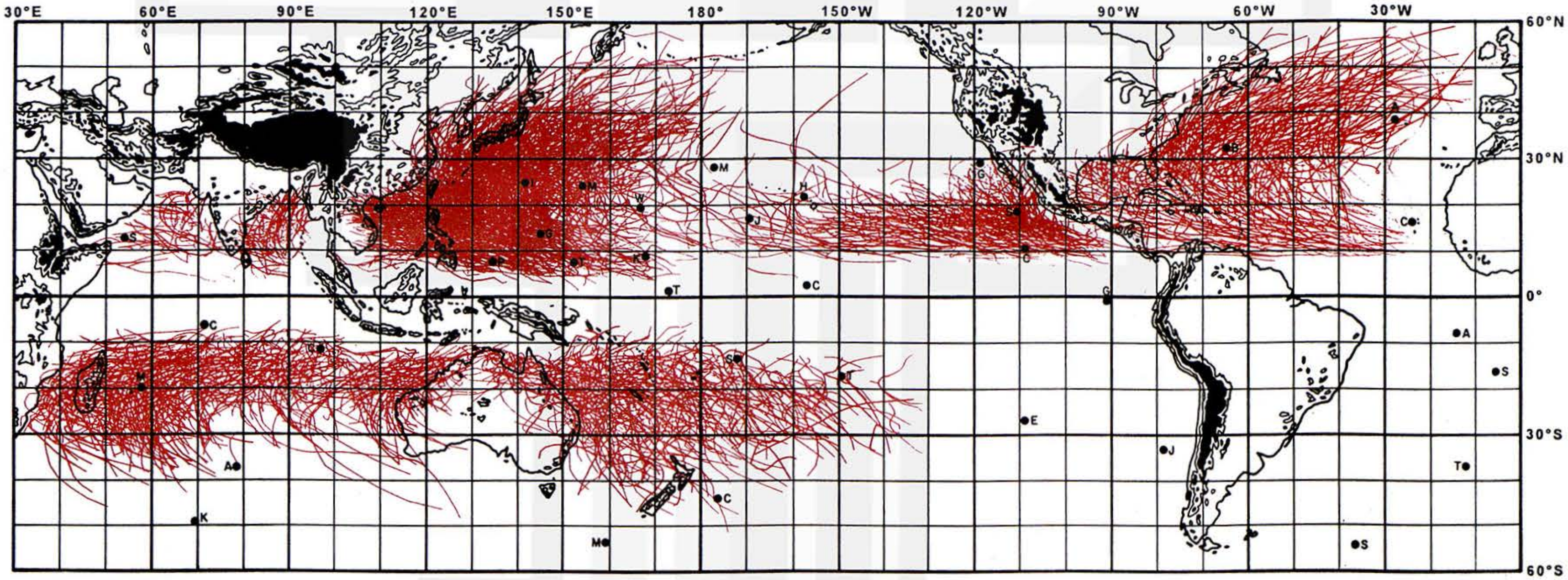

Fig. 3.10 1951-95

PPC (Total 45 years) Period ABC

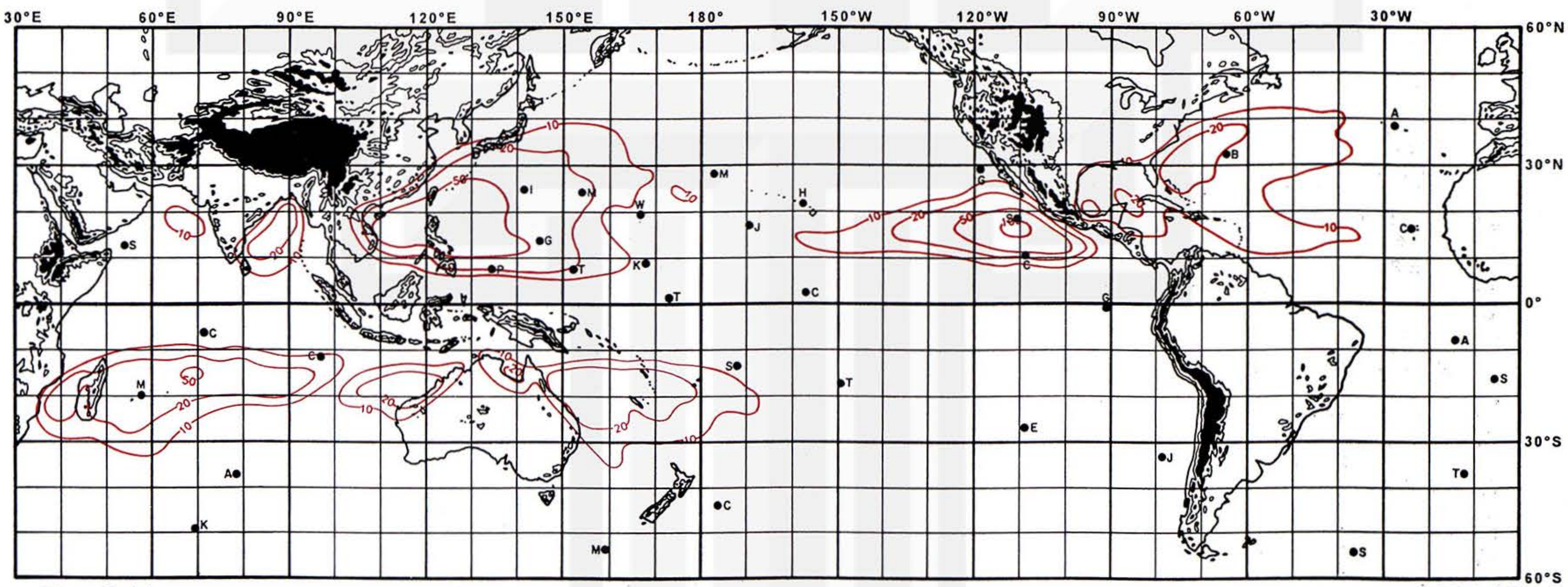

Fig. 3.11

1951-95

STORM PATHS (Period A) Area 1

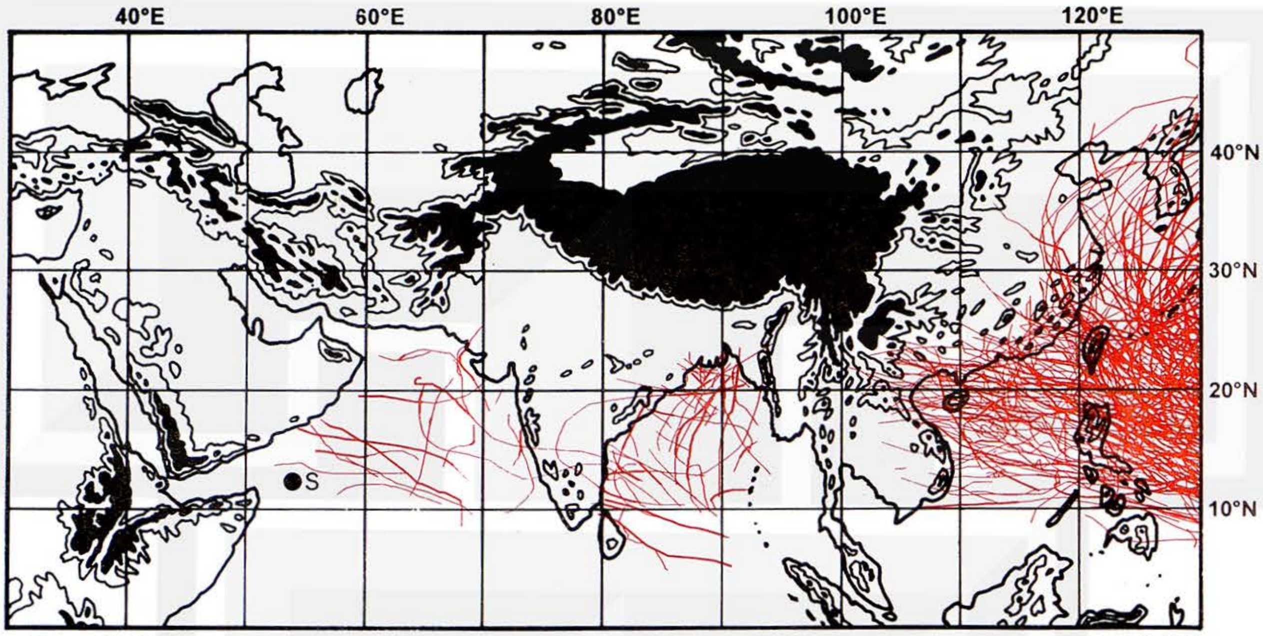

Fig. 3.12 1951-65

PPC (Period A) Area 1

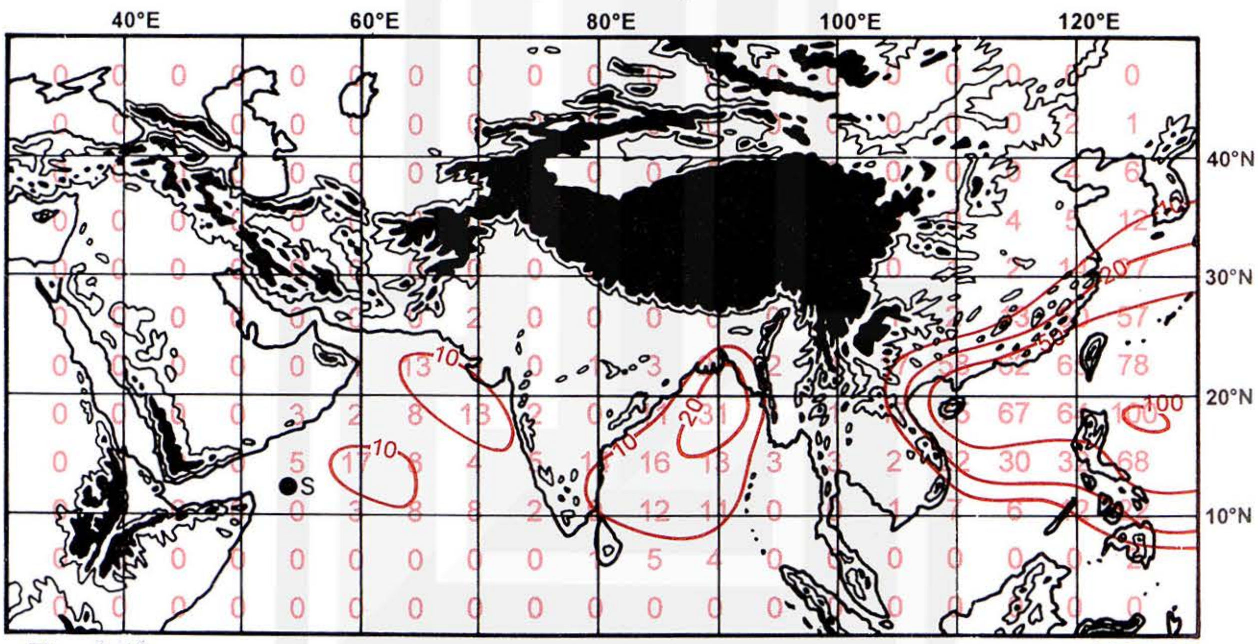

Fig. 3.13 1951-65

STORM PATHS (Period B) Area 1

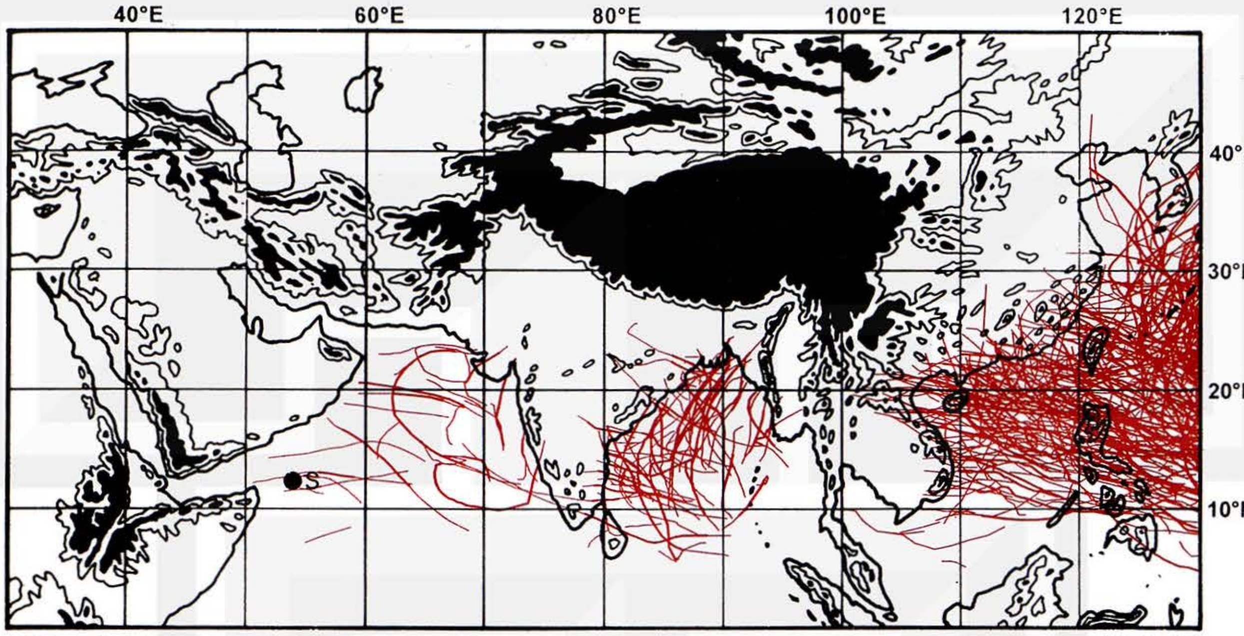

Fig. 3.14 1966-80

PPC (Period B) Area 1

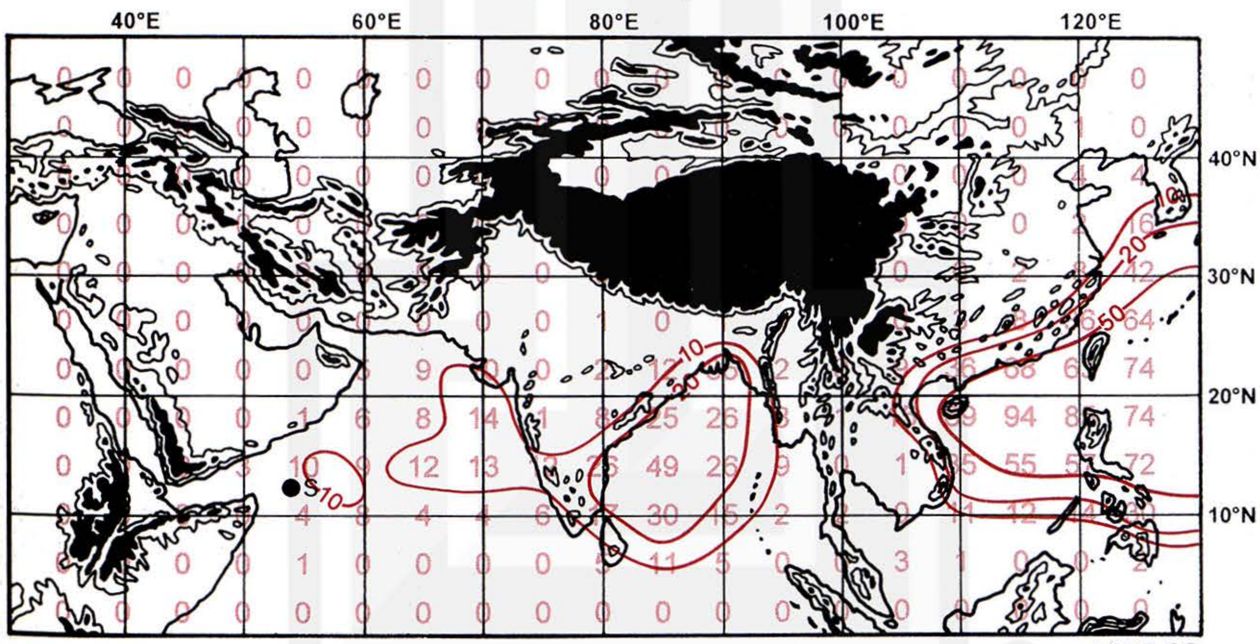

Fig. 3.15 1966-80

STORM PATHS (Period C) Area 1

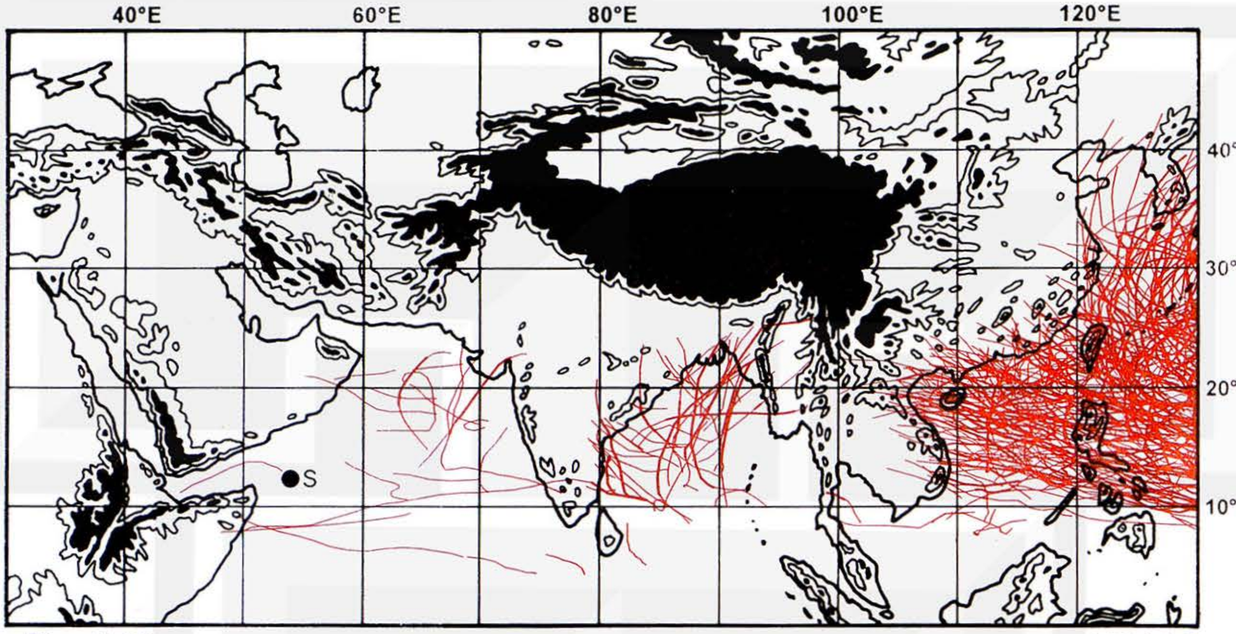

Fig. 3.16 1981-95

PPC (Period C) Area 1

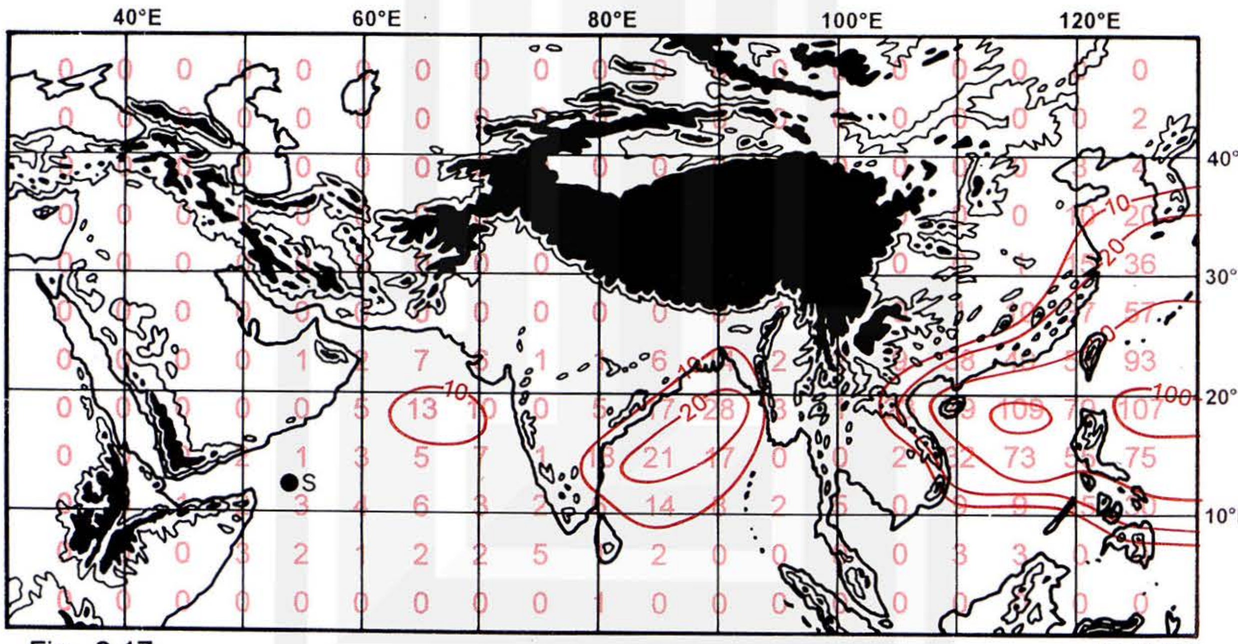

Fig. 3.17 1981-95

STORM PATHS (Period ABC) Area 1

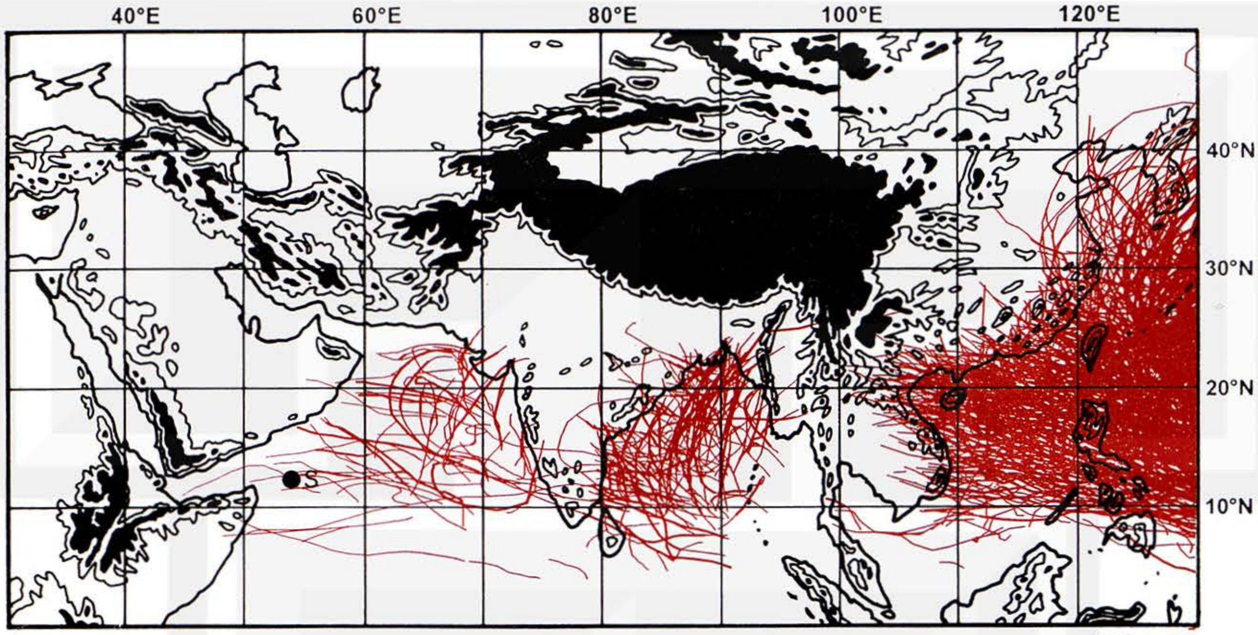

Fig. 3.18 1951-95

PPC (Period ABC) Area 1

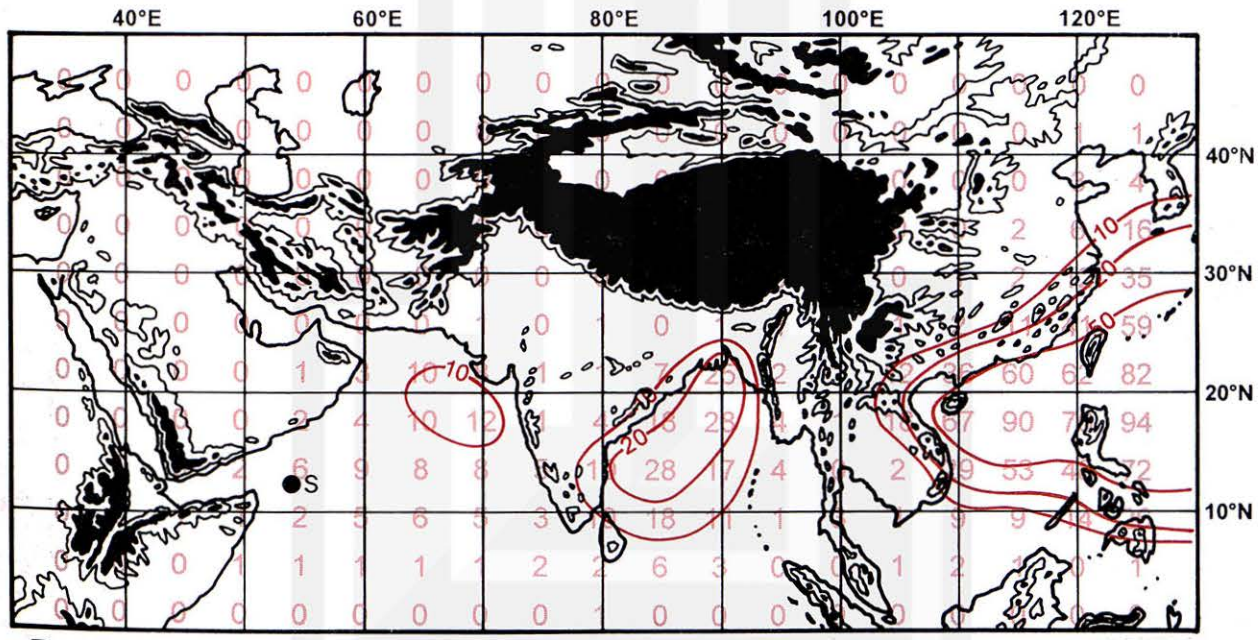

Fig. 3.19 1951-95

STORM PATHS (Period A) Area 2

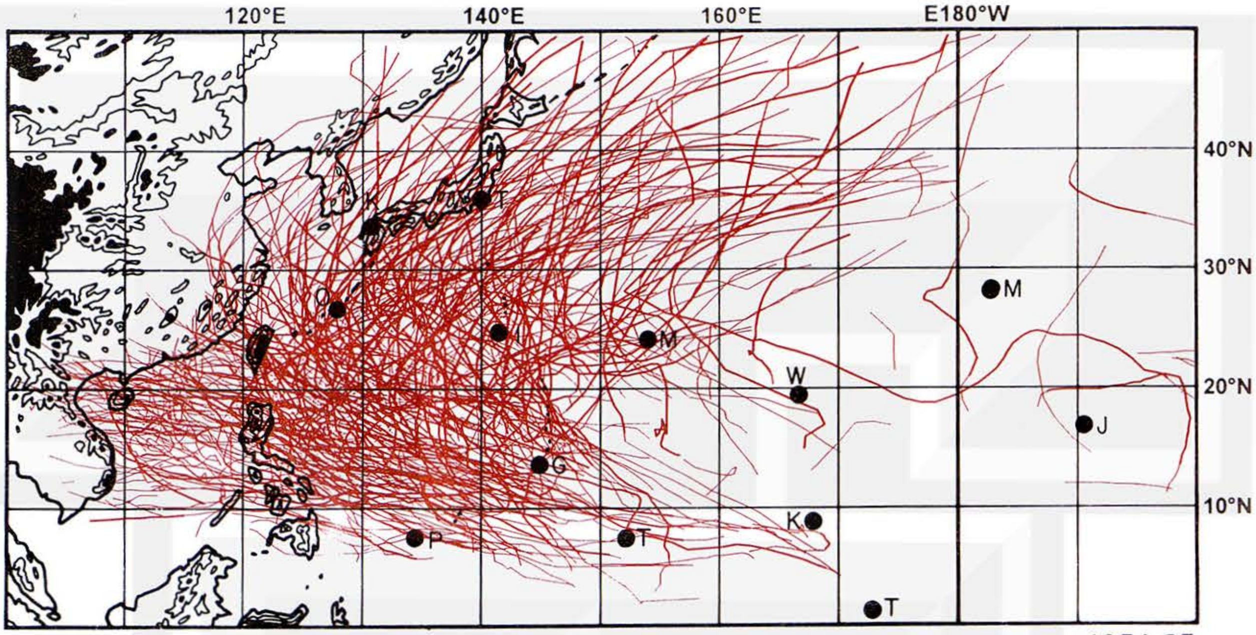

Fig. 3.20

1951-65

PPC (Period A) Area 2

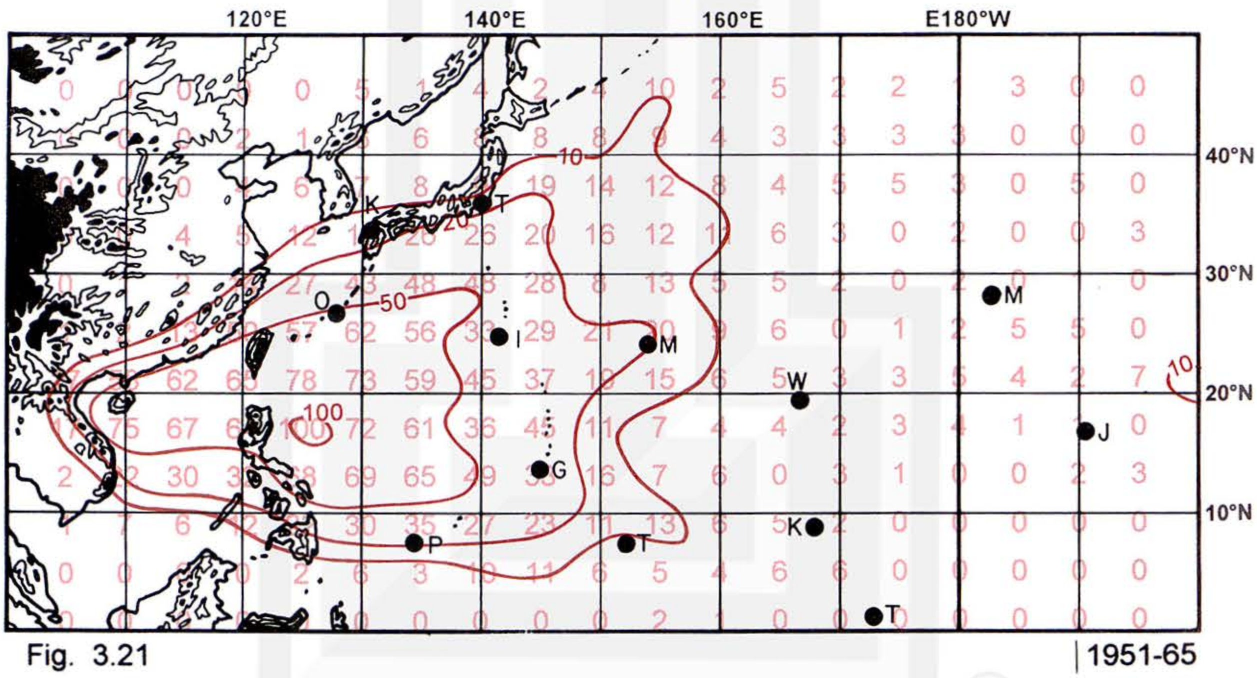

Fig. 3.21

1951-65

STORM PATHS (Period B) Area 2

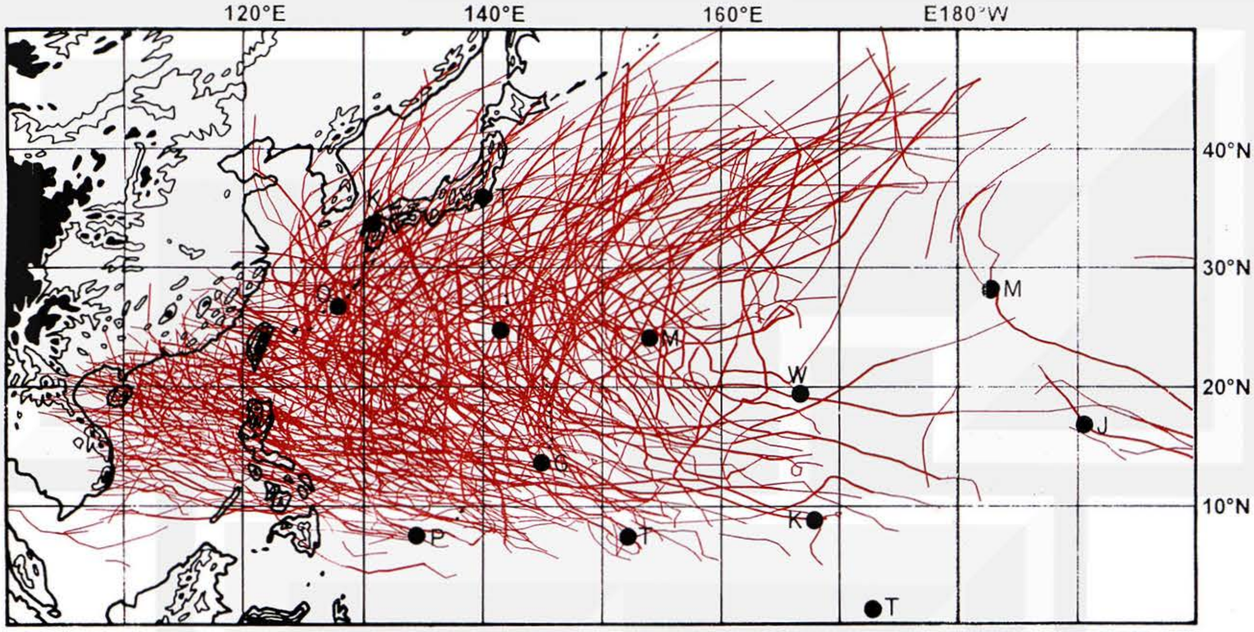

Fig. 3.22

PPC (Period B) Area 2

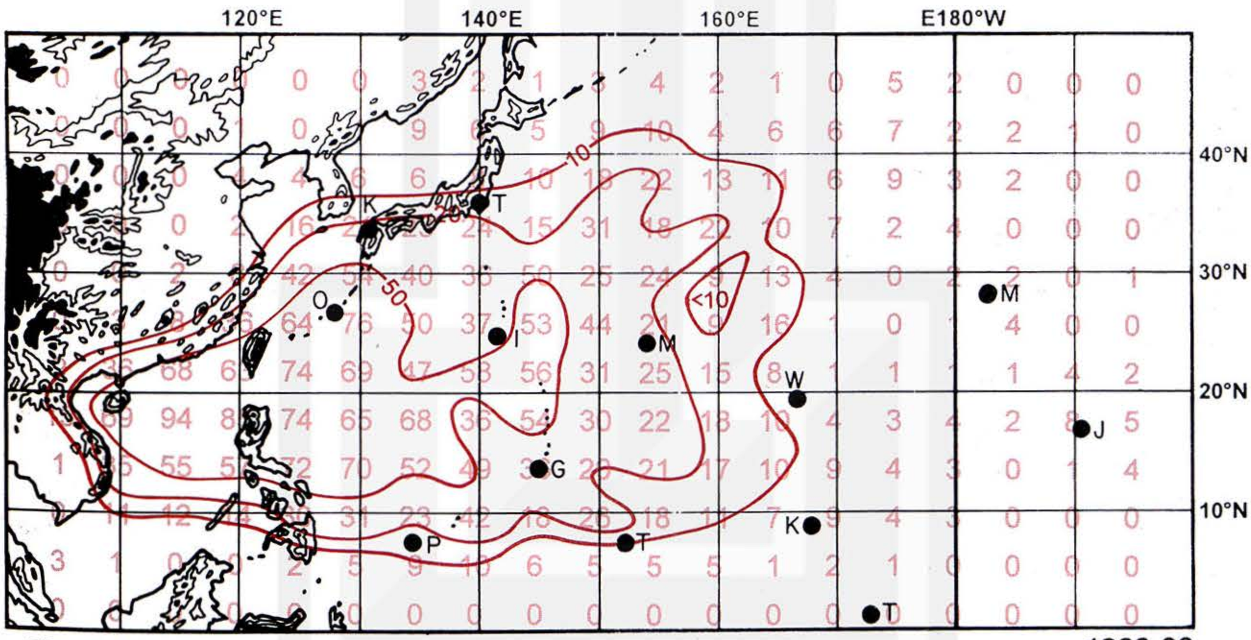

Fig. 3.23

STORM PATHS (Period C) Area 2

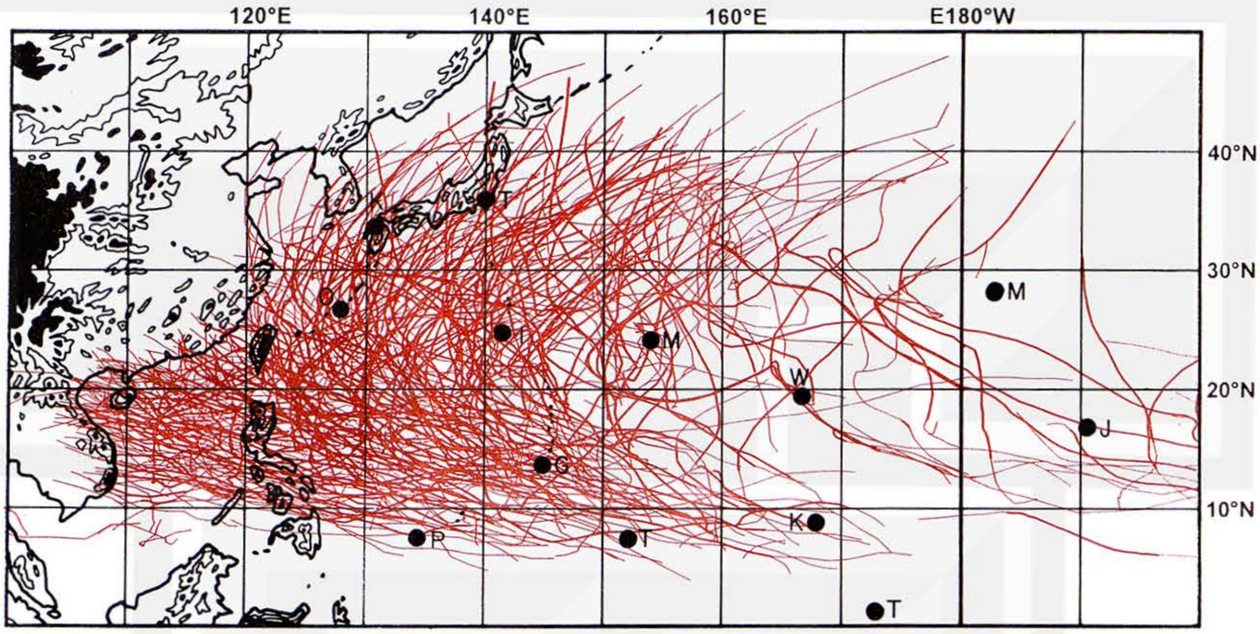

Fig. 3.24 1981-95

PPC (Period C) Area 2

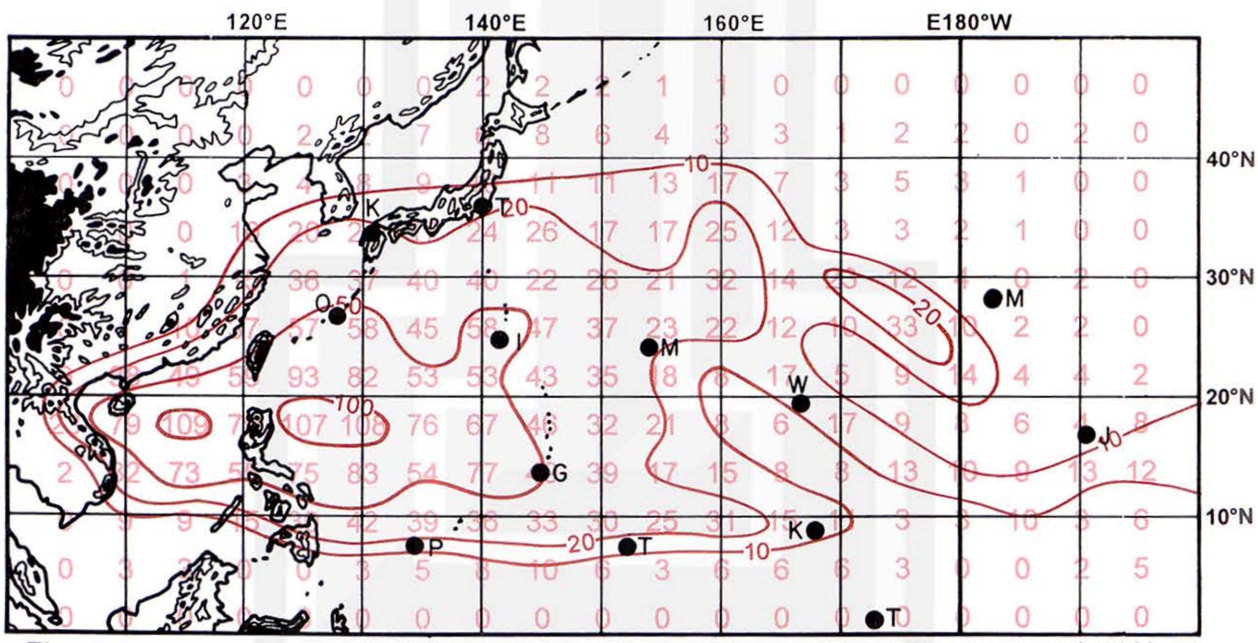

Fig. 3.25 1981-95

3.5 Local PPC Maps

STORM PATHS (Period ABC) Area 2

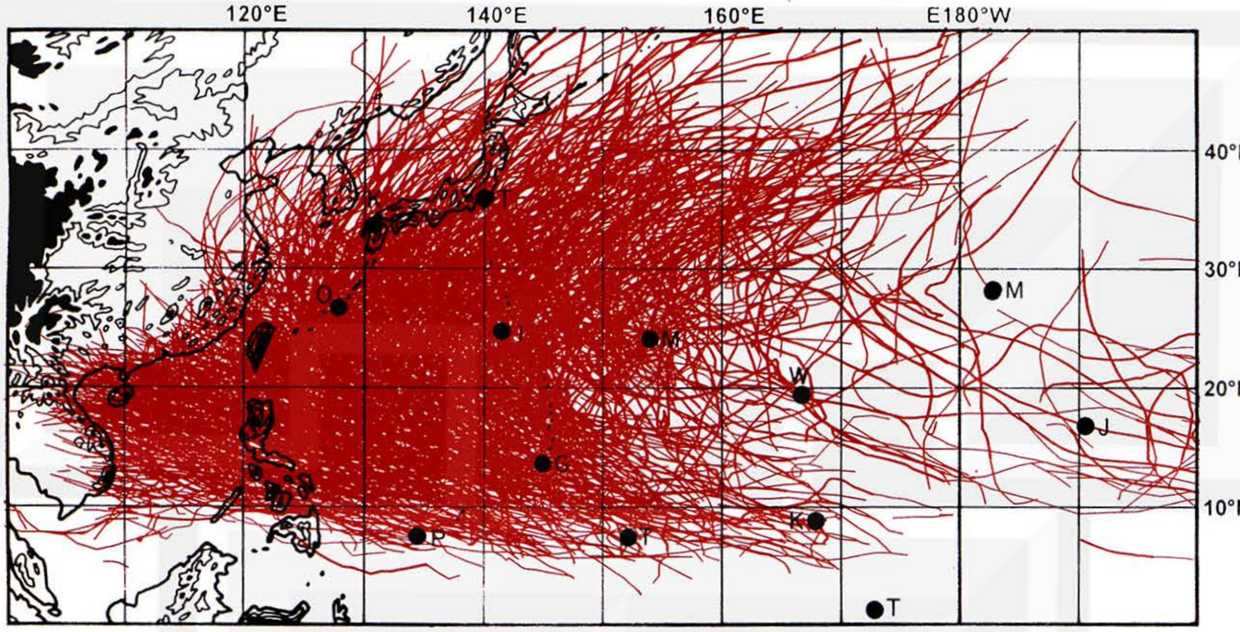

Fig. 3.26 1951-95

PPC (Period ABC) Area 2

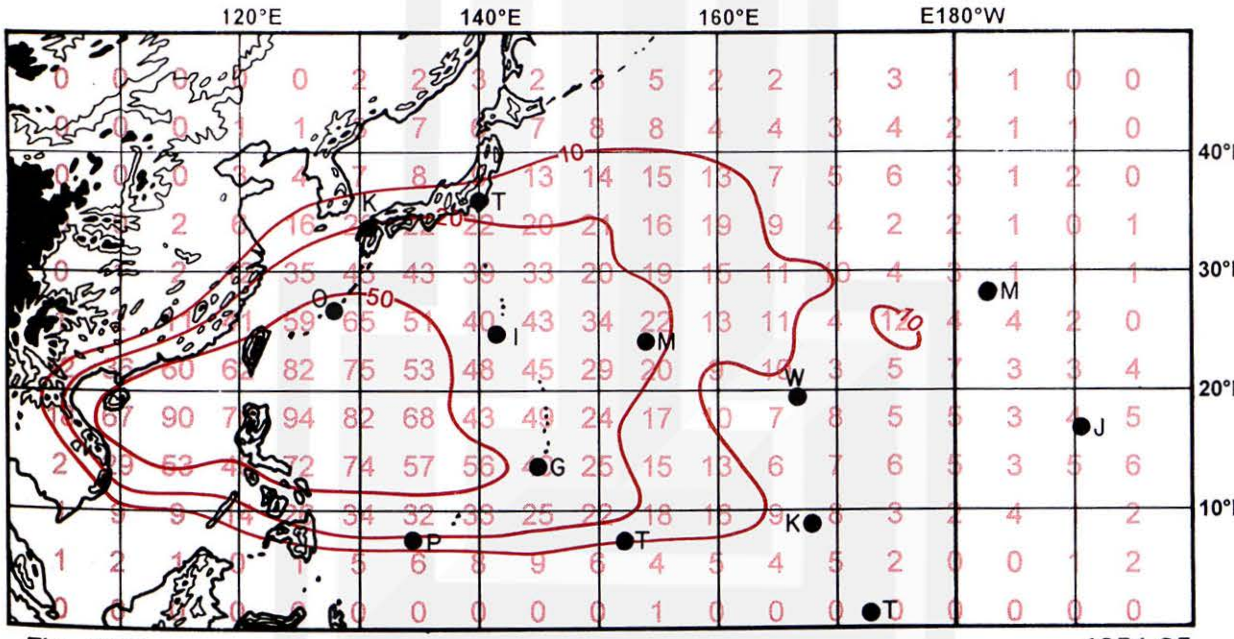

Fig. 3.27 1951-95

STORM PATHS (Period A) Area 3

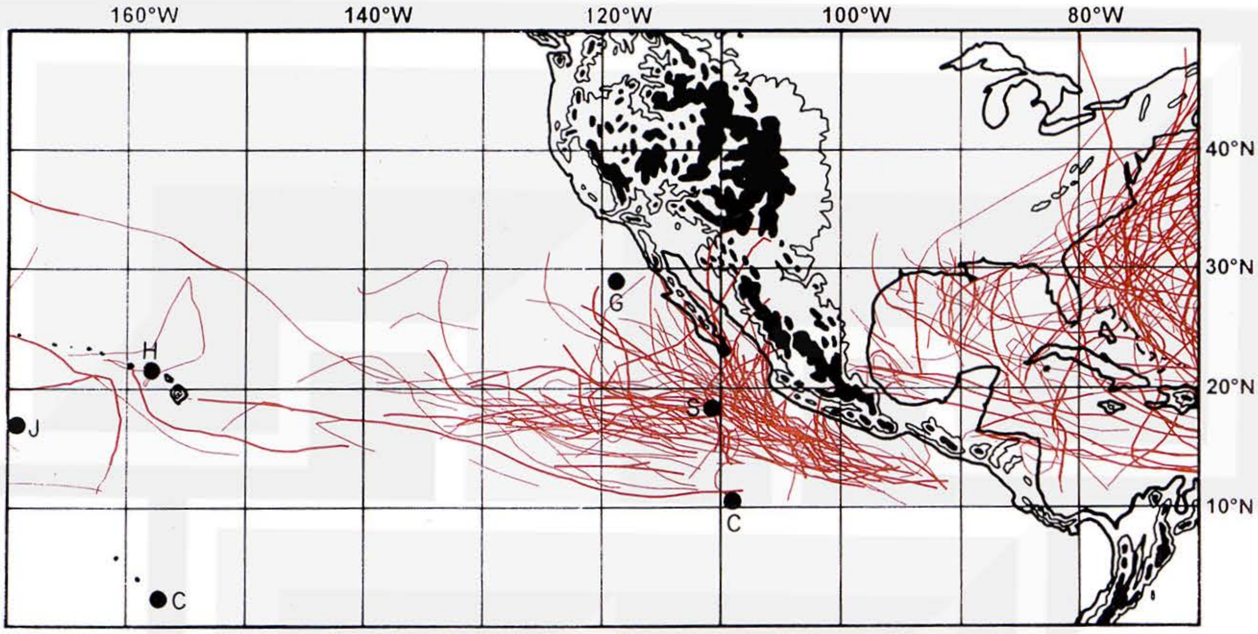

Fig. 3.28 1951-65

PPC (Period A) Area 3

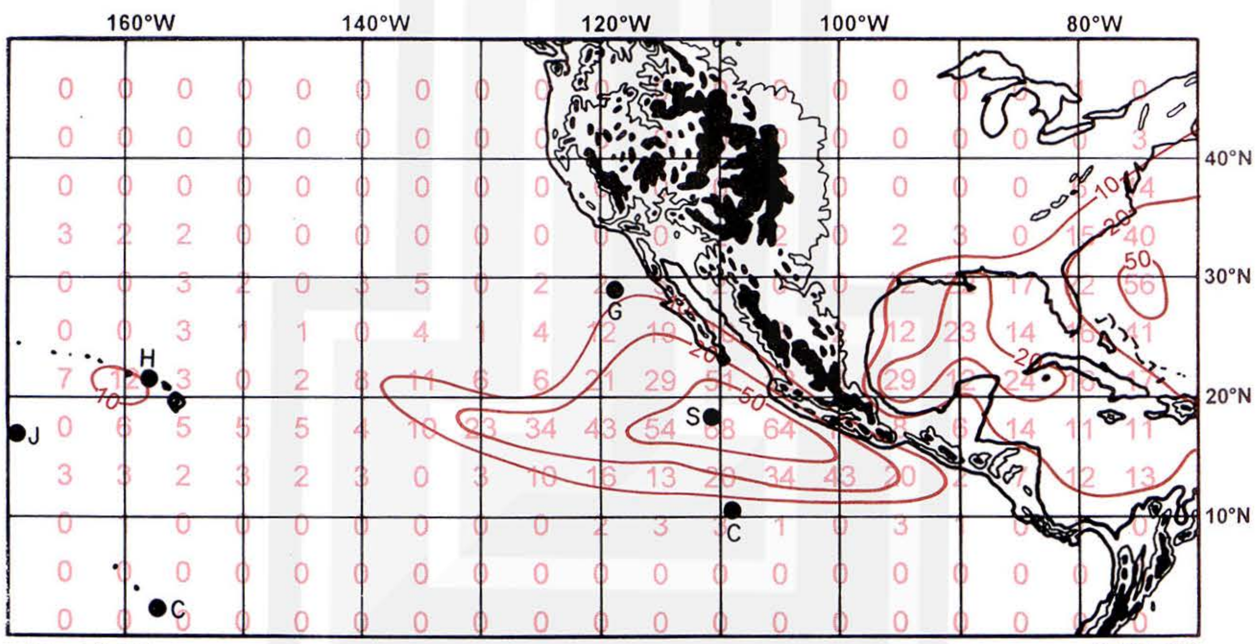

Fig. 3.29 1951-65

STORM PATHS (Period B) Area 3

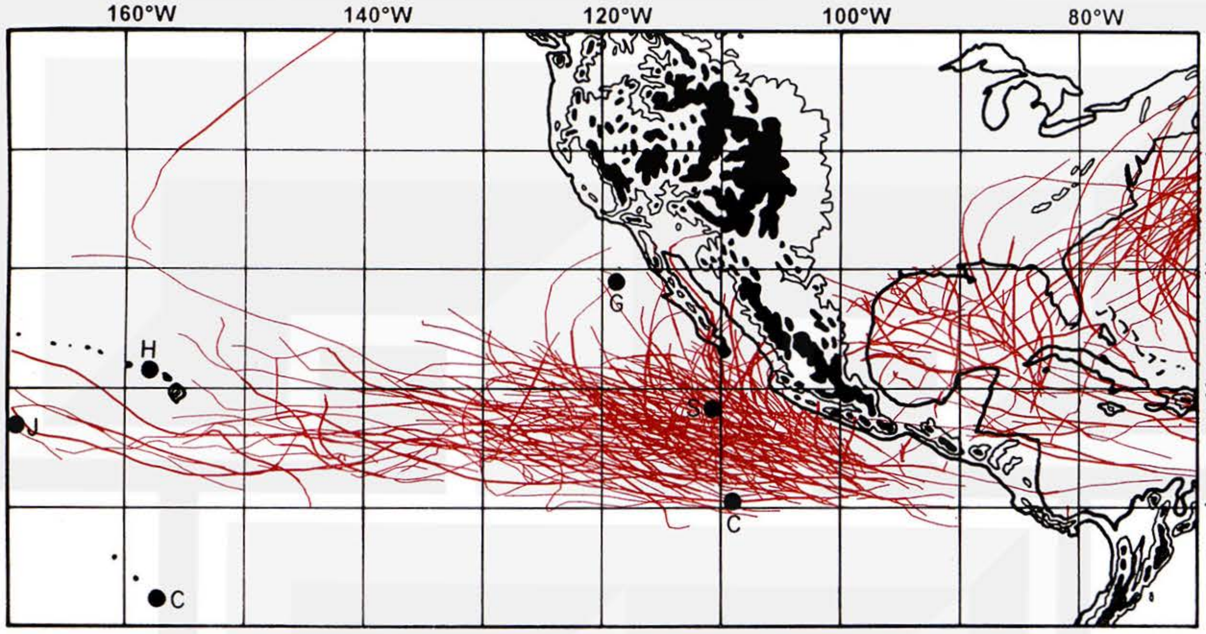

Fig. 3.30 1966-80

PPC (Period B) Area 3

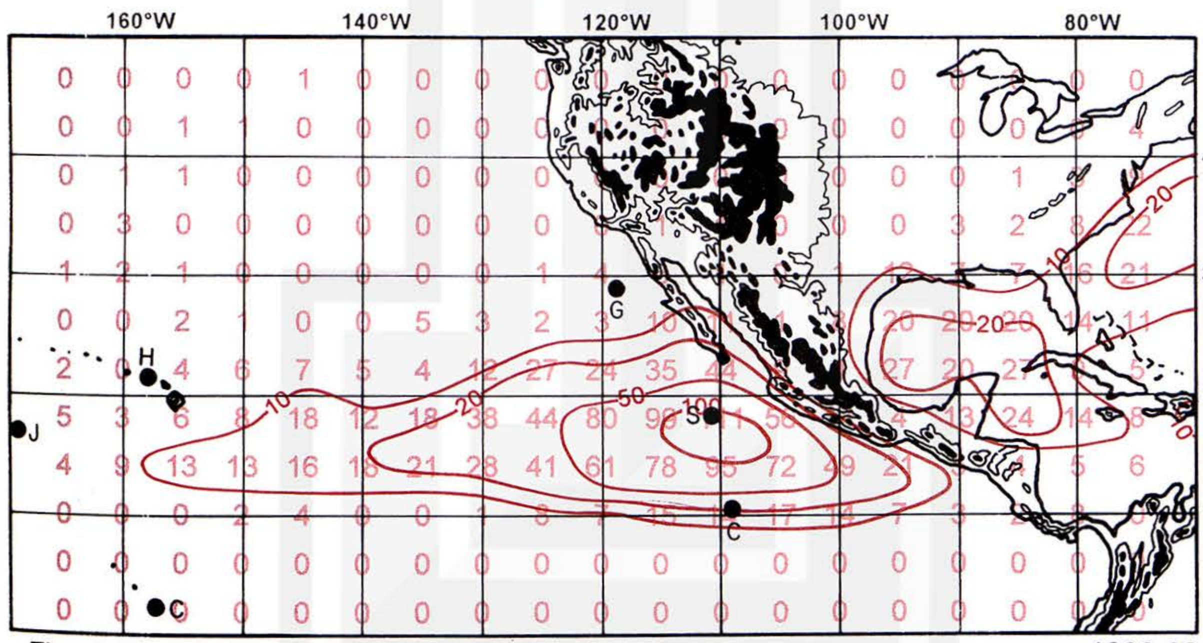

Fig. 3.31 1966-80

STORM PATHS (Period C) Area 3

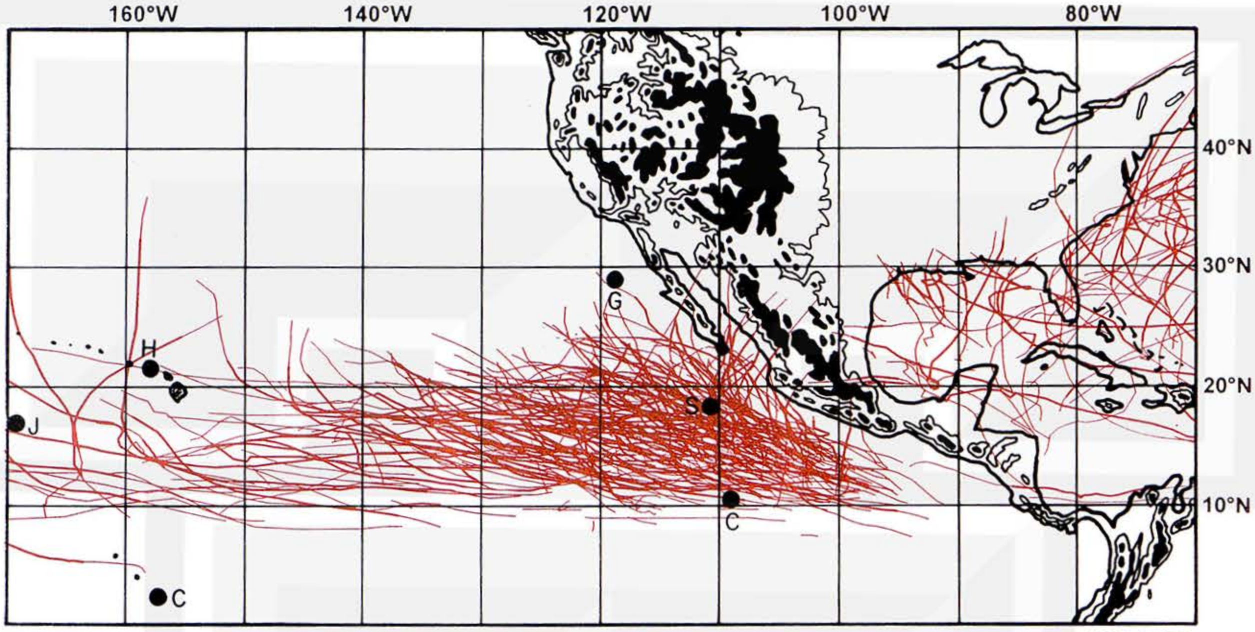

Fig. 3.32 1981-95

PPC (Period C) Area 3

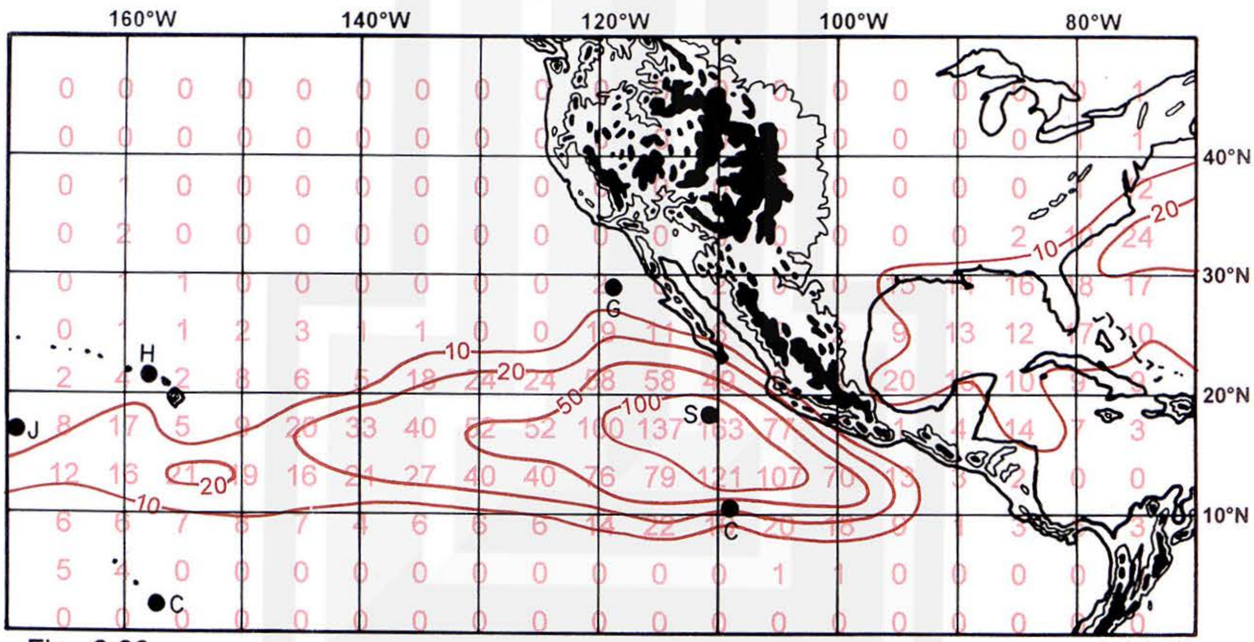

Fig. 3.33 1981-95

3.5 Local PPC Maps

STORM PATHS (Period ABC) Area 3

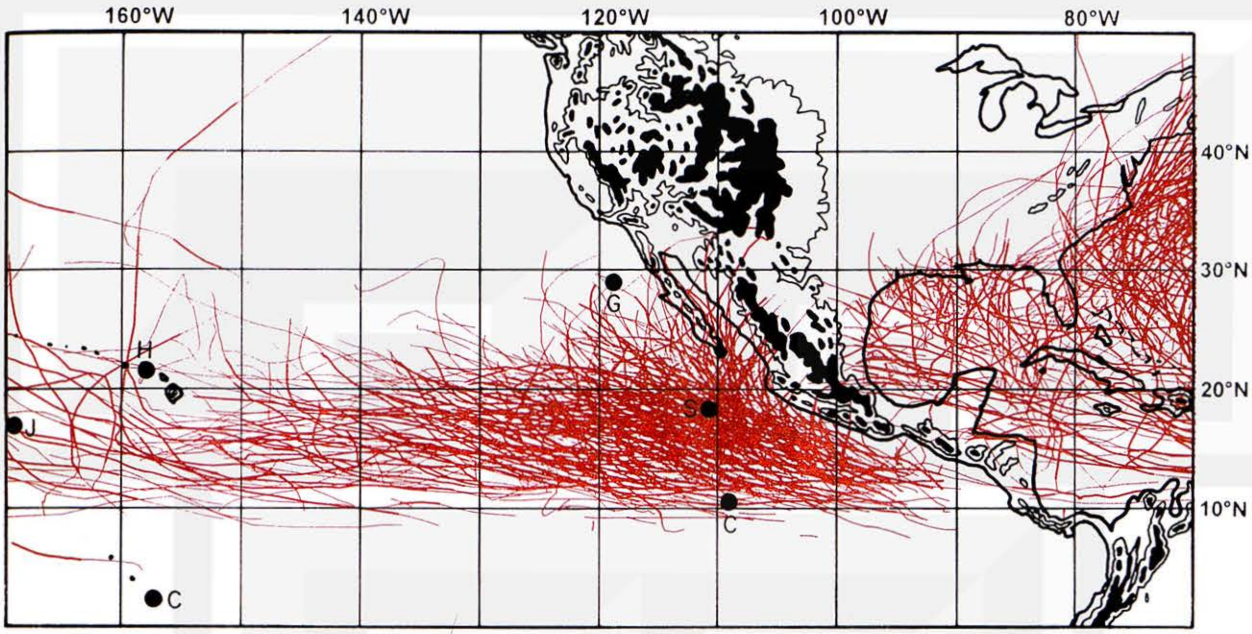

Fig. 3.34

1951-95

PPC (Period ABC) Area 3

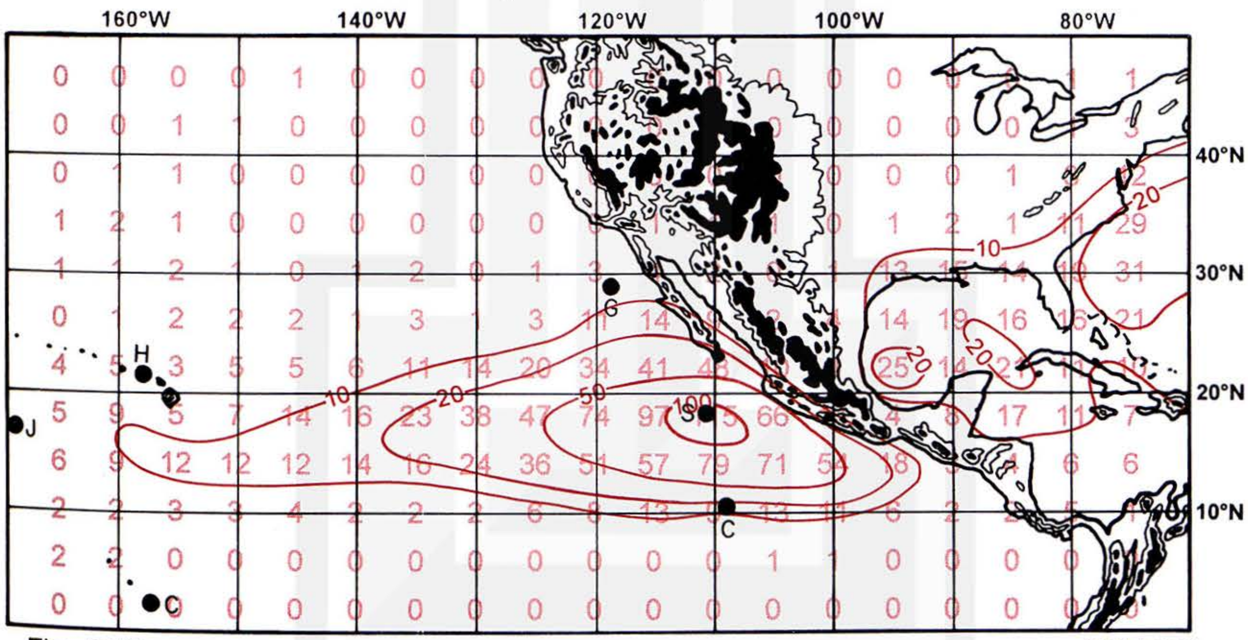

Fig. 3.35

1951-95

STORM PATHS (Period A) Area 4

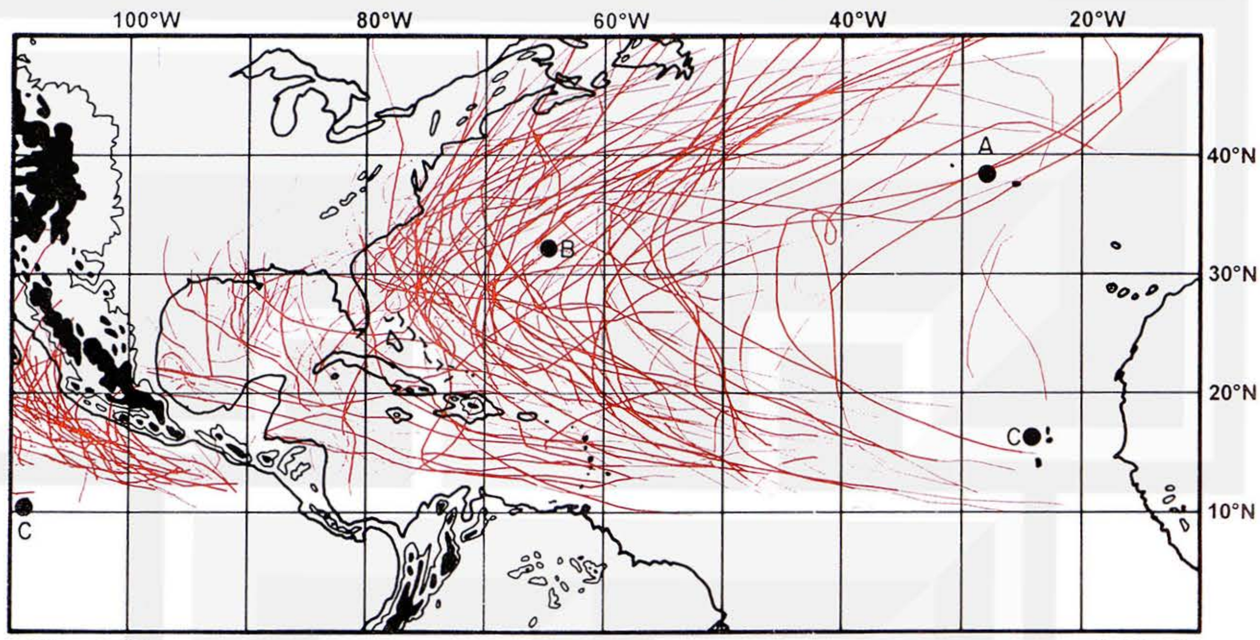

Fig. 3.36 1951-65

PPC (Period A) Area 4

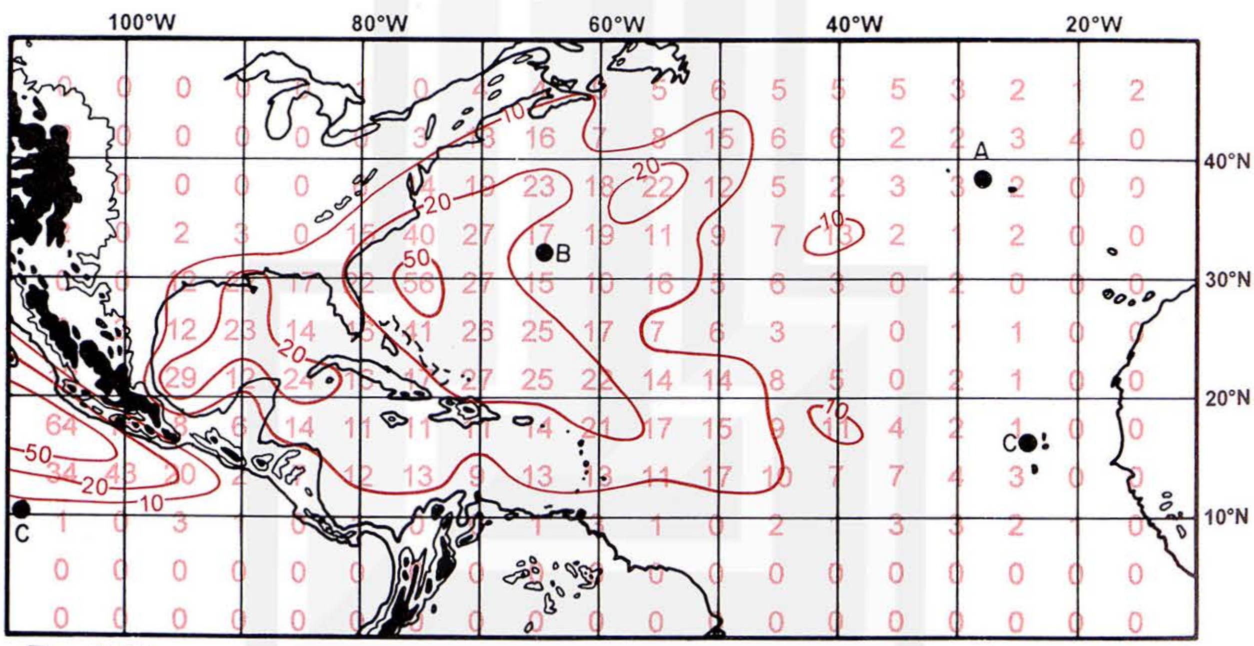

Fig. 3.37 1951-65

STORM PATHS (Period B) Area 4

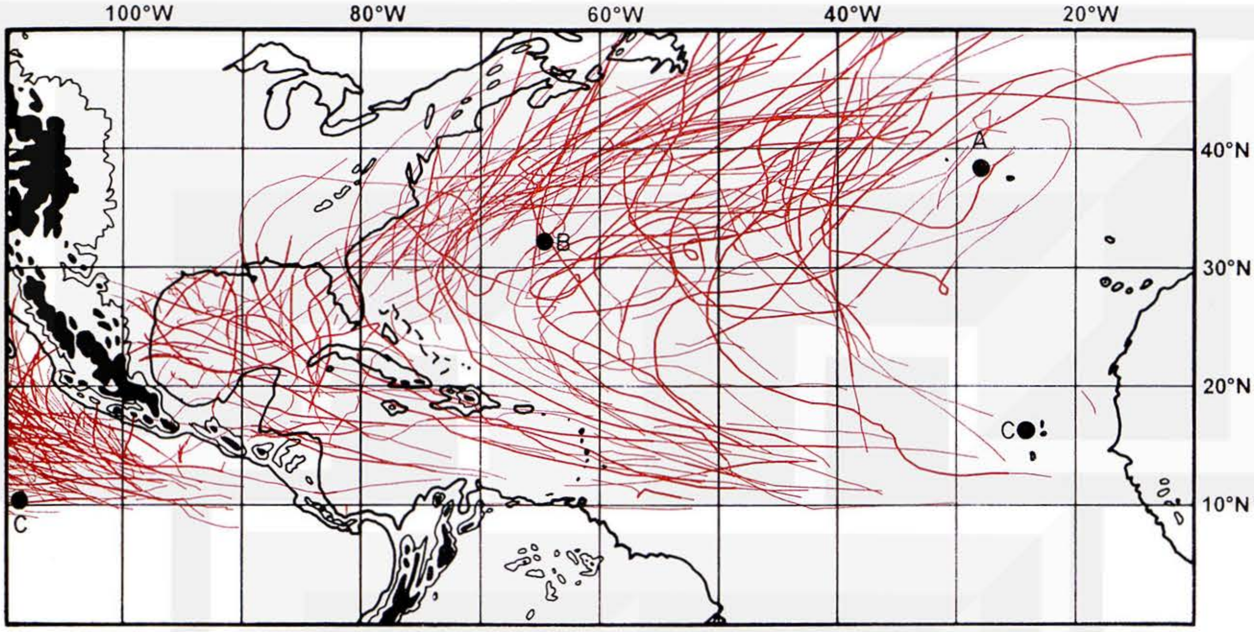

Fig. 3.38 1966-80

PPC (Period B) Area 4

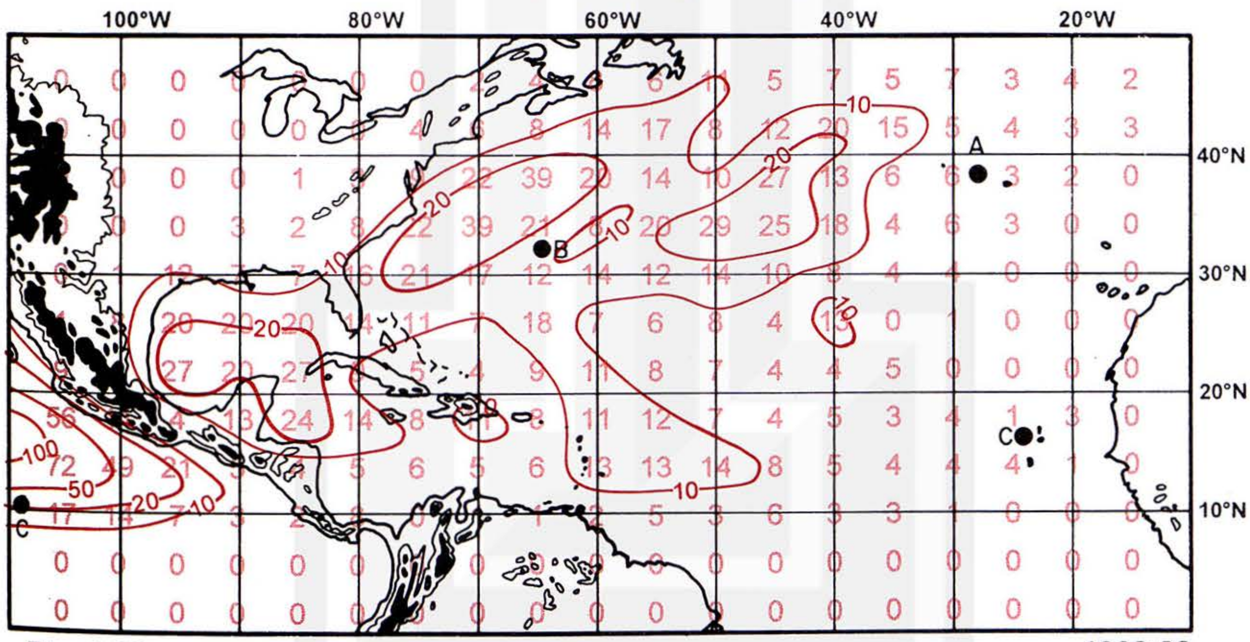

Fig. 3.39 1966-80

STORM PATHS (Period C) Area 4

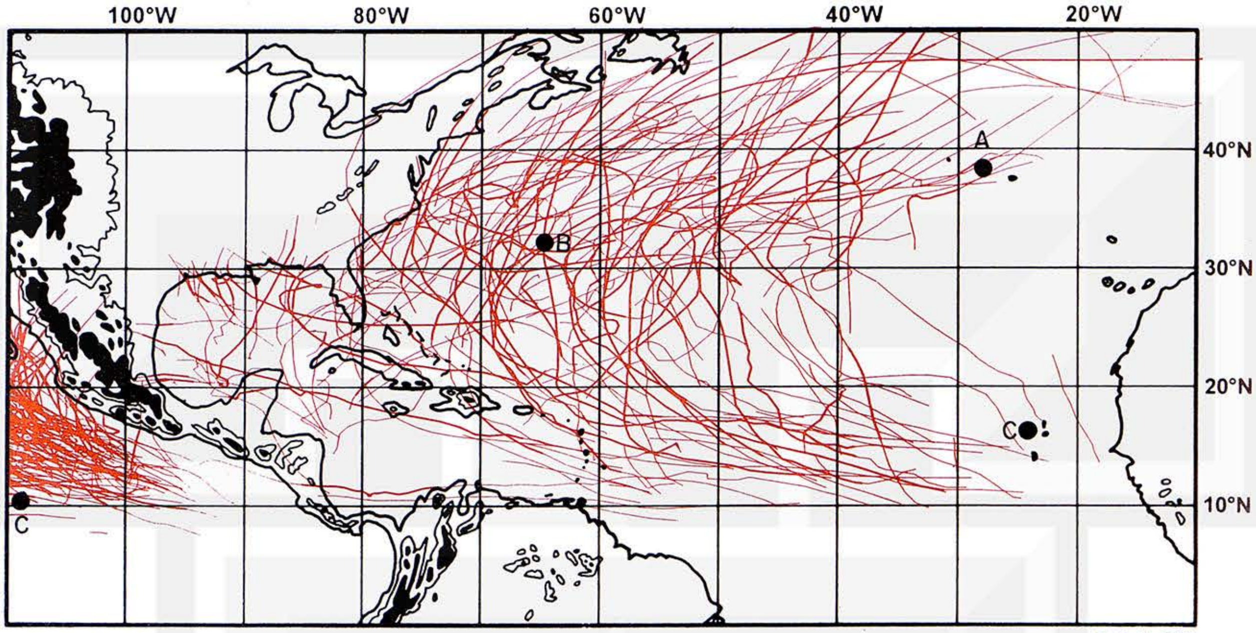

Fig. 3.40 1981-95

PPC (Period C) Area 4

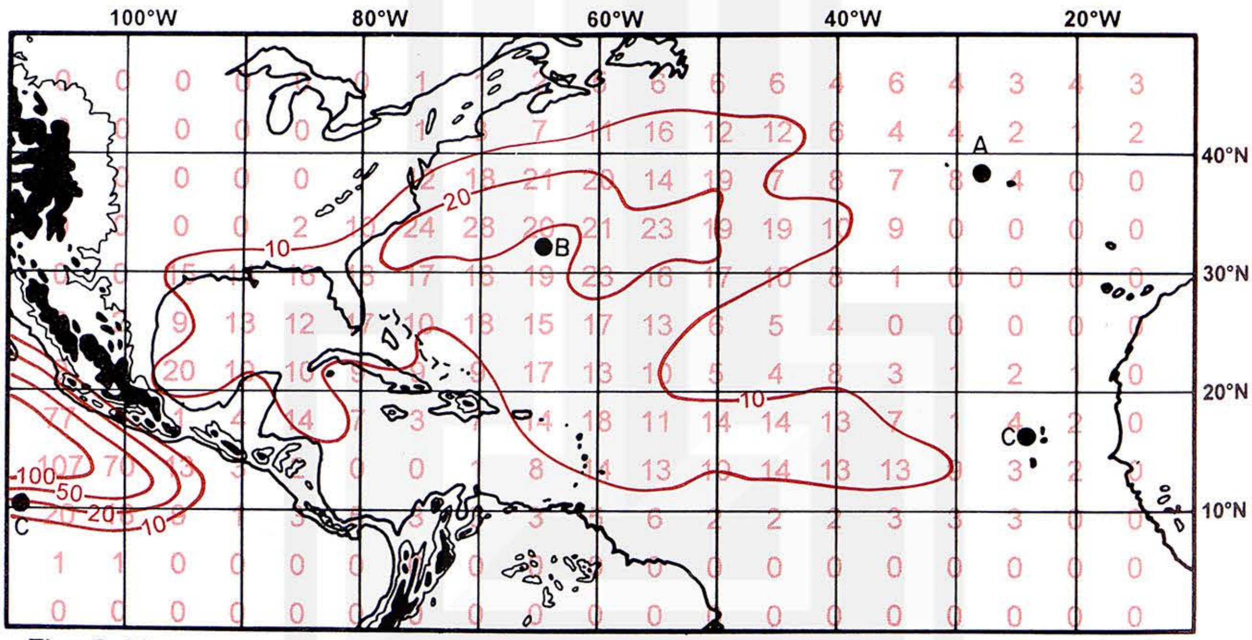

Fig. 3.41 1981-95

STORM PATHS (Period ABC) Area 4

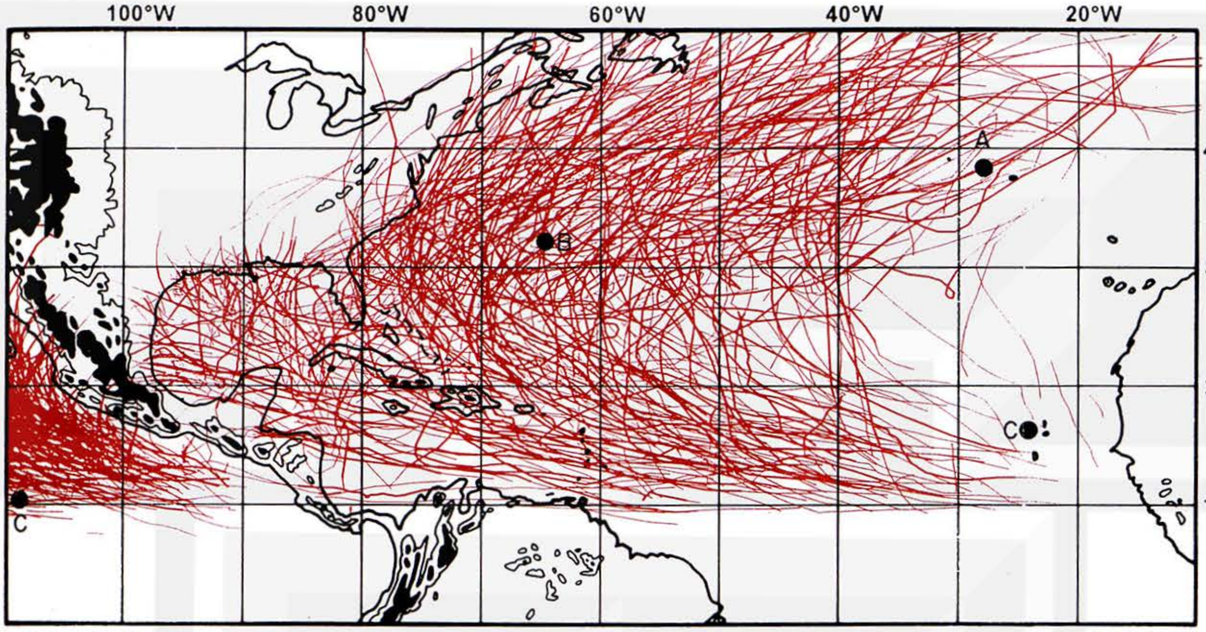

Fig. 3.42 1951-95

PPC (Period ABC) Area 4

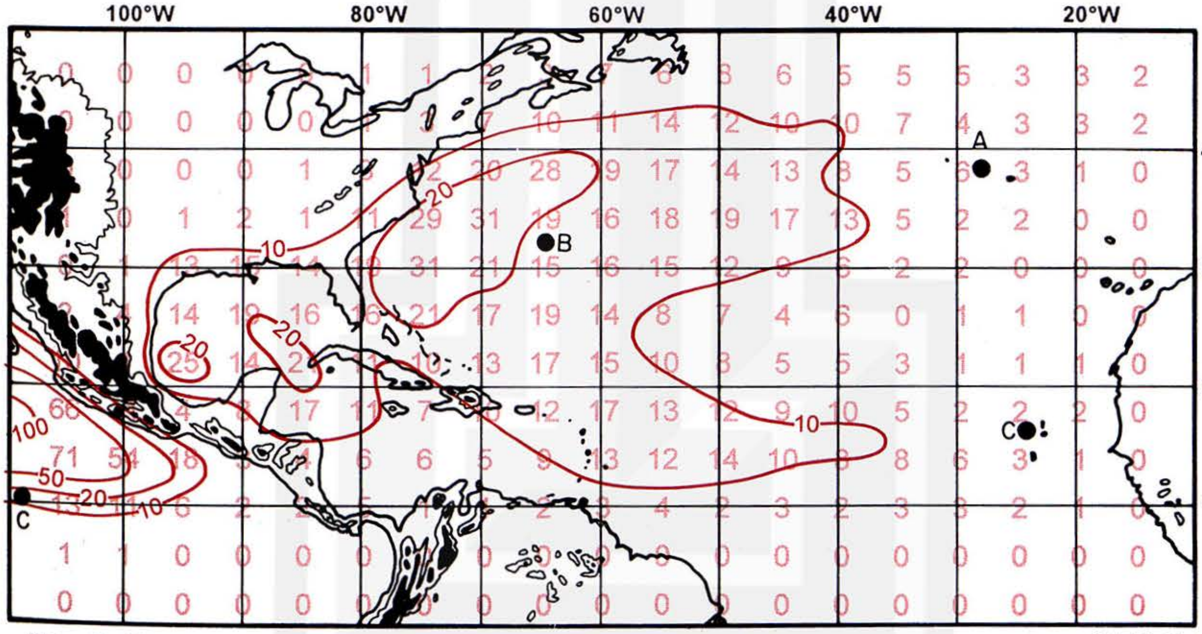

Fig. 3.43 1951-95

STORM PATHS (Period A) Area 5

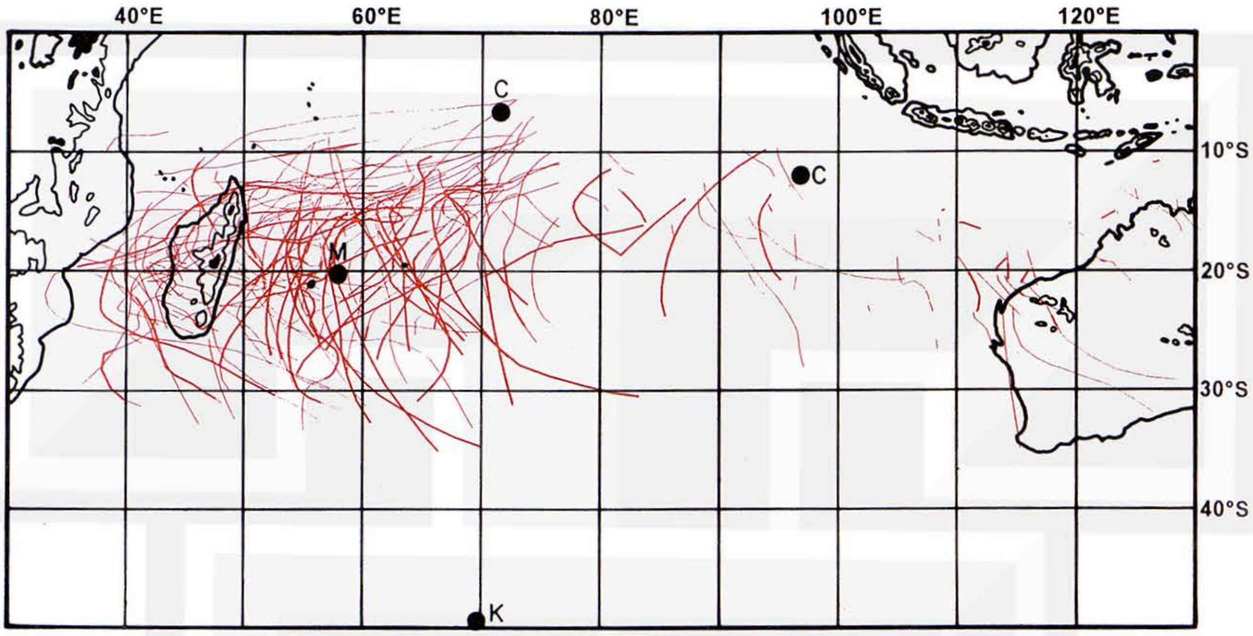

Fig. 3.44 1951-65

PPC (Period A) Area 5

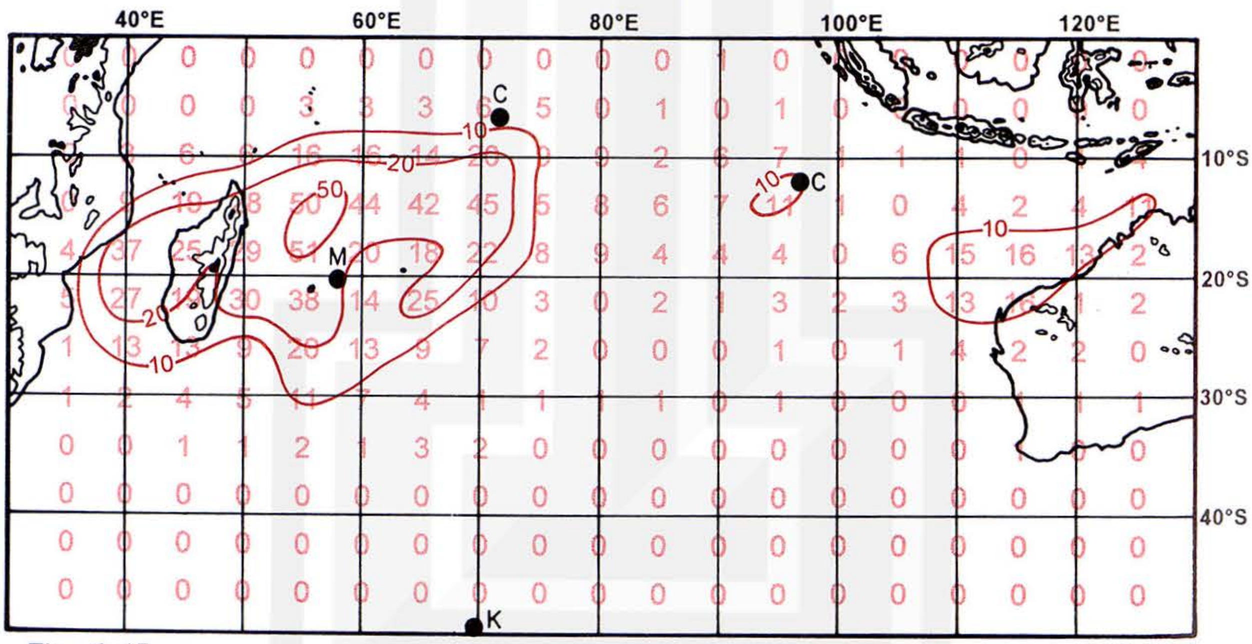

Fig. 3.45 1951-65

STORM PATHS (Period B) Area 5

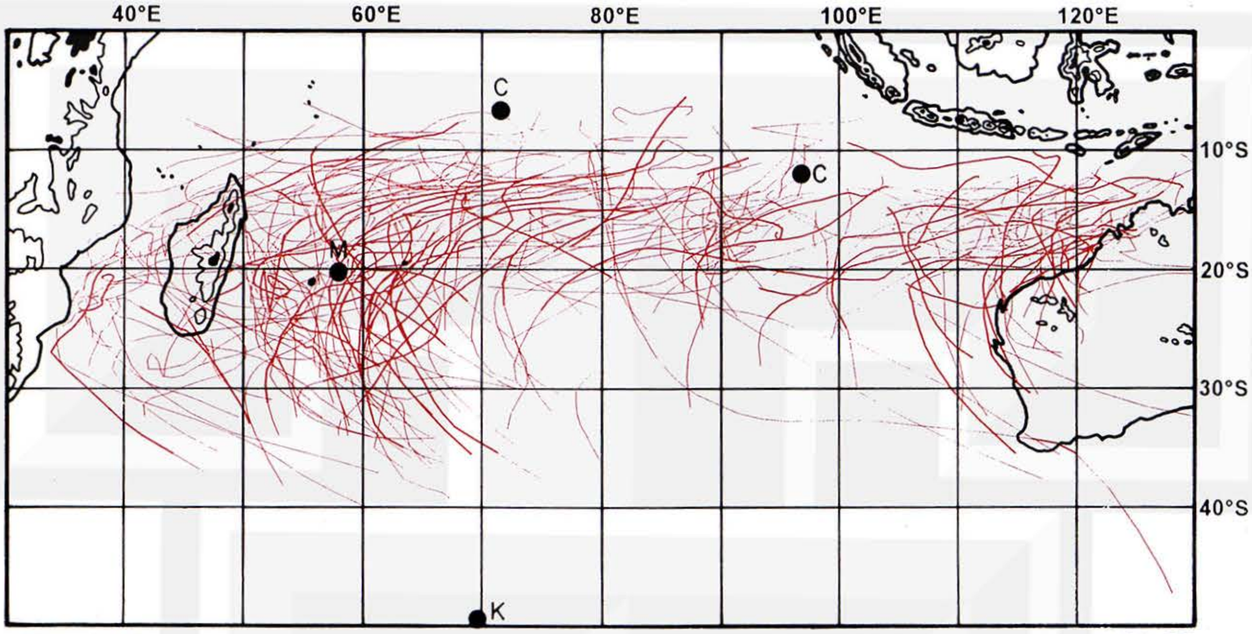

Fig. 3.46 1966-80

PPC (Period B) Area 5

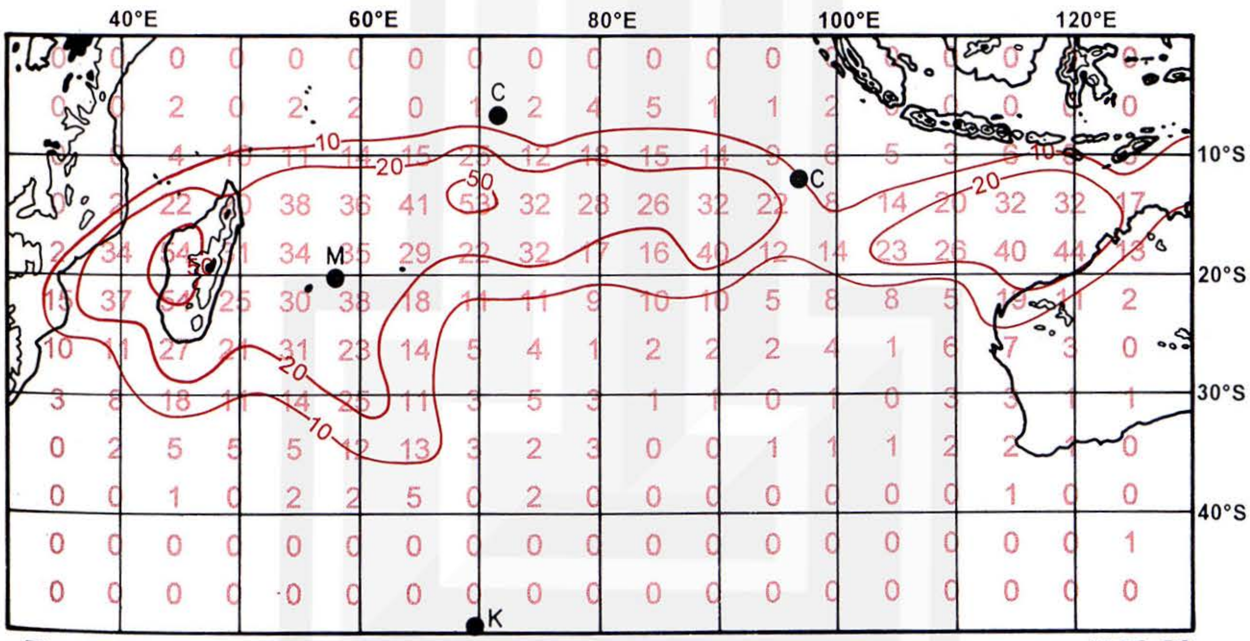

Fig. 3.47 1966-80

STORM PATHS (Period C) Area 5

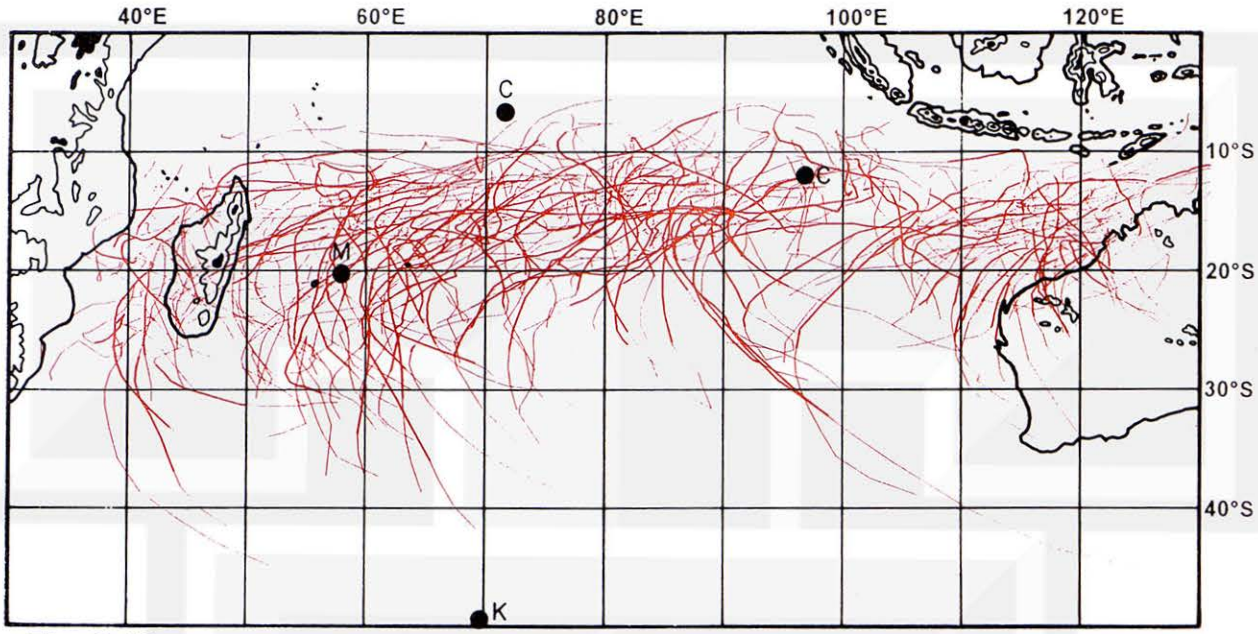

Fig. 3.48 1981-95

PPC (Period C) Area 5

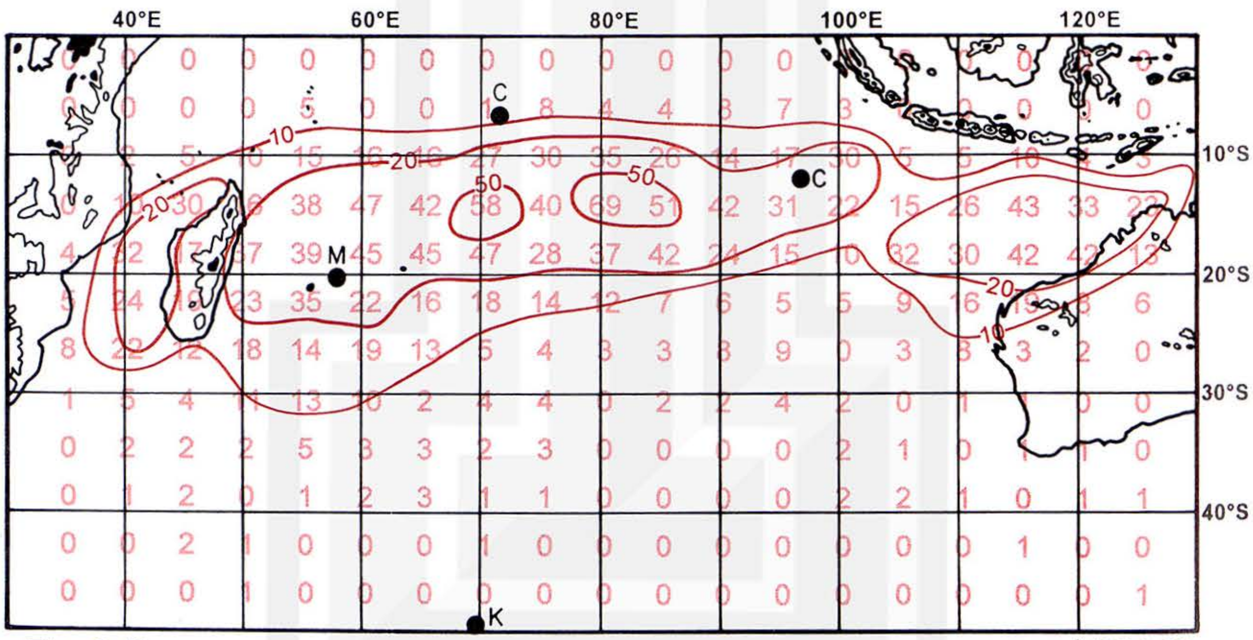

Fig. 3.49 1981-95

STORM PATHS (Period ABC) Area 5

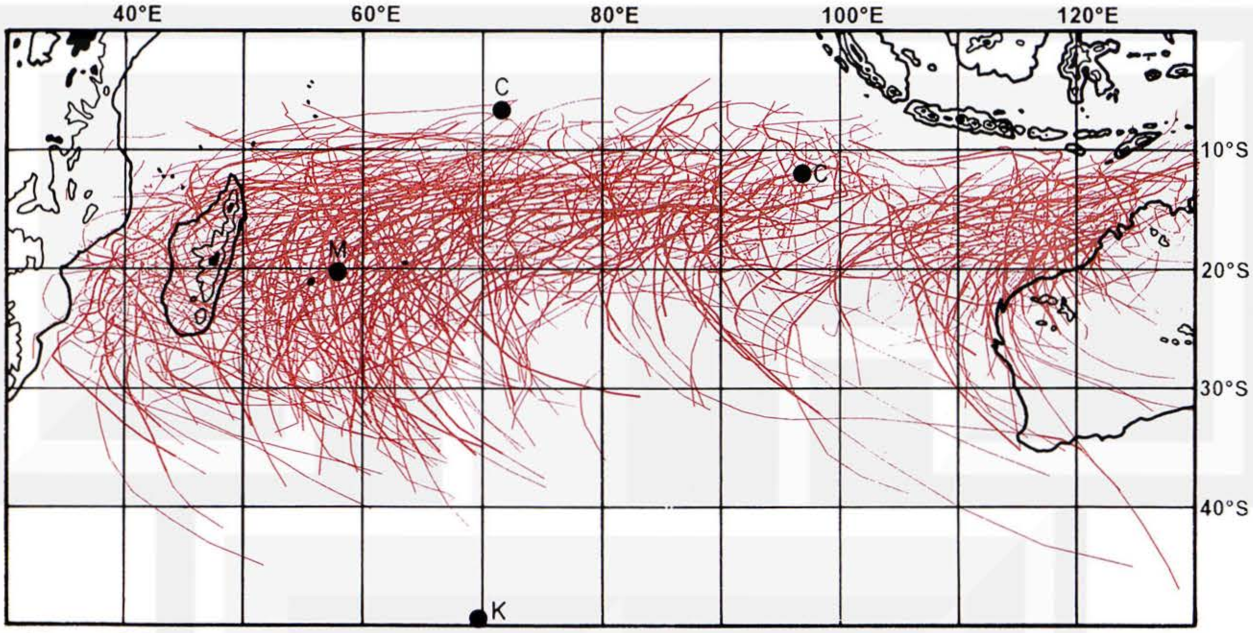

Fig. 3.50 1951-95

PPC (Period ABC) Area 5

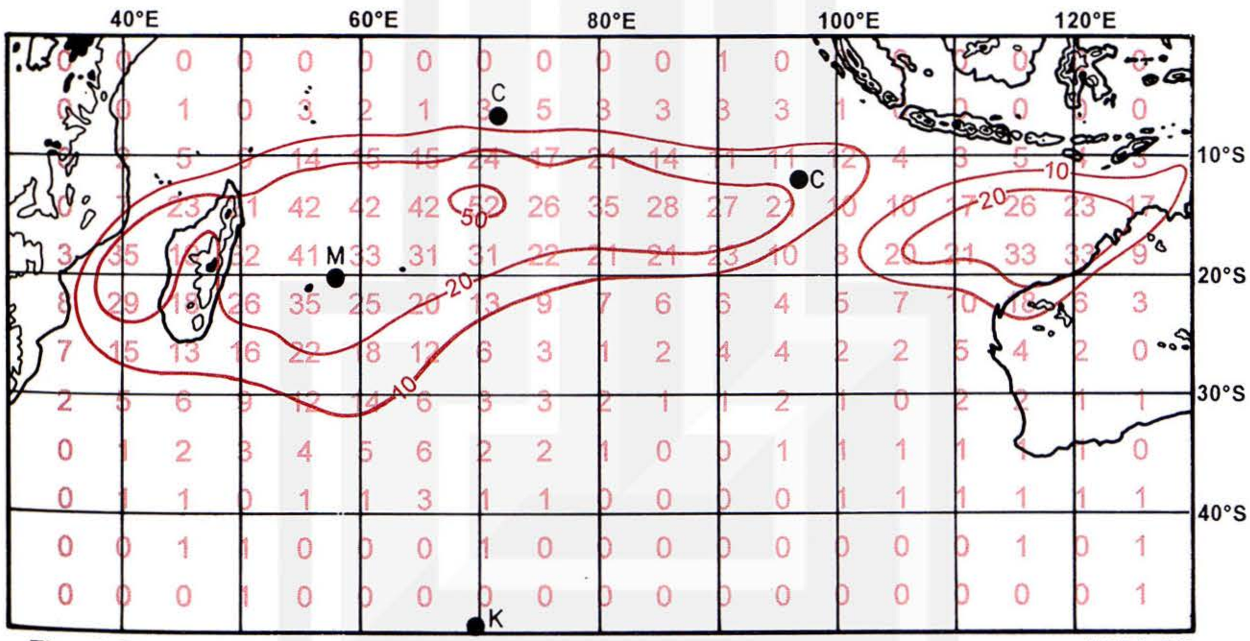

Fig. 3.51 1951-95

STORM PATHS (Period A) Area 6

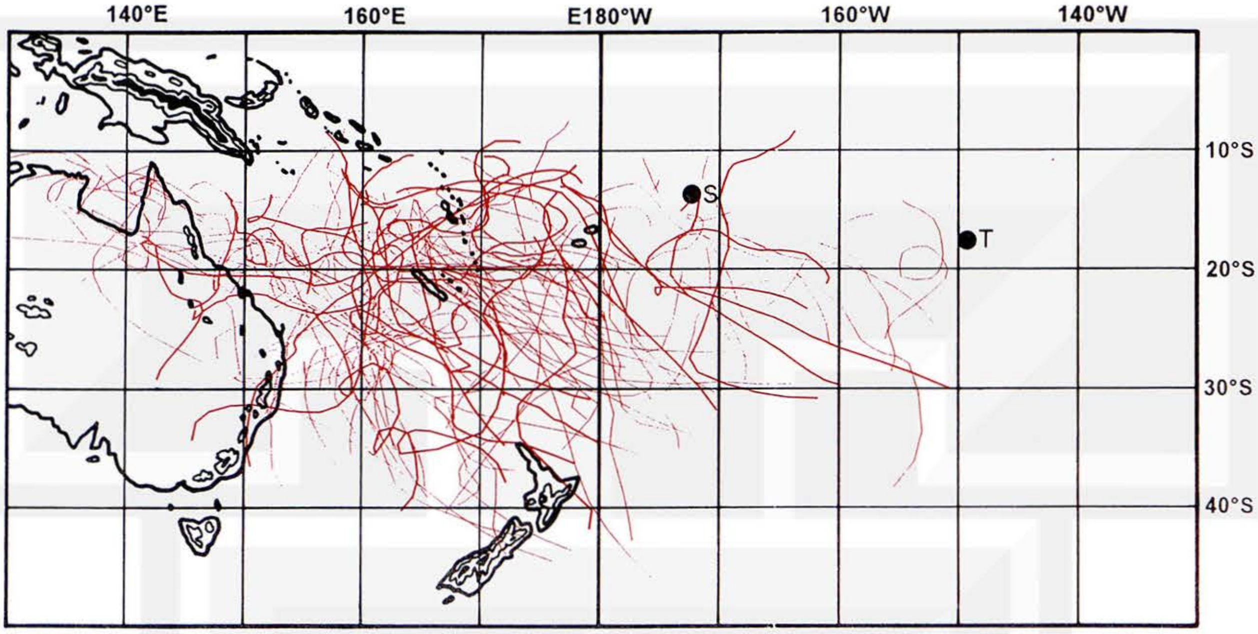

Fig. 3.52 1951-65

PPC (Period A) Area 6

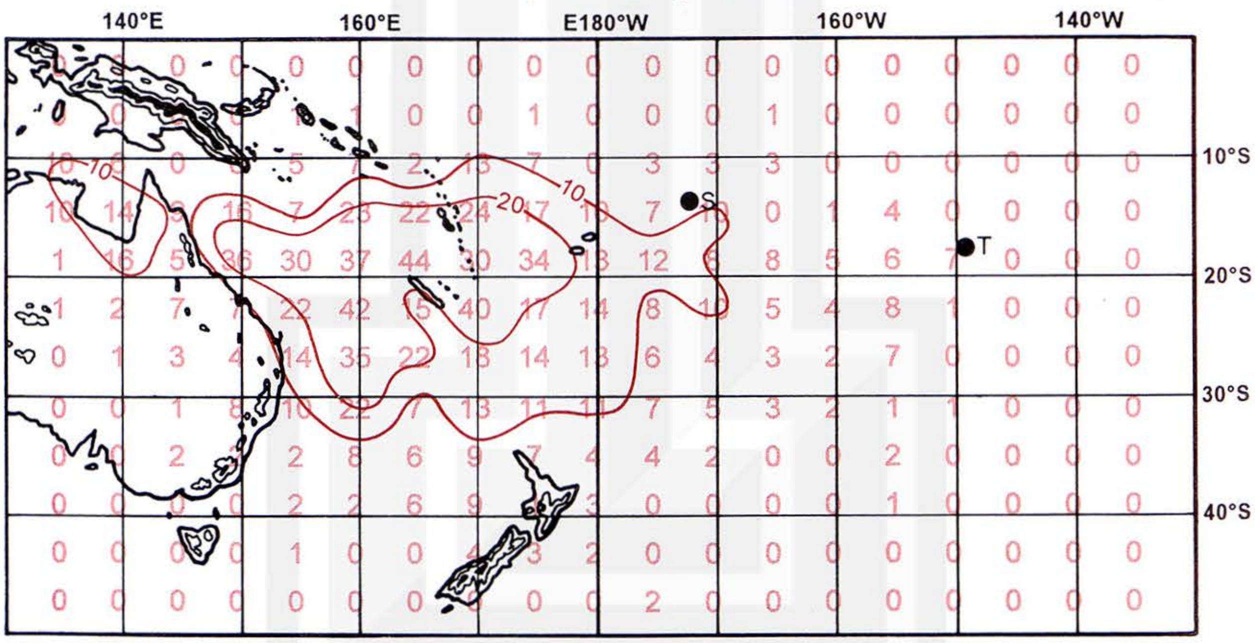

Fig. 3.53 1951-65

STORM PATHS (Period B) Area 6

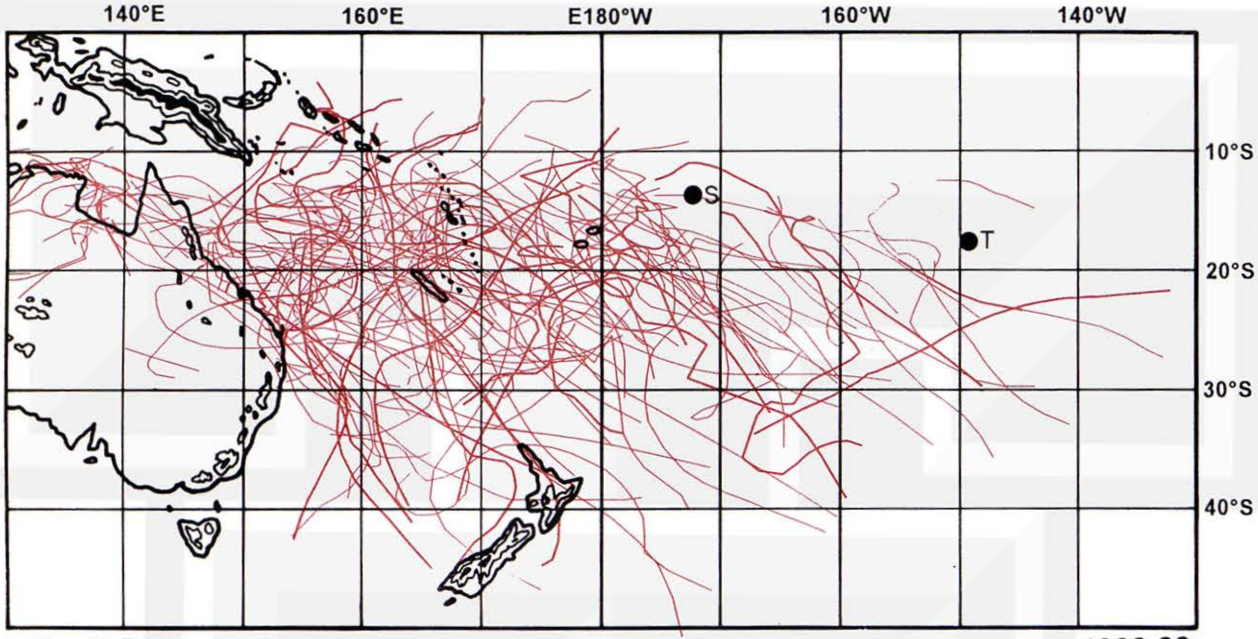

Fig. 3.54 1966-80

PPC (Period B) Area 6

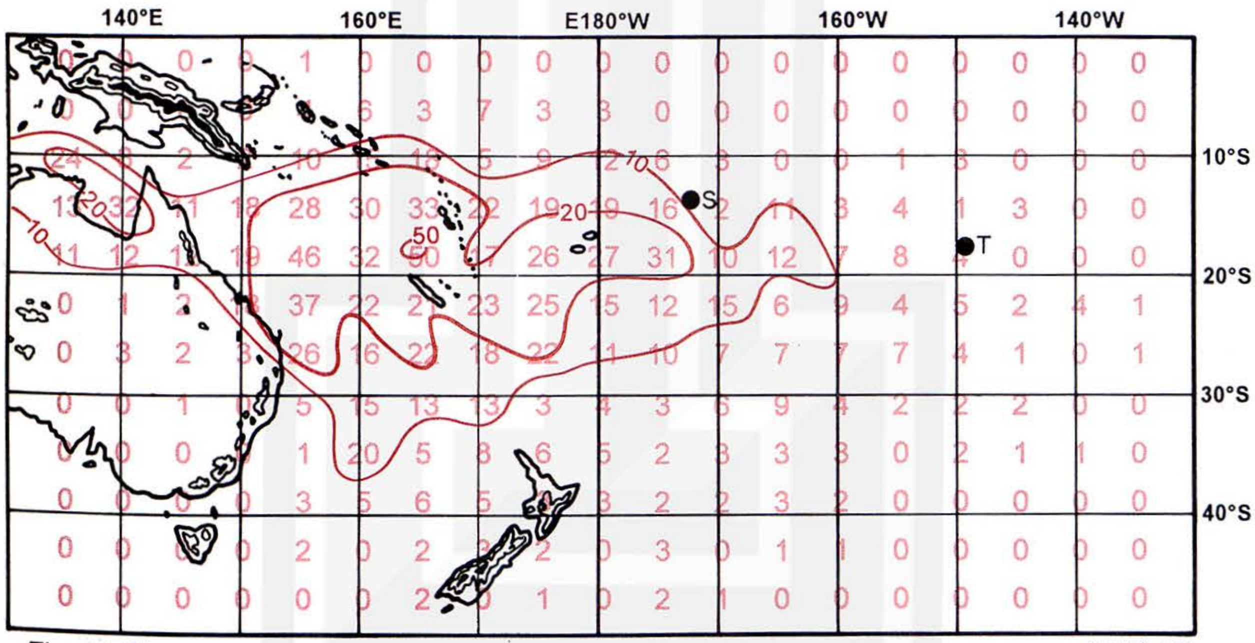

Fig. 3.55 1966-80

STORM PATHS (Period C) Area 6

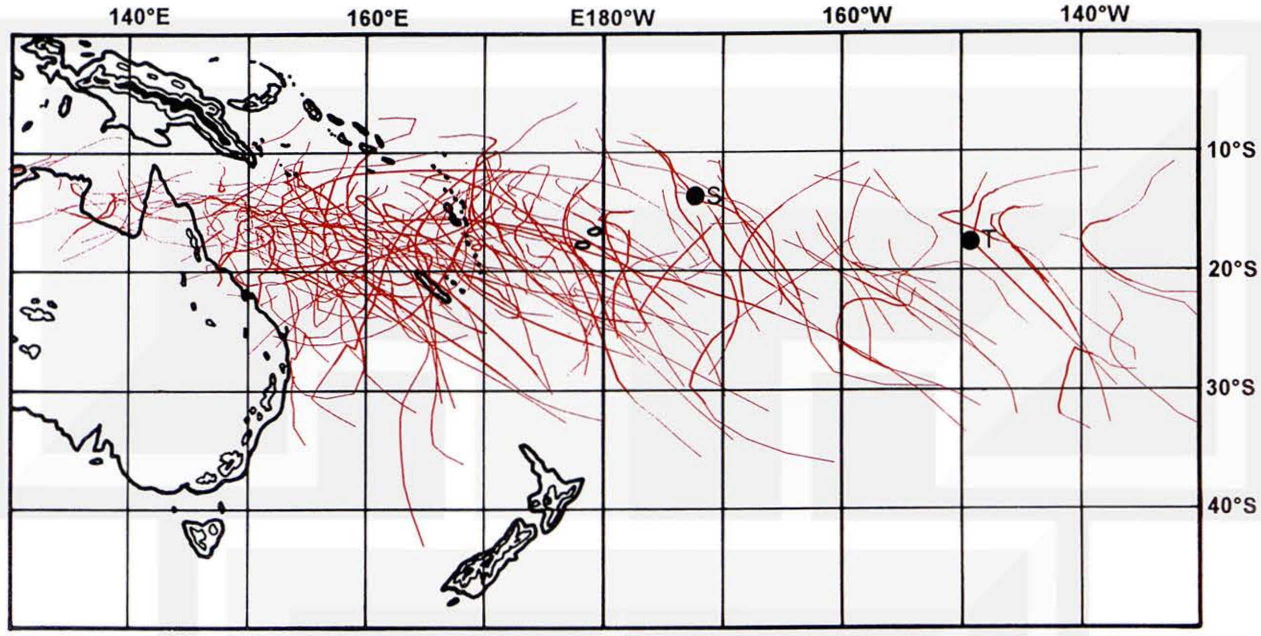

Fig. 3.56 1981-95

PPC (Period C) Area 6

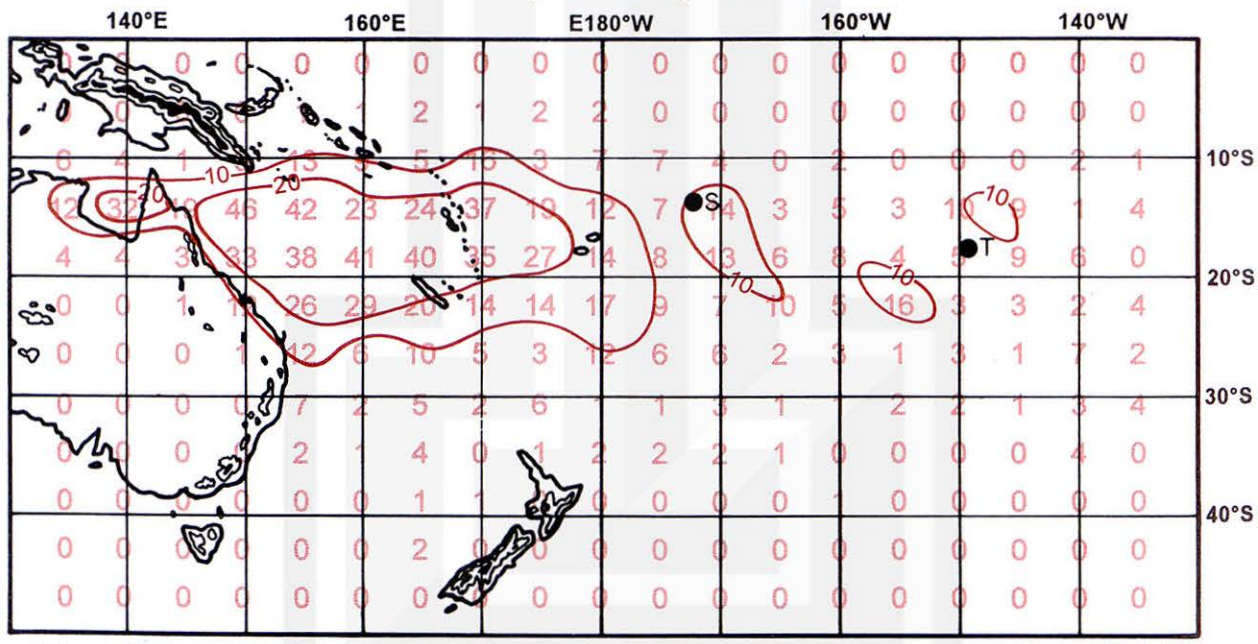

Fig. 3.57 1981-95

STORM PATHS (Period ABC) Area 6

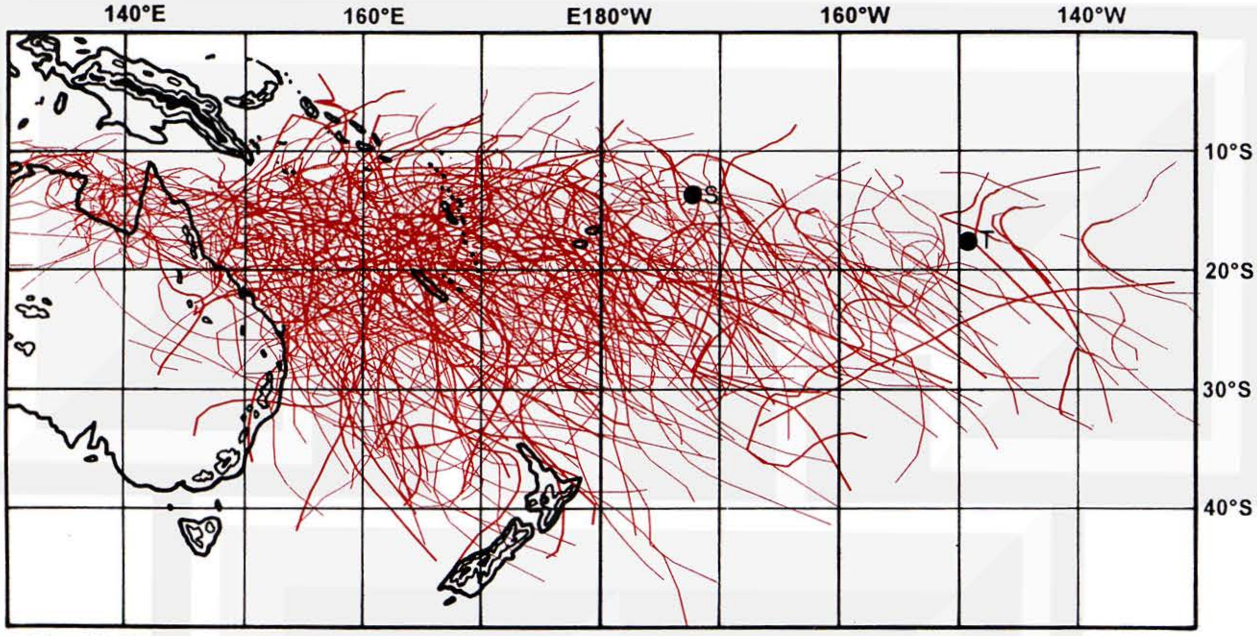

Fig. 3.58 1951-95

PPC (Period ABC) Area 6

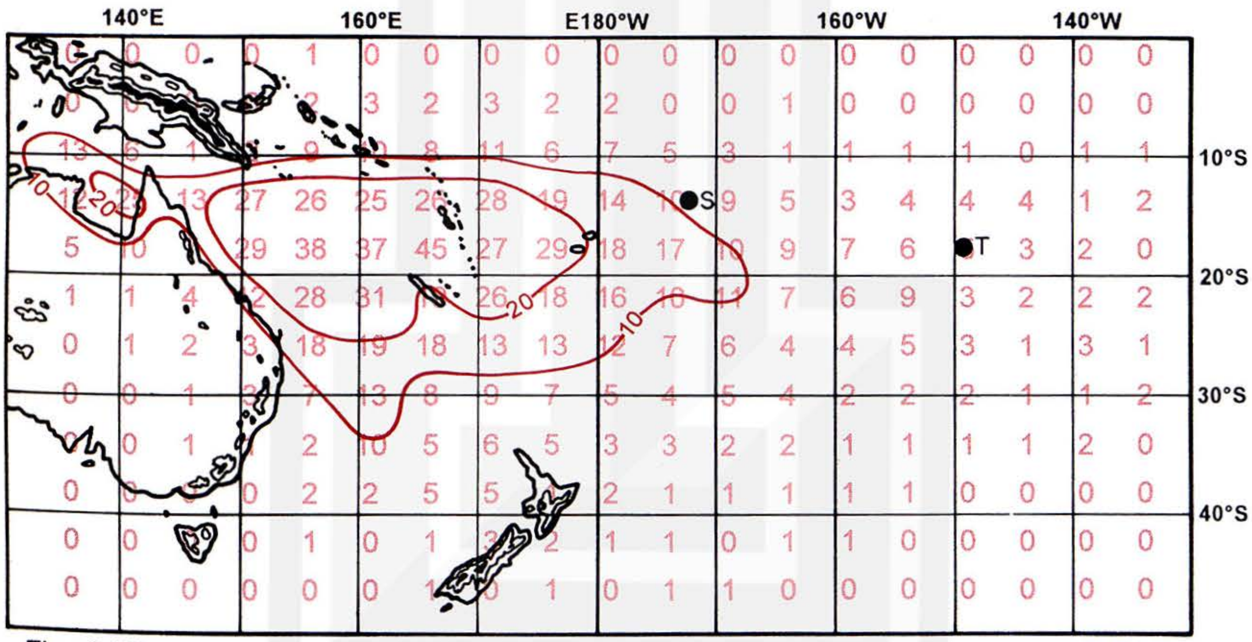

Fig. 3.59 1951-95

Chapter Four

Hurricane Hazard Indices

Introduction to Chapter Four

The PPC introduced in the previous chapter denotes the normalized density of storm positions. In order to assess the hazard imposed by the storms included in a specific PPC, it is necessary to take into consideration the destructive force of each storm included in the PPC. For this purpose, the Hazard Index (HI) for an individual storm was first defined as being the square of the windspeed ratio (WR), which is the storm's windspeed divided by 65 kts, the minimum windspeed of a hurricane. Thereafter, the Hurricane Hazard Index (HHI) was computed by adding up each position count weighted by Hazard Index (HI).

The HHI, thus computed, denotes the hazard induced by the PPC storms. In reality, however, the most destructive storm of PPC storms will induce a Maximum Hazard. Thus, the Maximum Hazard Index (MHI) denotes the worst hazard imposed by the most intense storm, and is taken from a single position count having the highest Hazard Index (HI). The MHI was found to be a better measure of hazard based on storm intensity, as the HHI heavily incorporates storm position recurrence resulting in analyses similar to those of PPC.

Produced in this chapter are MHI maps of the six local areas during the 45 storm years, 1951-95. It is of interest to find that the highest MHI in Area 1, 4.7 in North Indian Ocean, is located at the mouth of the Ganges River, while that of Area 2, 6.5 in North Atlantic Ocean, is at the mouth of the Mississippi River. MHI is clearly useful in determining the most dangerous storm areas around the world.

4.1 Principal of the Hazard Index (HI)

Tornado hazard is commonly expressed by the fastest ¼ mile wind used in the F-scale windspeed. By virtue of the large horizontal dimensions of hurricane winds, their speeds are expressed by the sustained windspeed averaged over a one-minute period.

In this atlas, the Windspeed Ratio (WR) denotes the ratio of the sustained windspeed divided by 65 knots, the lowest hurricane windspeed. Because the force of storm wind is proportional to the square of the windspeed, the Hazard Index (HI) is defined by the square of the windspeed ratio of an individual storm. The following table shows the WR and HI of storms with windspeeds between 35 kts and 200 kts.

	kts	mph	m/s	WR	HI
Tropical Storm	35-64	40-70	18-33	0.54-0.99	0.29-0.99
Hurricane	65	75	34	1.00	1.00
"	80	92	41	1.23	1.52
"	100	115	51	1.54	2.37
"	120	138	62	1.85	3.41
"	140	161	72	2.15	4.64
"	160	184	82	2.46	6.06
"	180	207	93	2.77	7.67
"	200	230	103	3.08	9.47

Table 4.1 Hazard Index (HI) computed as a function of storm windspeed ranging between 35 and 200 kts. The maximum sustained windspeed of hurricanes is approximately 180 kts.

4.2 Hurricane Hazard Index (HHI)

As explained in Chapter 3, position count is the simple count of 6-hourly positions of the storm centers irrespective of the storm windspeed at each position. In order to determine the storm hazard inside the latitude-longitude box in which 6-hourly positions are located, it is necessary to count the positions weighted by the wind force of the storm at each position inside the box. Thus the Hurricane Hazard Index (HHI) denotes the non-dimensional quantity defined by

$$HHI = (HI)_1 + (HI)_2 + (HI)_3 + \ldots\ldots\ (HI)_{PC}$$

where 1, 2, 3, etc., are individual 6-hourly positions inside the latitude-longitude box and PC, the last position counted. HHI is therefore a cumulative hazard index that largely incorporates PPC, resulting in analyses similar to those of PPC as seen below.

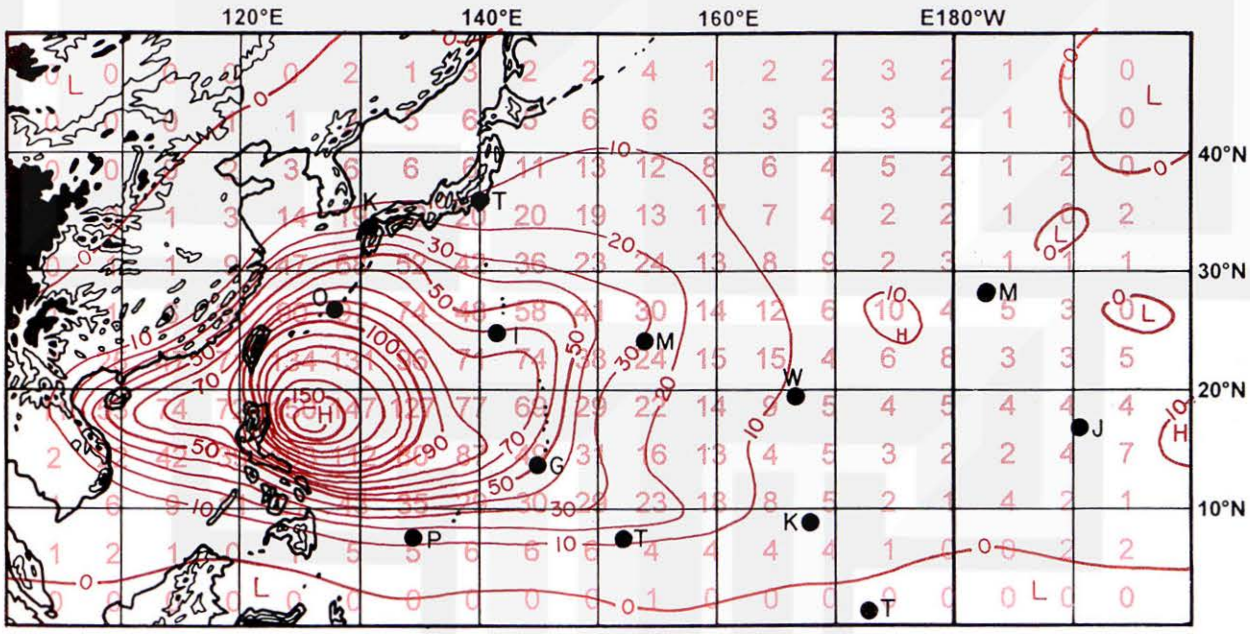

Fig. 4.1 An example of an HHI analysis mapping of Area 2, Western Pacific for the 45-year period 1951-95 storm years. The map shows a peak HHI of 150 just to the east of the Philippines.

4.3 Maximum Hazard Index (MHI)

Maximum Hazard Index (MHI), denoting the highest degree of hazard imposed by the most intense storm, is derived from a single 6-hourly position and is defined as the highest value of Hazard Index (HI) in a specific latitude-longitude box during a specific statistical period. Presented on the following pages 66 through 71 are maps of Maximum Hazard Index based on the 45-year period 1951-95 storm years for each of the six local areas, along with storm path maps for comparison. In contrast to HHI, note that MHI analyses deviate more from those of PPC. Plotted data values (in green) are 10 times that of actual computed values (i.e. a computed value of 5.2 is plotted as 52).

4.3 Maximum Hazard Index (MHI)

STORM PATHS (45-Yr Period) Area 1

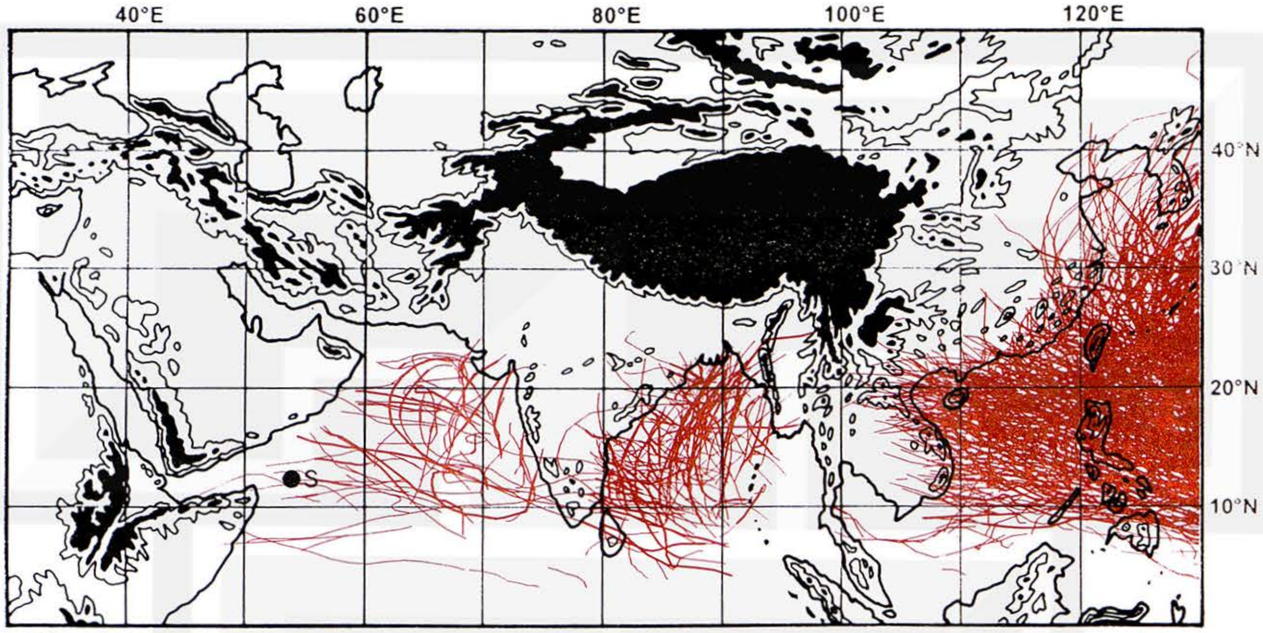

Fig. 4.2 1951-95

MAXIMUM HAZARD INDEX (MHI) (45-Yr Period) Area 1

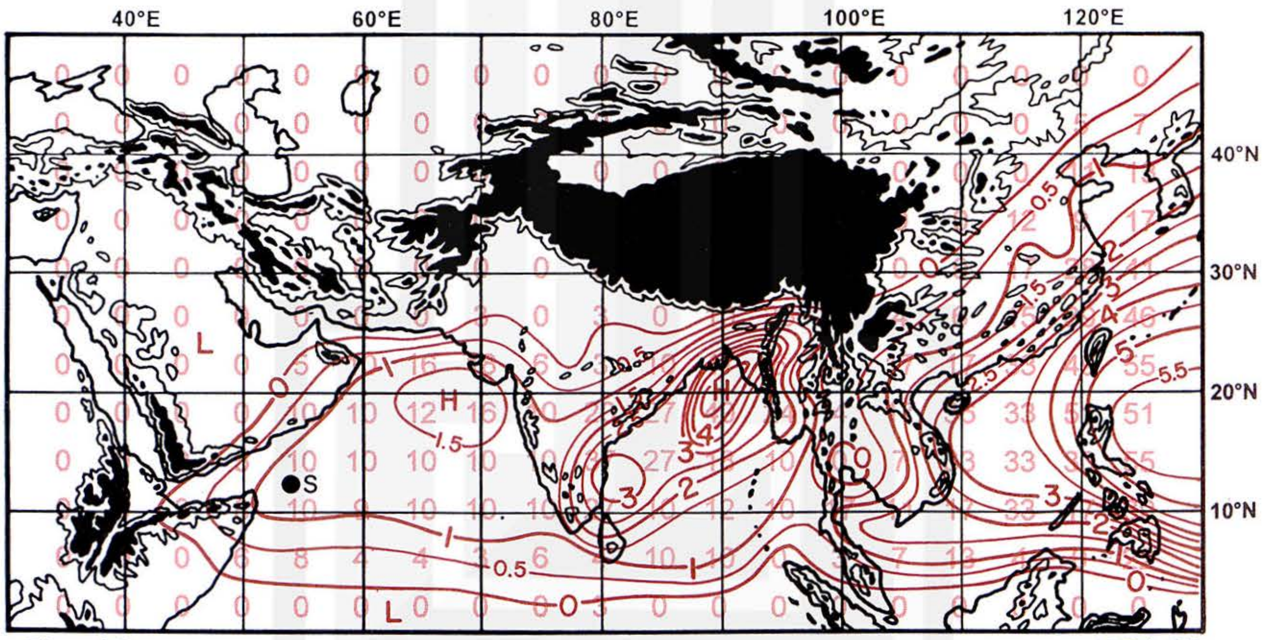

Fig. 4.3 1951-95

STORM PATHS (45-Yr Period) Area 2

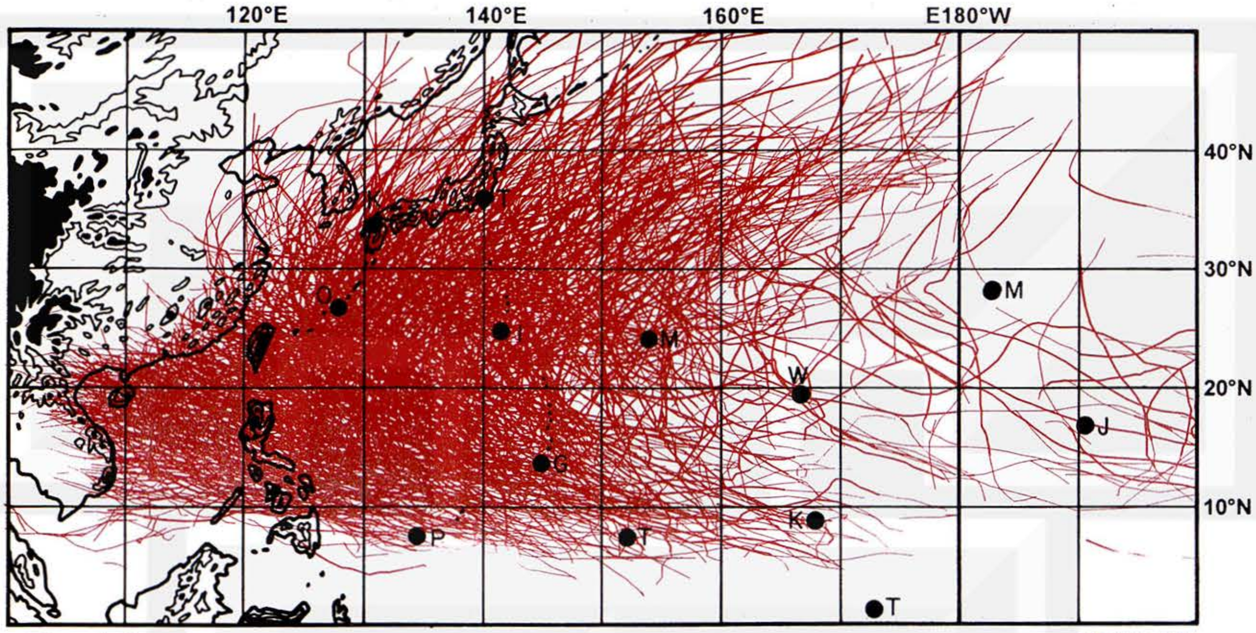

Fig. 4.4 1951-95

MAXIMUM HAZARD INDEX (MHI) (45-Yr Period) Area 2

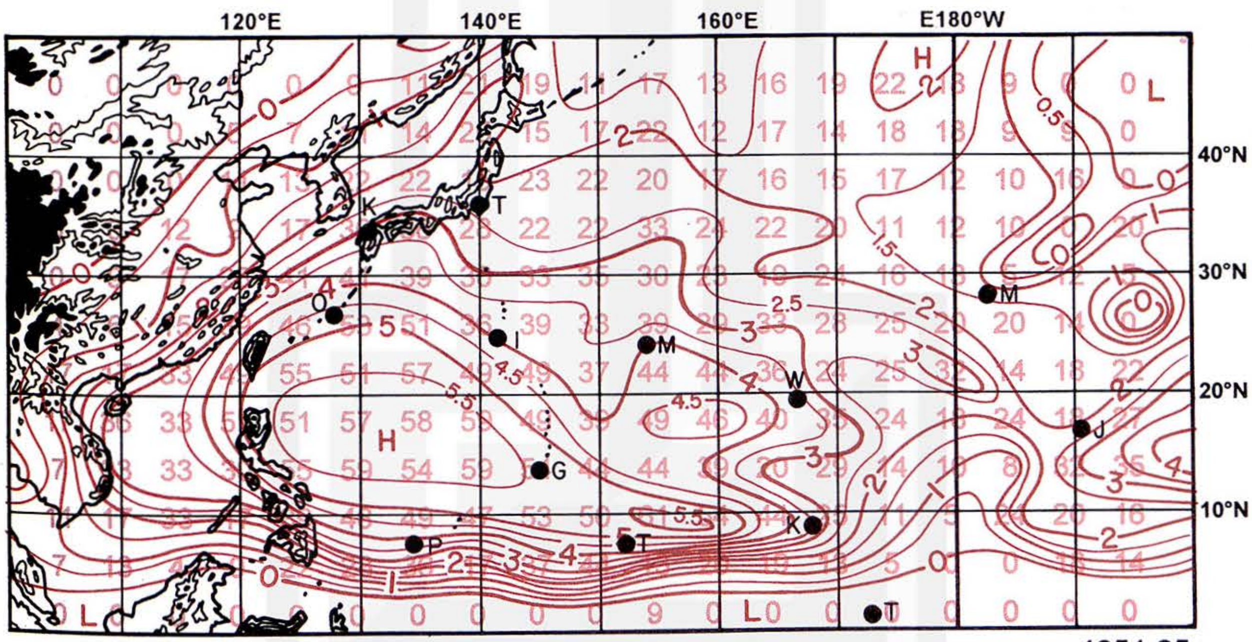

Fig. 4.5 1951-95

STORM PATHS (45-Yr Period) Area 3

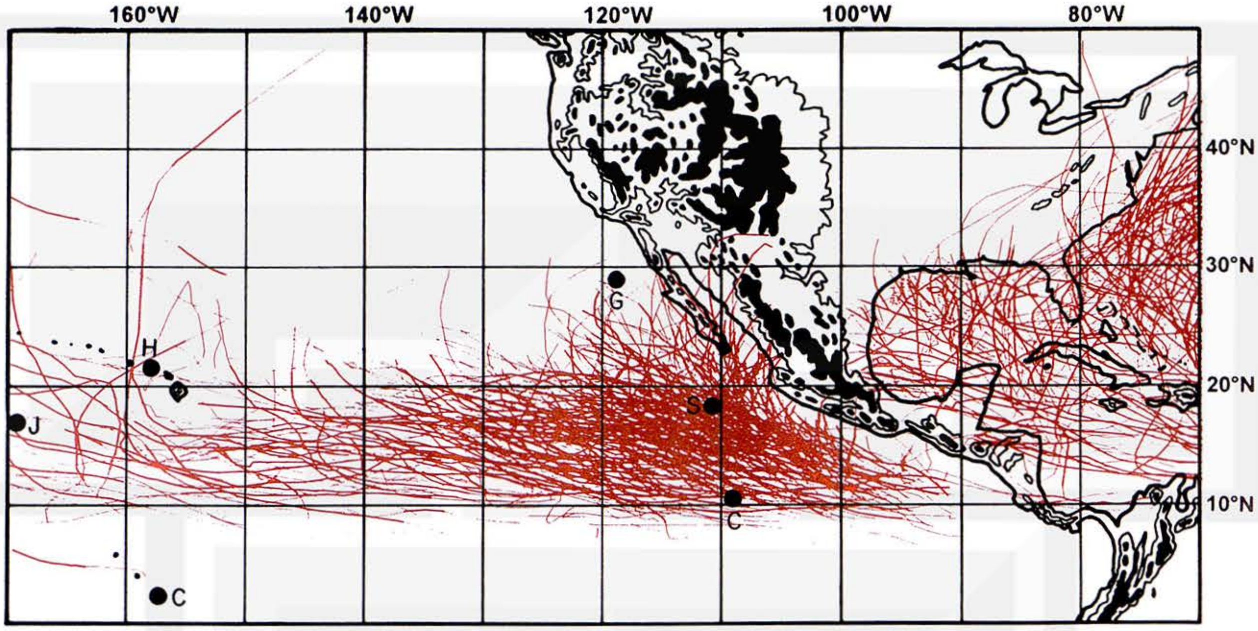

Fig. 4.6 1951-95

MAXIMUM HAZARD INDEX (MHI) (45-Yr Period) Area 3

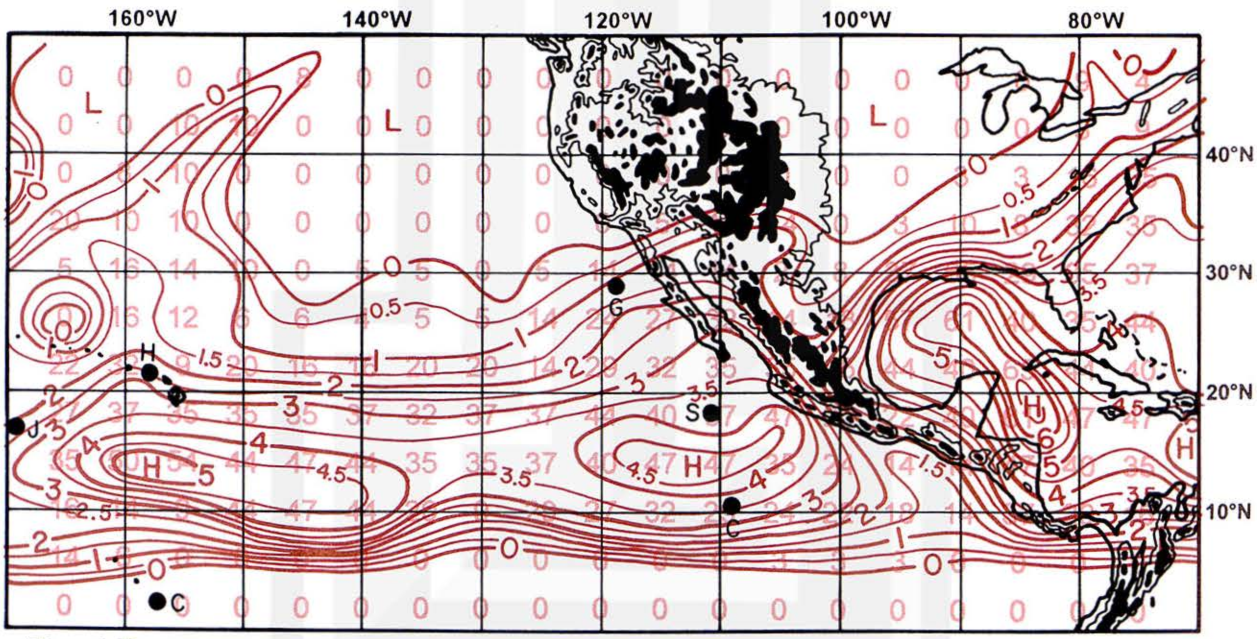

Fig. 4.7 1951-95

STORM PATHS (45-Yr Period) Area 4

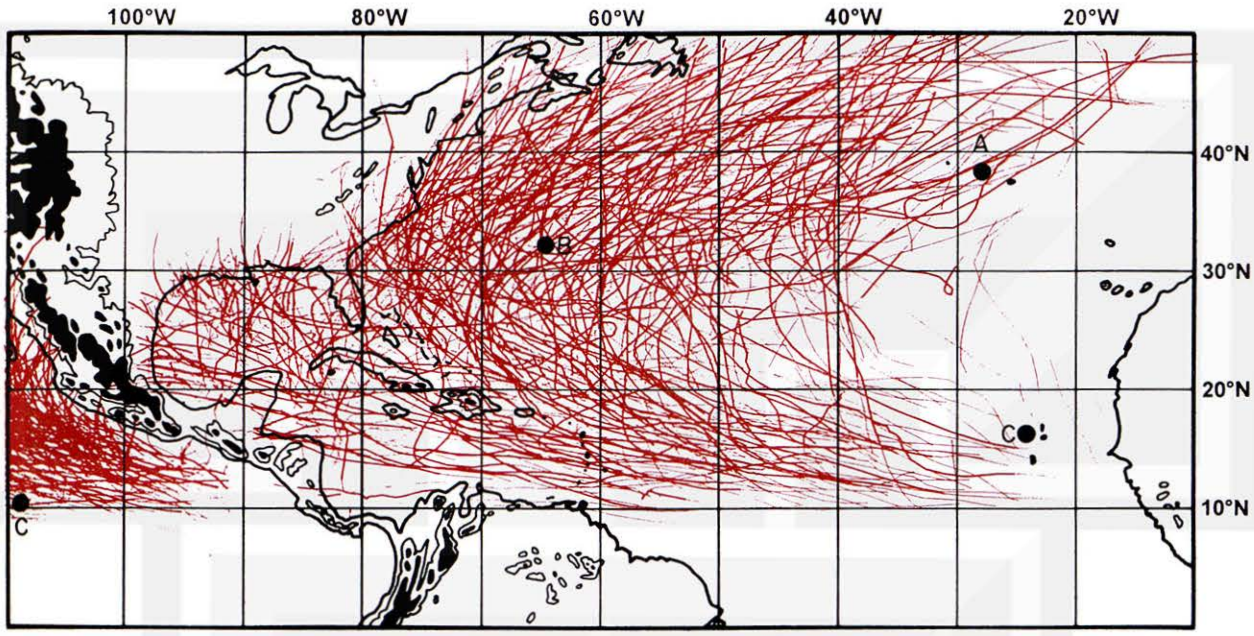

Fig. 4.8 1951-95

MAXIMUM HAZARD INDEX (MHI) (45-Yr Period) Area 4

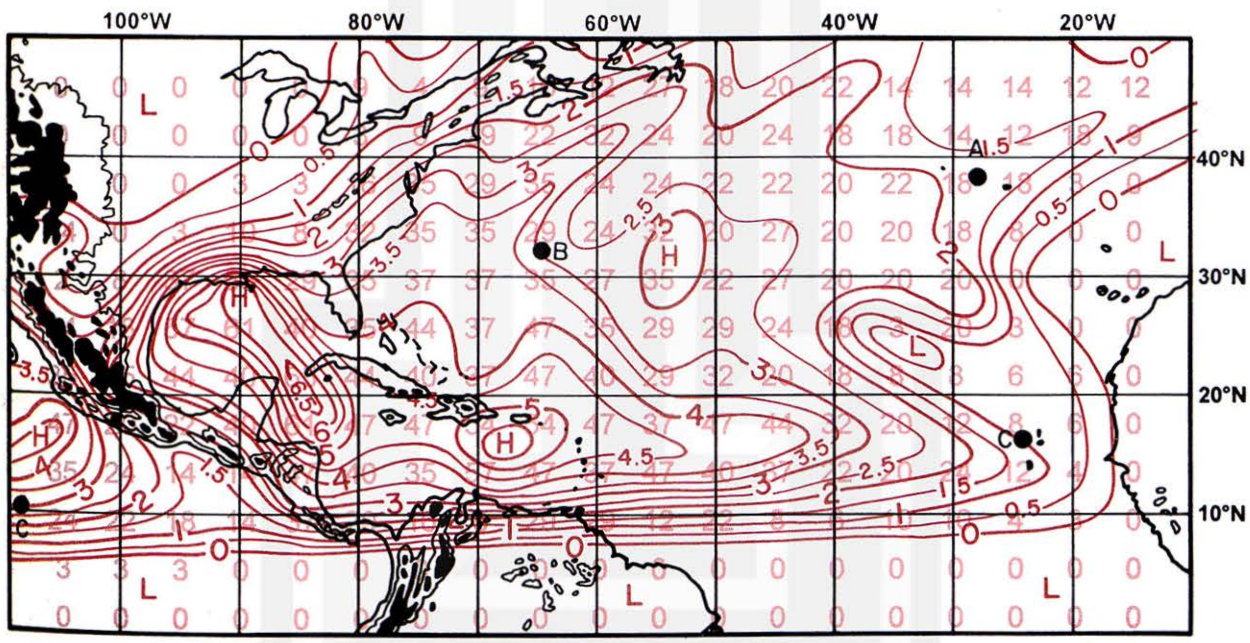

Fig. 4.9 1951-95

4.3 Maximum Hazard Index (MHI)

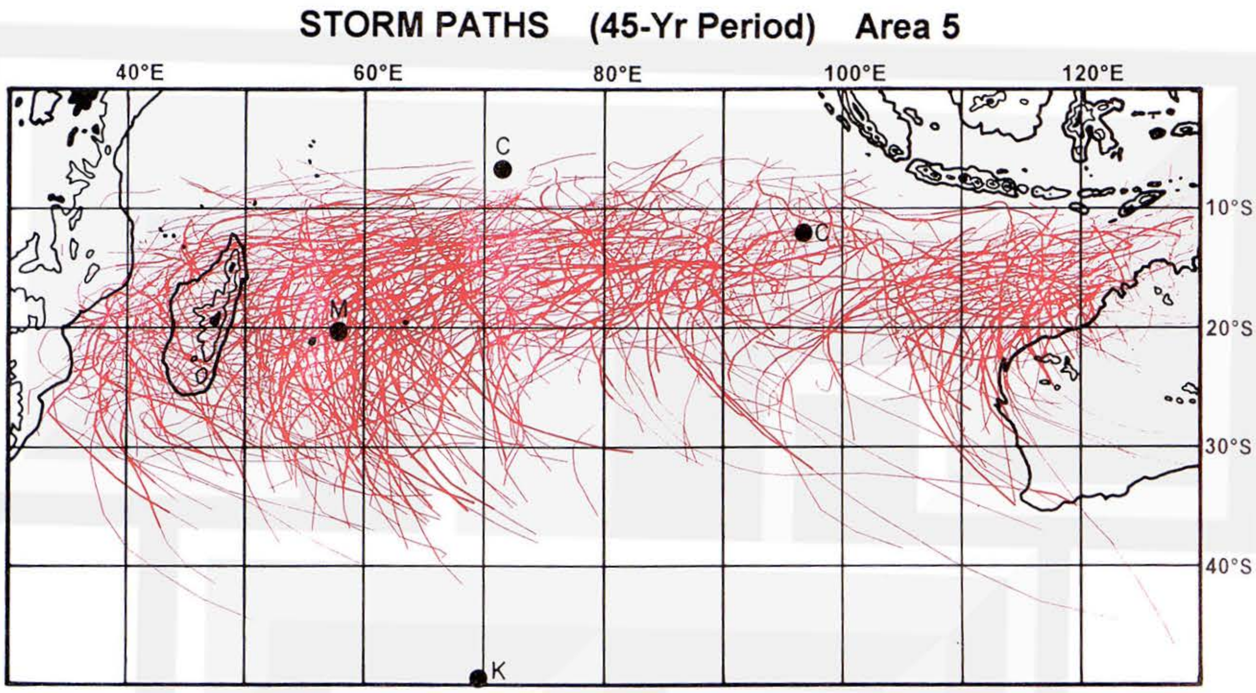

Fig. 4.10 1951-95

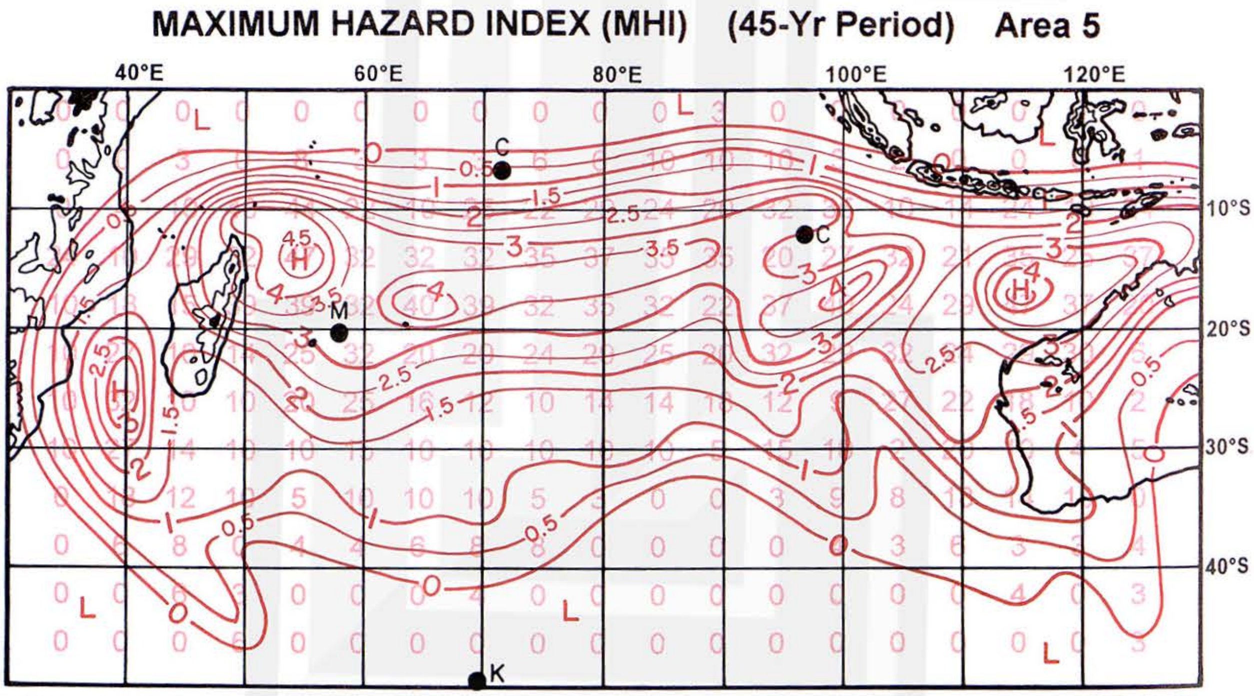

Fig. 4.11 1951-95

4.3 Maximum Hazard Index (MHI)

STORM PATHS (45-Yr Period) Area 6

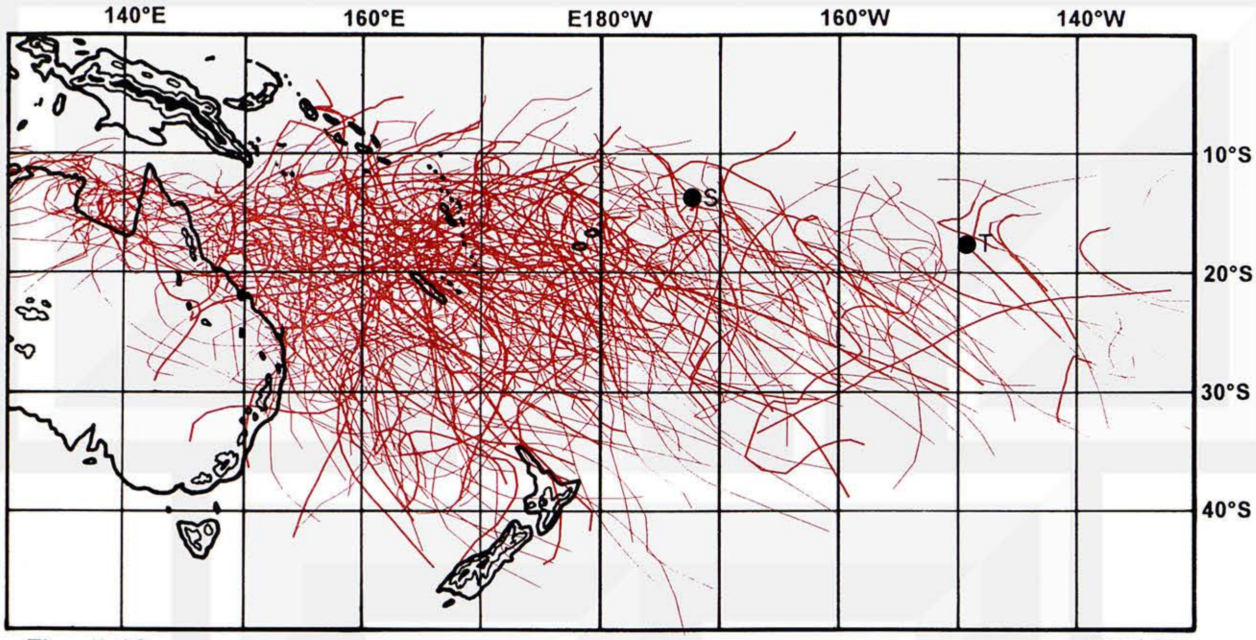

Fig. 4.12 1951-95

MAXIMUM HAZARD INDEX (MHI) (45-Yr Period) Area 6

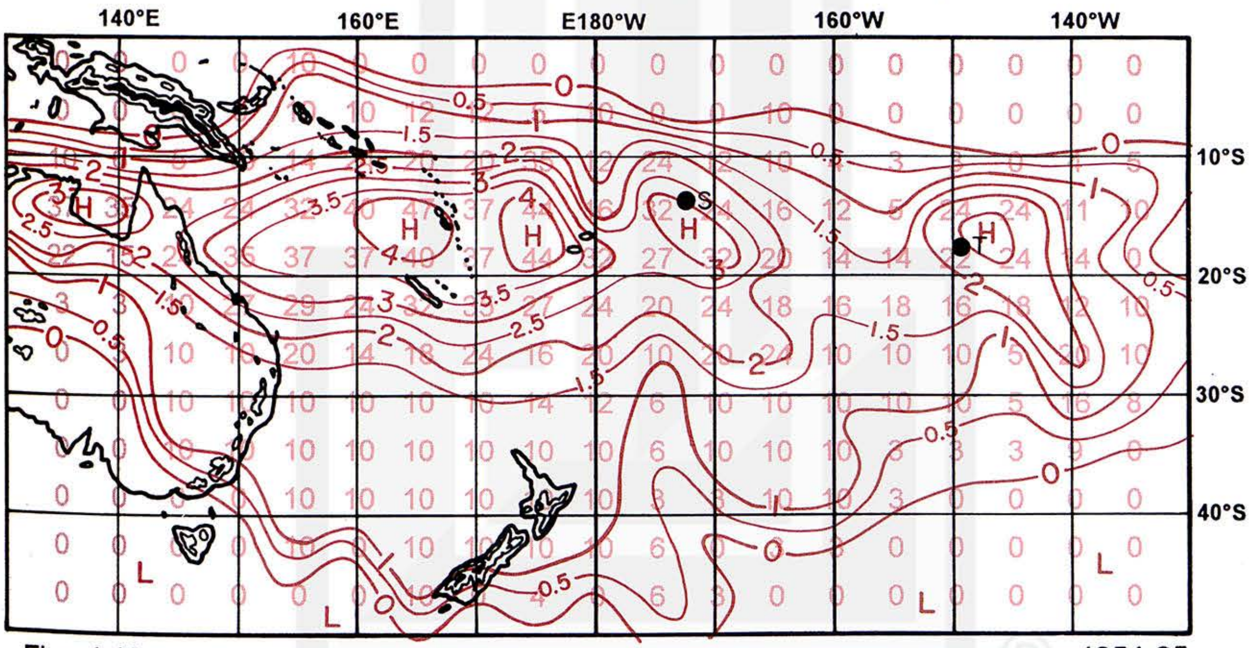

Fig. 4.13 1951-95

Chapter Five

Influence of El Niño and La Niña

Introduction to Chapter Five

It has long been known that sea surface temperature (SST) anomalies, especially the large localized anomalies of El Niño and La Niña, affect the weather around the world. Undoubtedly, these events influence storm activity as well, although this influence has not been revealed very well either quantitatively or even qualitatively. In this Atlas, however, the use of new SST anomalies as applicable to northern and southern hemisphere "storm years" improved the relatability of storm activity to specific El Niño / La Niña events, allowing Top 10 El Niño and Top 10 La Niña "storm years" to be selected for each hemisphere from the 45-year data base. Furthermore, new parameter PPC provides a means to numerically determine storm activity for the Top 10 El Niño and Top 10 La Niña years. From the PPC ratio of El Niño / La Niña the variance in storm activity could then be established.

Based on these new concepts, the PPC ratio of El Niño / La Niña decreases eastward from +19% and +24% in the North Indian Ocean and Western Pacific Ocean to -24% in the Atlantic Ocean in the Northern Hemisphere. It also decreases eastward from -7% to -12% in the southern hemisphere. Of particular note in Area 2, the Western Pacific, is the localized variance of storm activity in its southeast quadrant near the island of Kwajalein. This source region for storms experiences significantly less activity during La Niña years as opposed to El Niño years. Results for the global percent change in storm activity in El Niño versus La Niña years have been presented in Figure 4.2 from <u>Mystery of El Niño and Hurricanes</u> (WRL Research Paper 249), which is also presented here as Figure A.4 in the Appendix.

5.1 Top 10 El Niño and Top 10 La Niña Years

To determine storm years of greatest El Niño and La Niña influence in the northern and southern hemispheres, SST anomalies for the four Japan Meteorological Agency watch areas (Fig. 5.1) were examined for the 45-year data base. Anomalies of the Fujita EP (Equatorial Pacific) 2 area (JMA Region B) were found to correspond best with variations in storm activity. Also, the EP 2 area is geographically aligned to the mean location of El Niño / La Niña occurrence. The top 10 years of largest positive and negative storm-season SST anomalies in the EP 2 area were then selected for each of the northern and southern hemispheres, from which comparisons could be made in both storm paths and PPC distributions to reveal the effects of El Niño and La Niña on storm activity.

JMA Identification (1)	JMA Identification (2)	FUJITA Identification	Average SST
NINO 1+2	Region C	EP 1	22.9°C
NINO 3	Region B	EP 2	25.6°C
NINO 4	Region A	EP 3	28.3°C
NINO West	Region D	EP 4	28.9°C

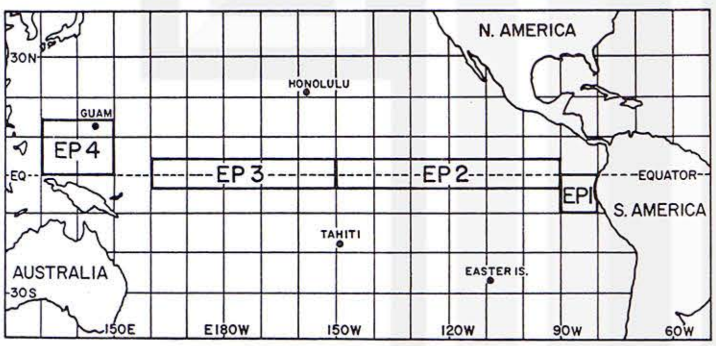

LEFT: Fig. 5.1 Geographical locations of the Japan Meteorological Agency watch areas in the equatorial Pacific with alternate identifications and average sea-surface temperatures indicated in an accompanying table.

BELOW: Table 5.1 Lists of the Top 10 El Niño and Top 10 La Niña years selected from the 45-year data base (1951-95 storm years) for each of the northern and southern hemispheres based on the magnitude of the storm-season SST anomaly for the EP 2 area.

Top 10 El Niño and Top 10 La Niña Years for Northern and Southern Hemisphere Storm Years

El Niño

Northern Hemisphere		Southern Hemisphere	
Year	Anomaly	Year	Anomaly
1951	1.3°C	1952	0.5°C
1957	1.3	1958	1.0
1963	1.0	1966	0.4
1965	1.1	1969	0.8
1969	0.7	1970	0.4
1972	1.6	1973	0.8
1976	1.1	1977	0.7
1982	1.5	1983	2.3
1987	1.0	1987	0.8
1991	0.7	1992	1.0

La Niña

Northern Hemisphere		Southern Hemisphere	
Year	Anomaly	Year	Anomaly
1954	-0.8°C	1955	-0.7°C
1955	-1.2	1956	-0.6
1964	-0.7	1967	-0.4
1970	-1.3	1968	-0.8
1973	-1.1	1971	-1.0
1975	-0.8	1974	-0.8
1984	-0.6	1976	-0.6
1985	-0.7	1985	-0.8
1988	-1.6	1986	-0.4
1995	-0.7	1989	-1.1

5.2 El Niño / La Niña PPC Ratios for Areas 1 through 6

Prorated Position Counts (PPC) were evaluated for each of Areas 1 through 6 for the Top 10 El Niño and Top 10 La Niña years. The PPC ratios of the El Niño years versus La Niña years were then computed to reveal the percent change. The greatest difference in storm activity was found to exist in the North Atlantic with a 24% decrease during El Niño vs. La Niña. Lesser but still substantial decreases of -7% and -12% were also found to exist in the South Indian Ocean (Area 5) and South Pacific Ocean (Area 6), respectively. Alternately, large increases of +17% and +19% were revealed for the North Indian Ocean (Area 1) and Western Pacific Ocean (Area 2), respectively.

Area	1	2	3	4	5	6
PPC (El Niño Yrs)	380	2786	1409	1198	1449	1137
PPC (La Niña Yrs)	325	2343	1398	1582	1556	1298
Average PPC	353	2564	1404	1390	1503	1218
EL / LA Ratio	1.17	1.19	1.01	0.76	0.93	0.88
% Change	+17%	+19%	+1%	-24%	-7%	-12%

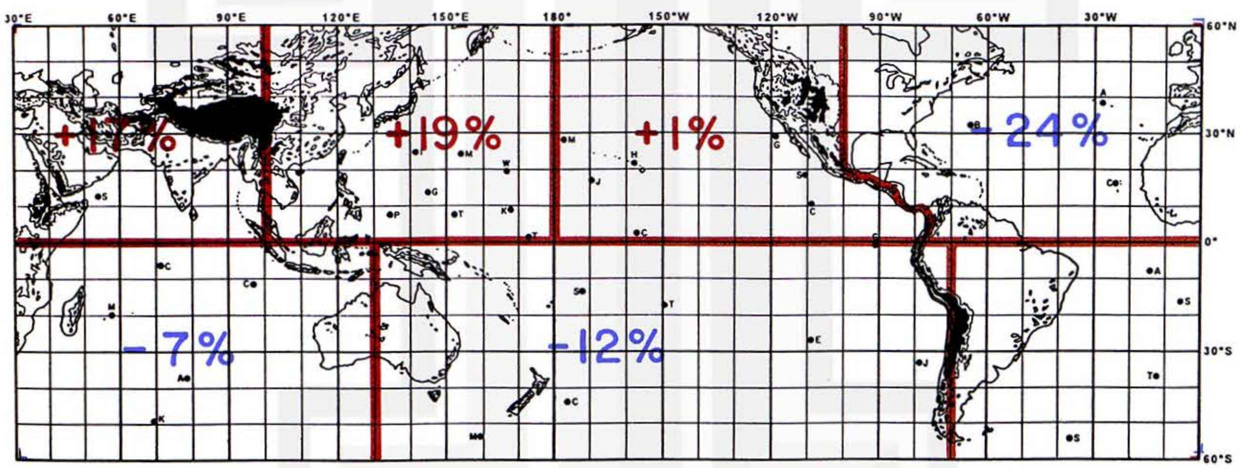

Table & Fig. 5.2 Percent change in storm activity for Areas 1 through 6 based on PPC ratios (El Niño vs. La Niña) of the top 10 El Niño and top 10 La Niña storm years.

On following pages are global (section 5.3, pages 76-79) and local (section 5.4, pages 80-91) maps showing distributions of storm paths and PPC during the Top 10 El Niño Years and Top 10 La Niña Years as indicated. Examples of Maximum Hazard Index (MHI) mapping for Area 2 are shown in section 5.5, pages 93 and 94, depicting how risk can vary with occurrence of El Niño vs. La Niña.

STORM PATHS El Niño (Top 10 Yrs)

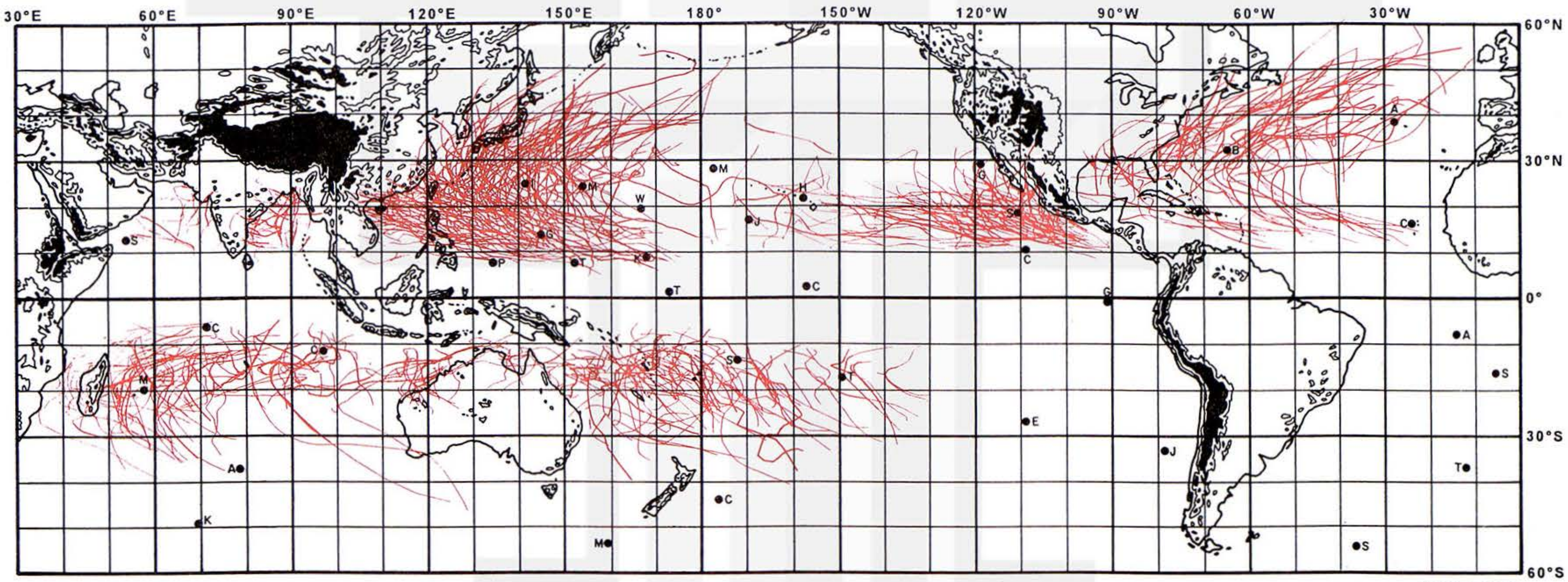

Fig. 5.3

1951-95

STORM PATHS La Niña (Top 10 Yrs)

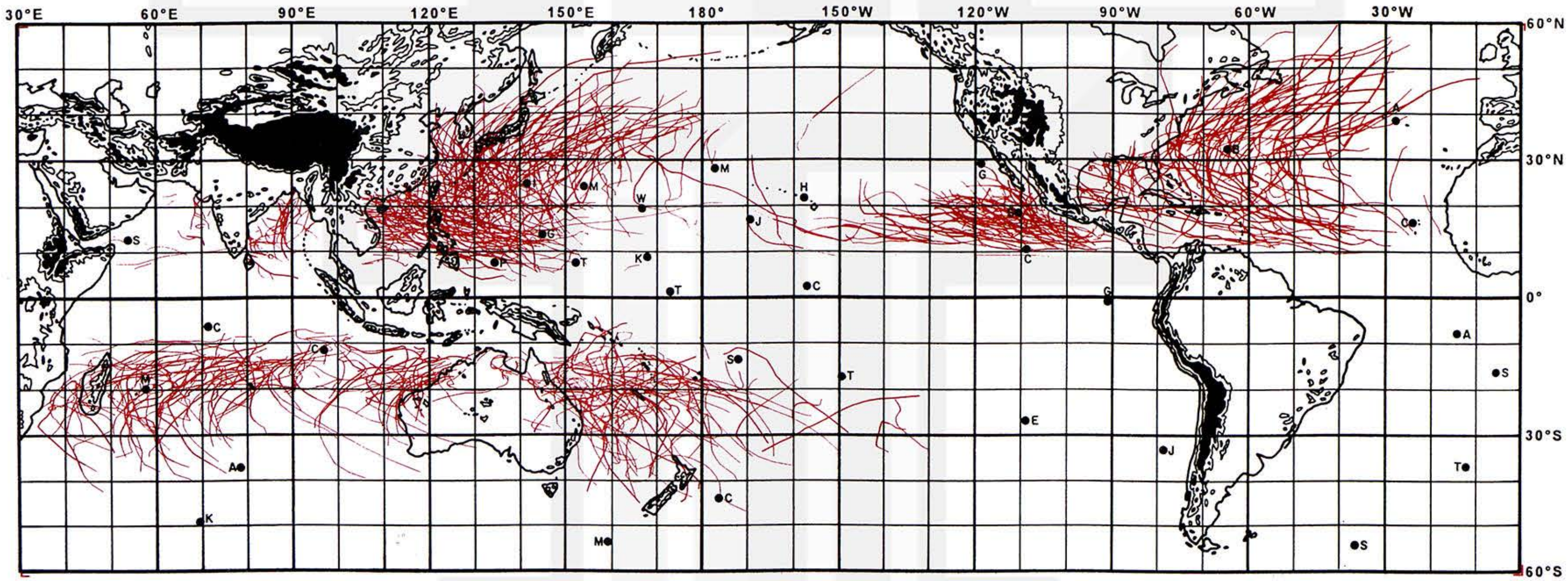

Fig. 5.4

1951-95

PPC El Niño (Top 10 Yrs)

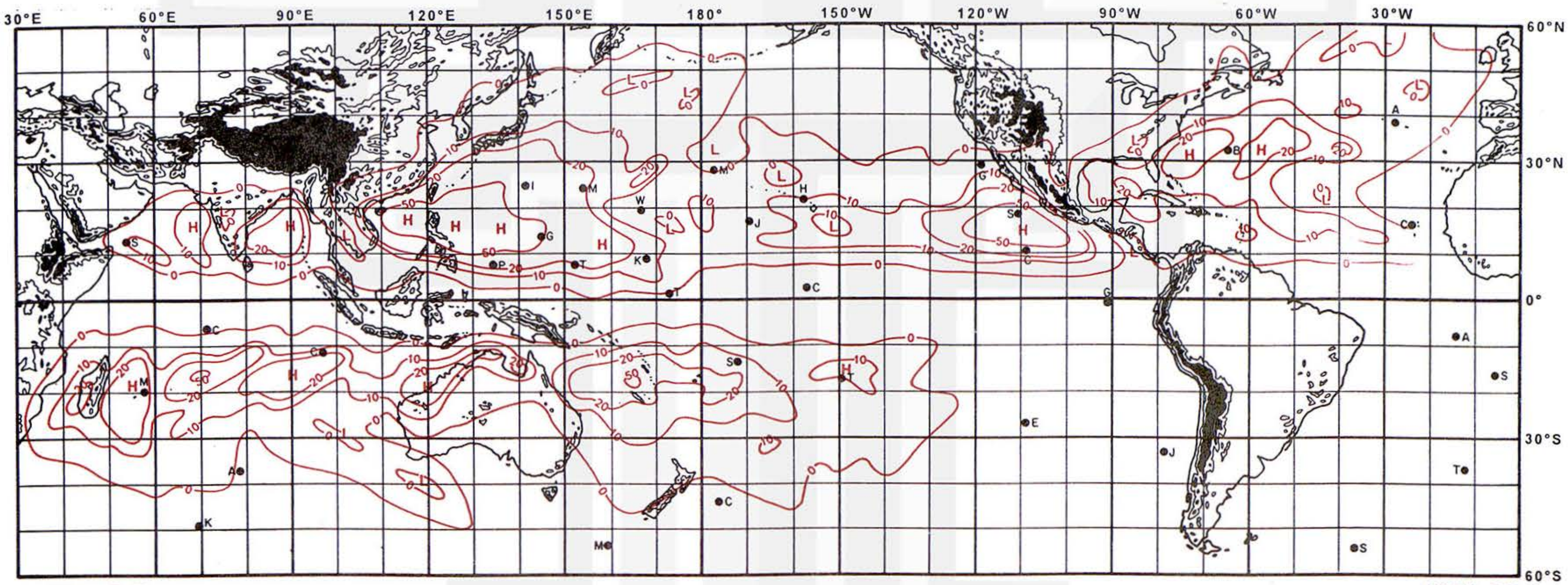

Fig. 5.5 1951-95

PPC La Niña (Top 10 Yrs)

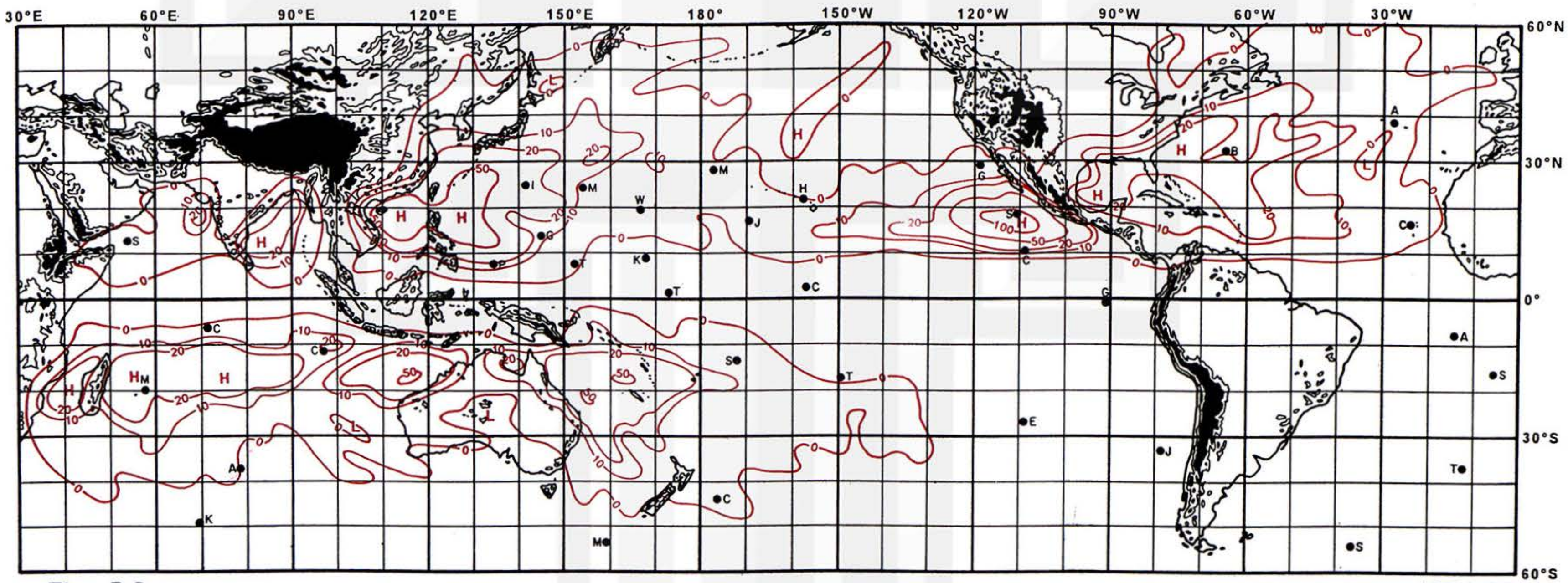

Fig. 5.6

1951-95

STORM PATHS El Niño (Top 10 Yrs) Area 1

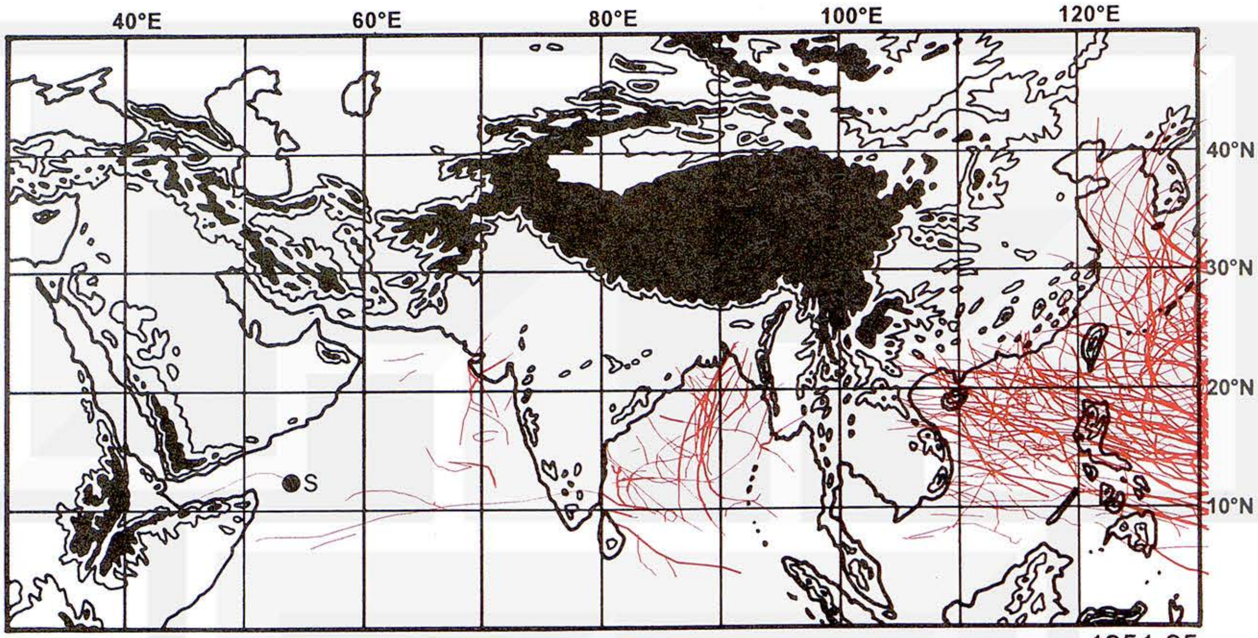

Fig. 5.7 1951-95

PPC El Niño (Top 10 Yrs) Area 1

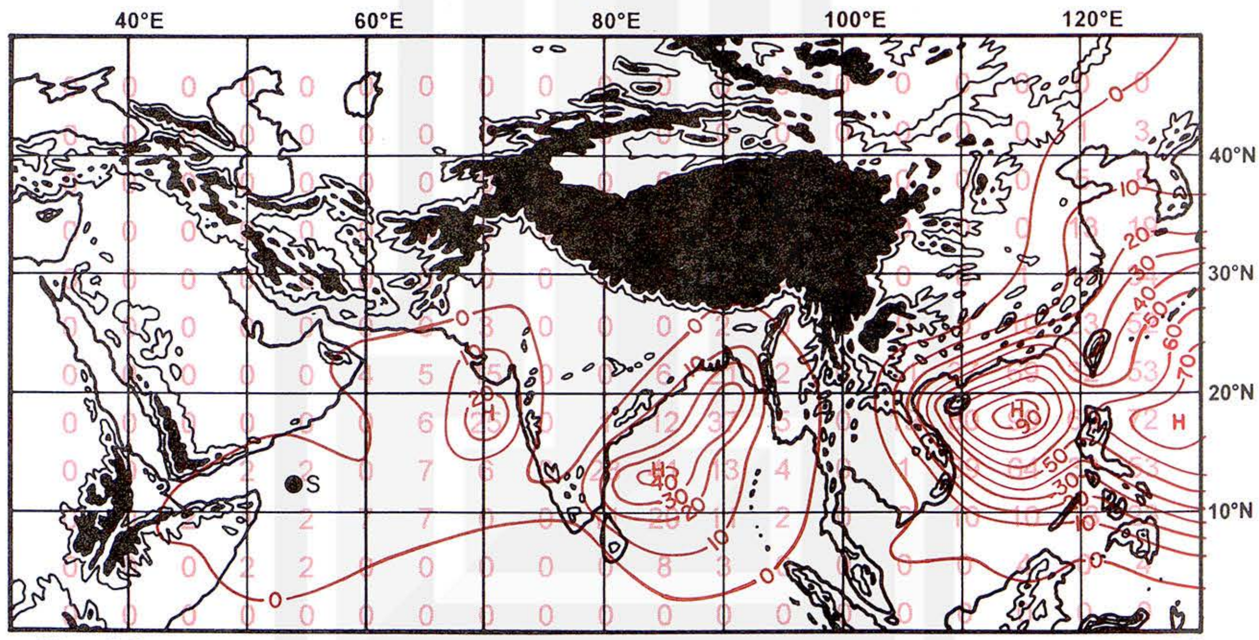

Fig. 5.8 1951-95

STORM PATHS La Niña (Top 10 Yrs) Area 1

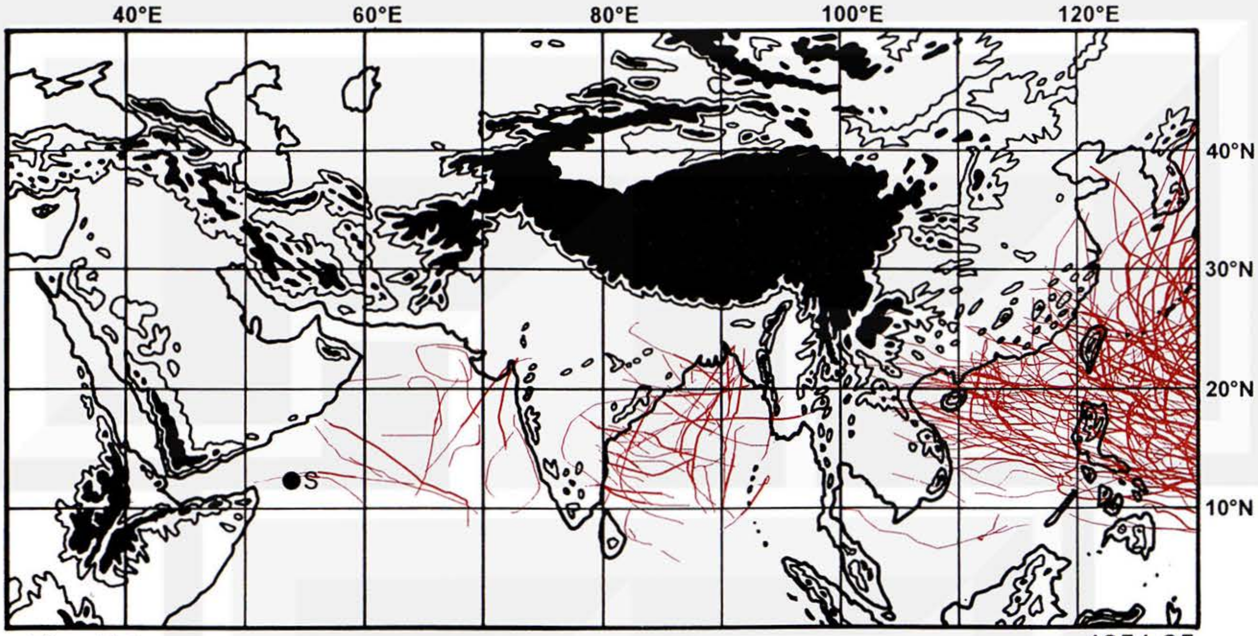

Fig. 5.9 1951-95

PPC La Niña (Top 10 Yrs) Area 1

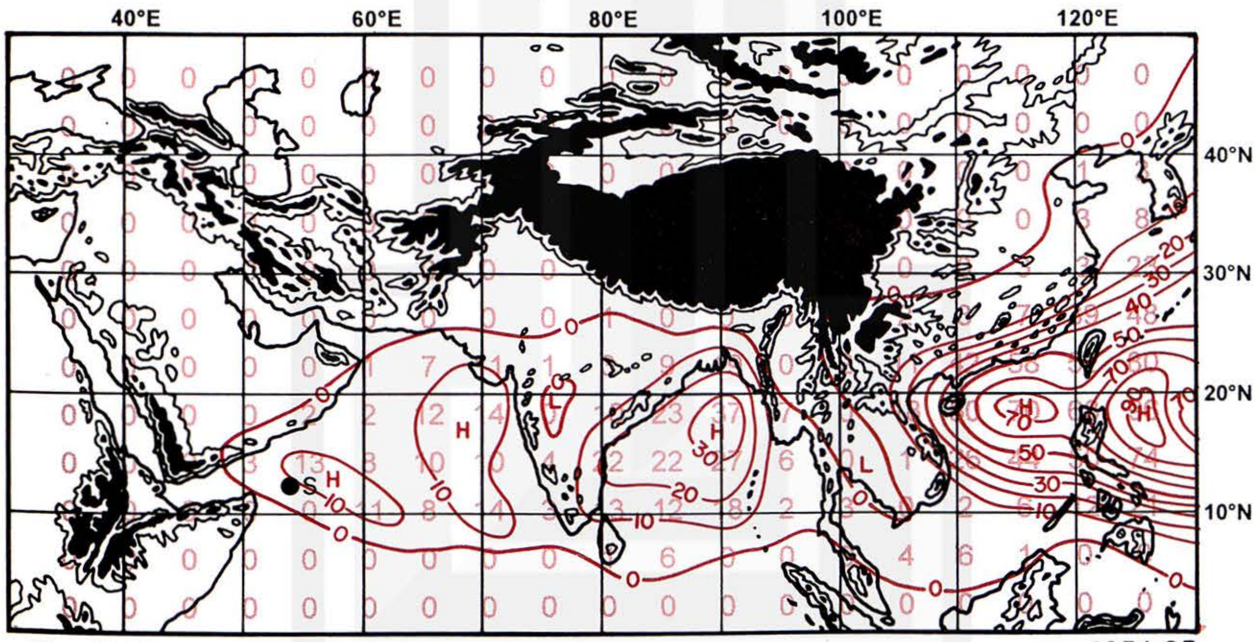

Fig. 5.10 1951-95

STORM PATHS El Niño (Top 10 Yrs) Area 2

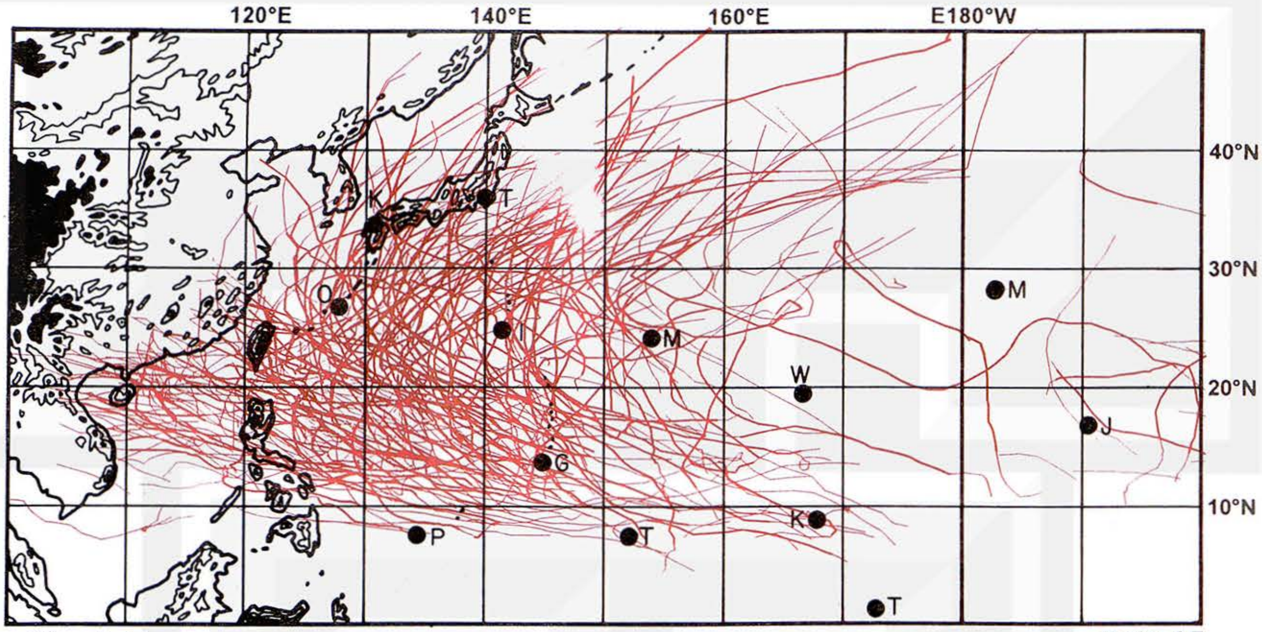

Fig. 5.11 1951-95

PPC El Niño (Top 10 Yrs) Area 2

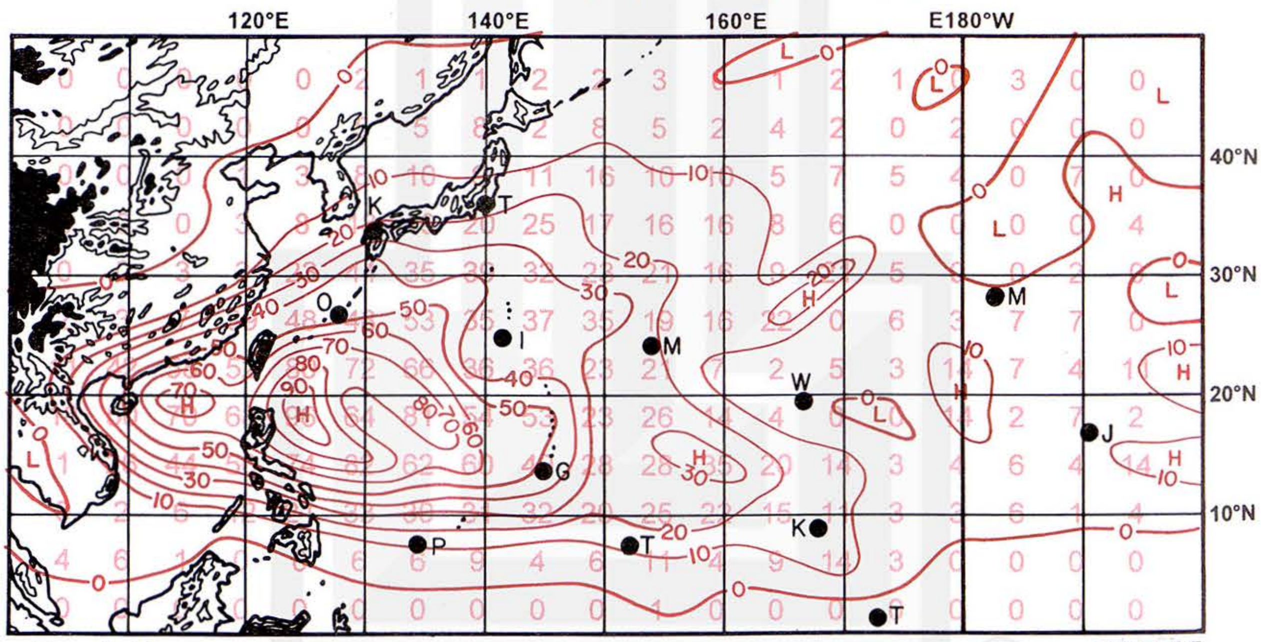

Fig. 5.12 1951-95

STORM PATHS La Niña (Top 10 Yrs) Area 2

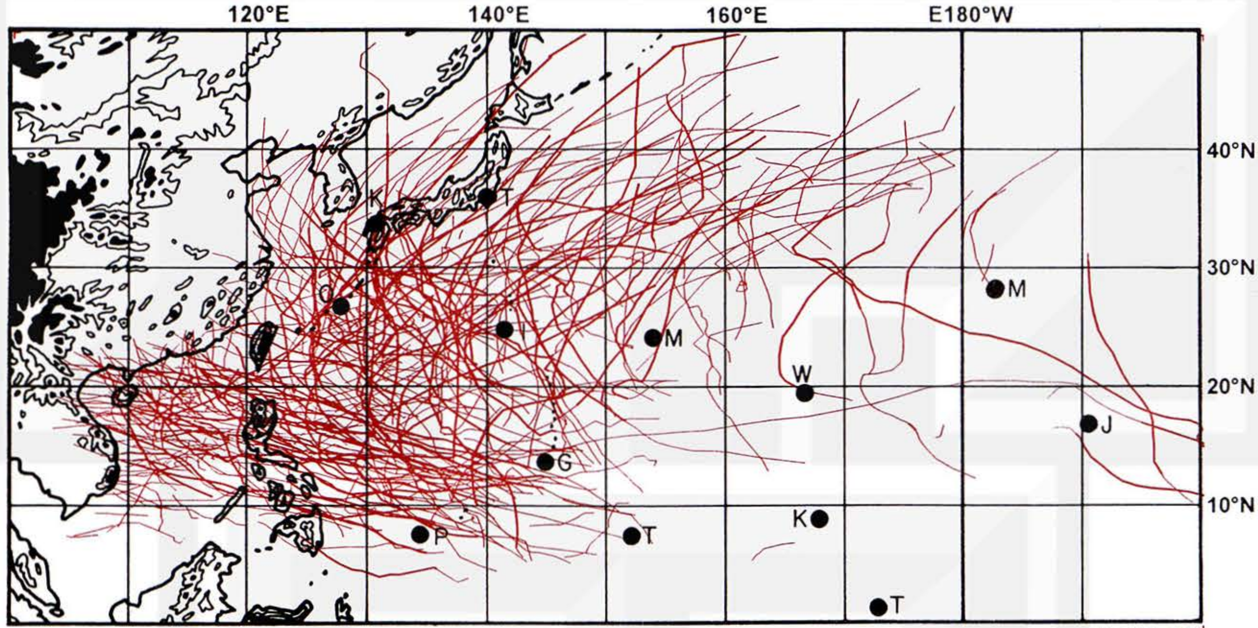

Fig. 5.13 1951-95

PPC La Niña (Top 10 Yrs) Area 2

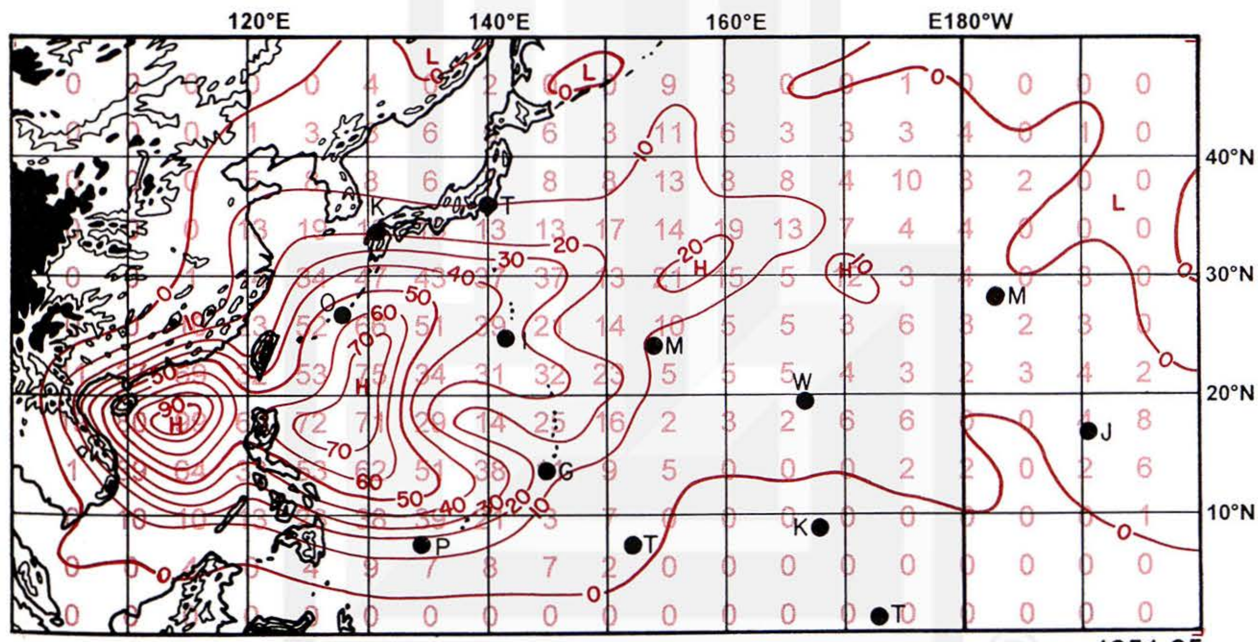

Fig. 5.14 1951-95

STORM PATHS El Niño (Top 10 Yrs) Area 3

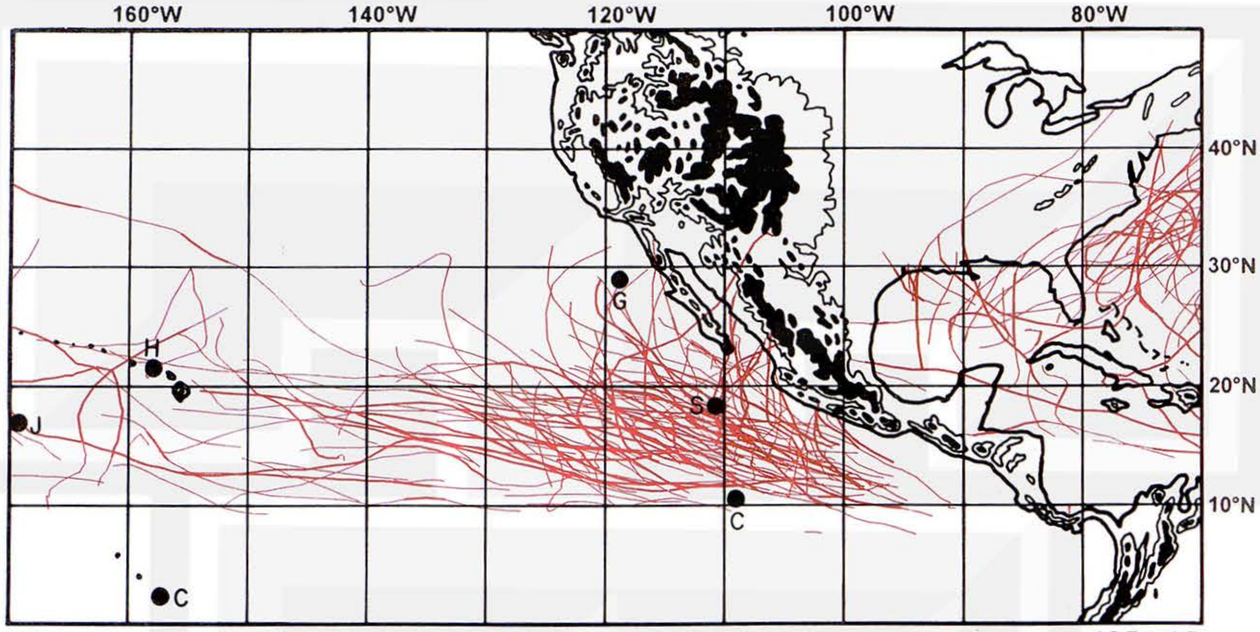

Fig. 5.15 1951-95

PPC El Niño (Top 10 Yrs) Area 3

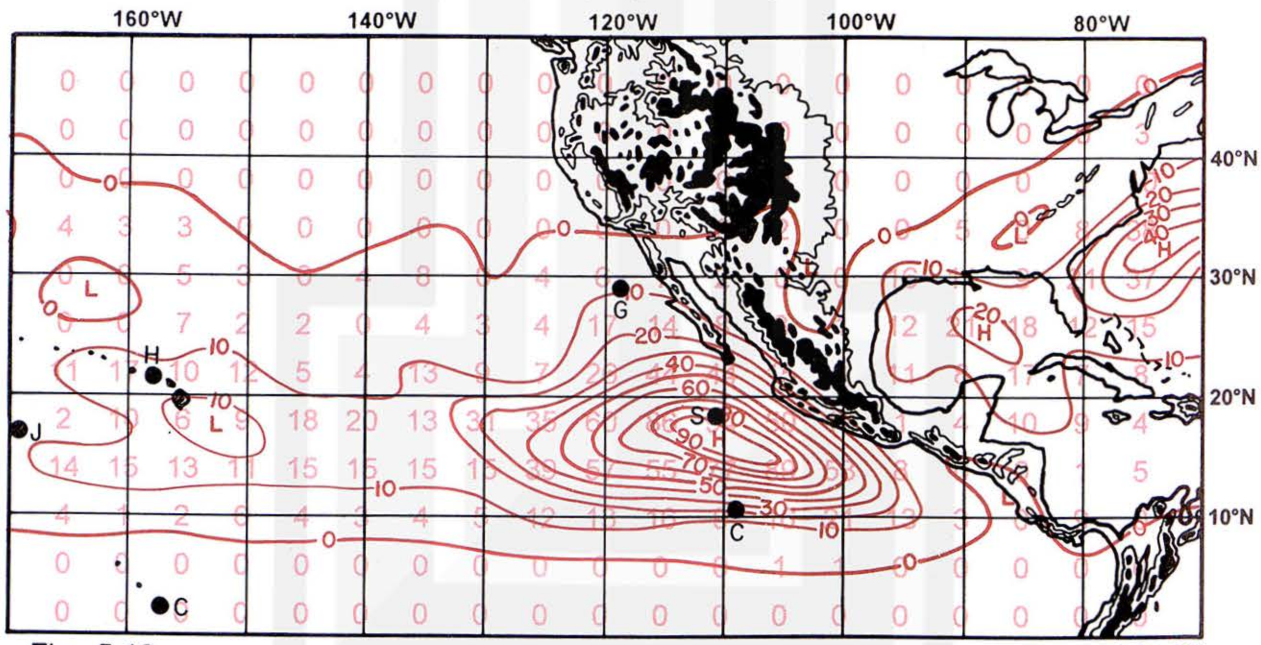

Fig. 5.16 1951-95

STORM PATHS La Niña (Top 10 Yrs) Area 3

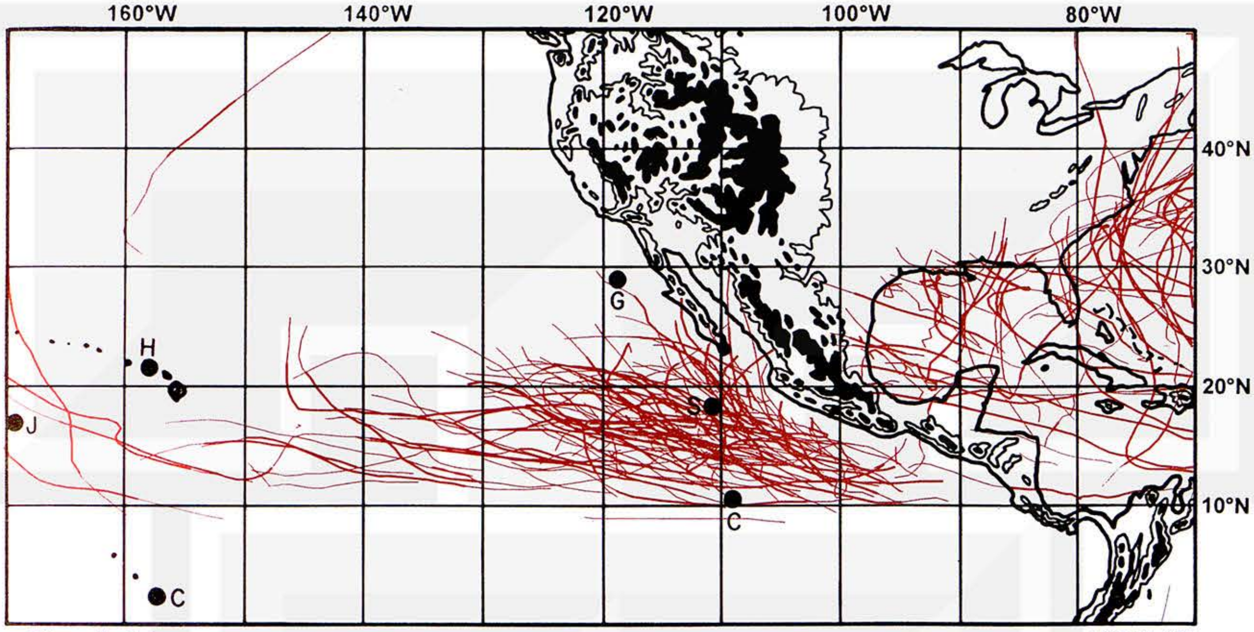

Fig. 5.17 1951-95

PPC La Niña (Top 10 Yrs) Area 3

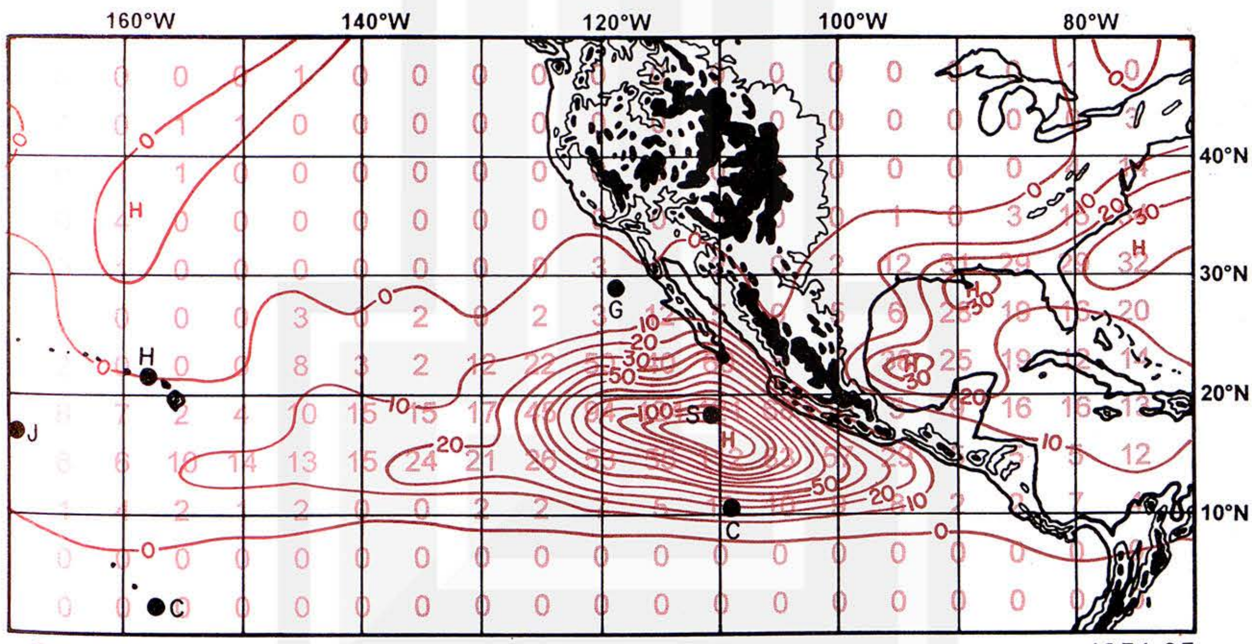

Fig. 5.18 1951-95

STORM PATHS El Niño (Top 10 Yrs) Area 4

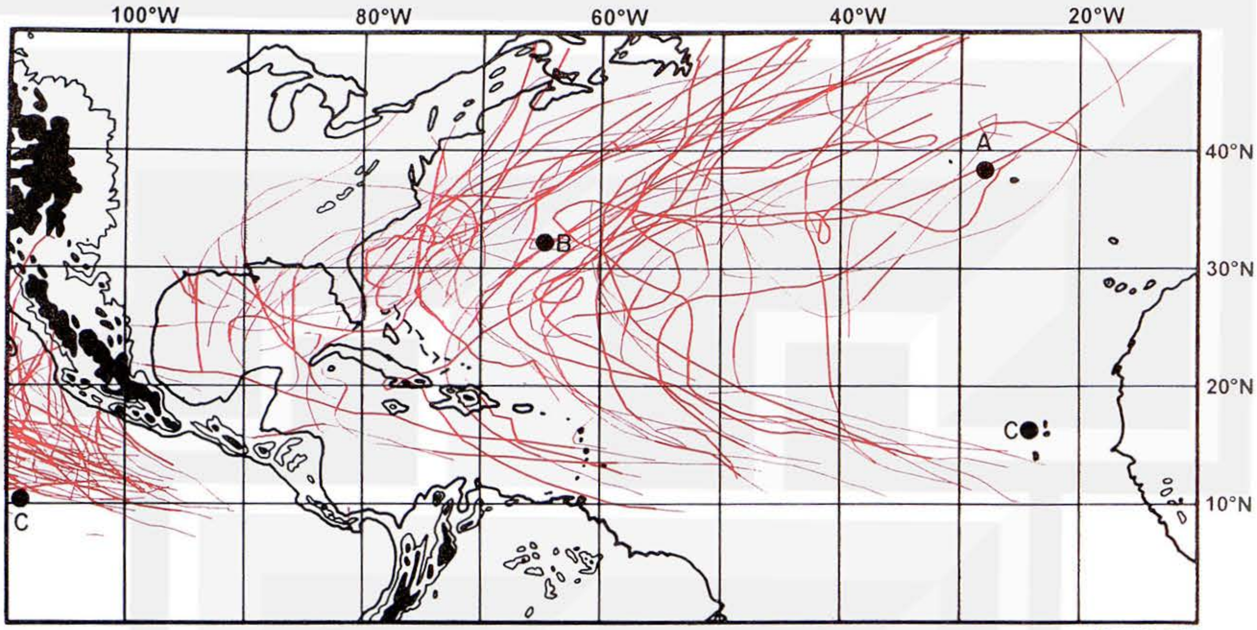

Fig. 5.19 1951-95

PPC El Niño (Top 10 Yrs) Area 4

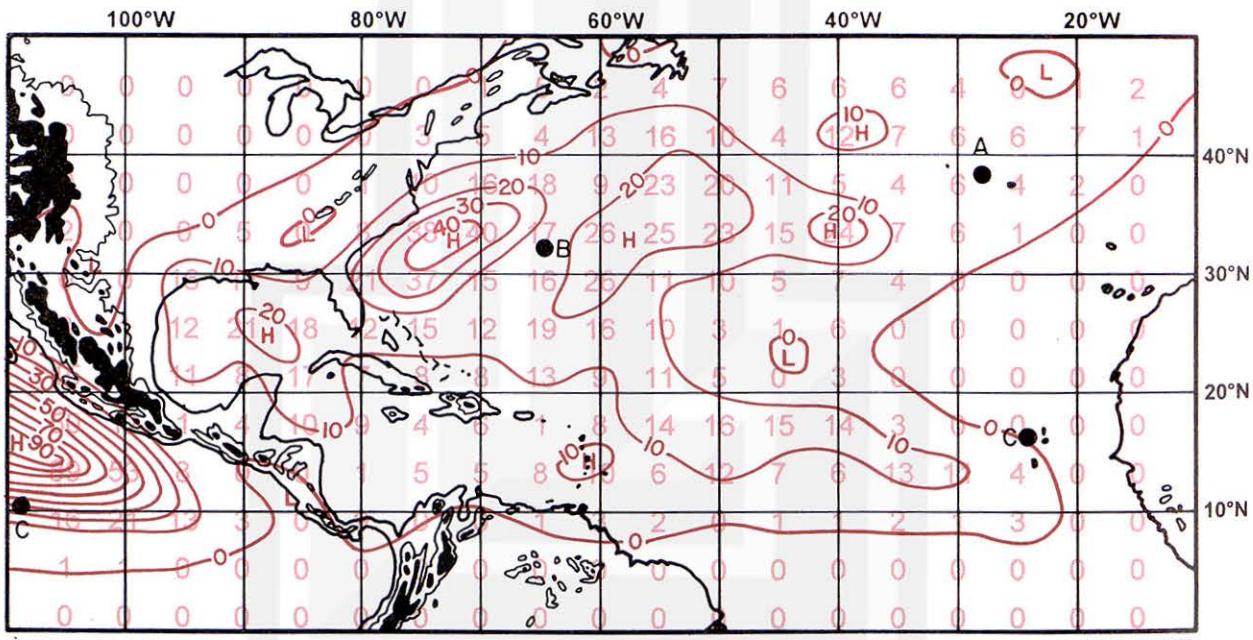

Fig. 5.20 1951-95

STORM PATHS La Niña (Top 10 Yrs) Area 4

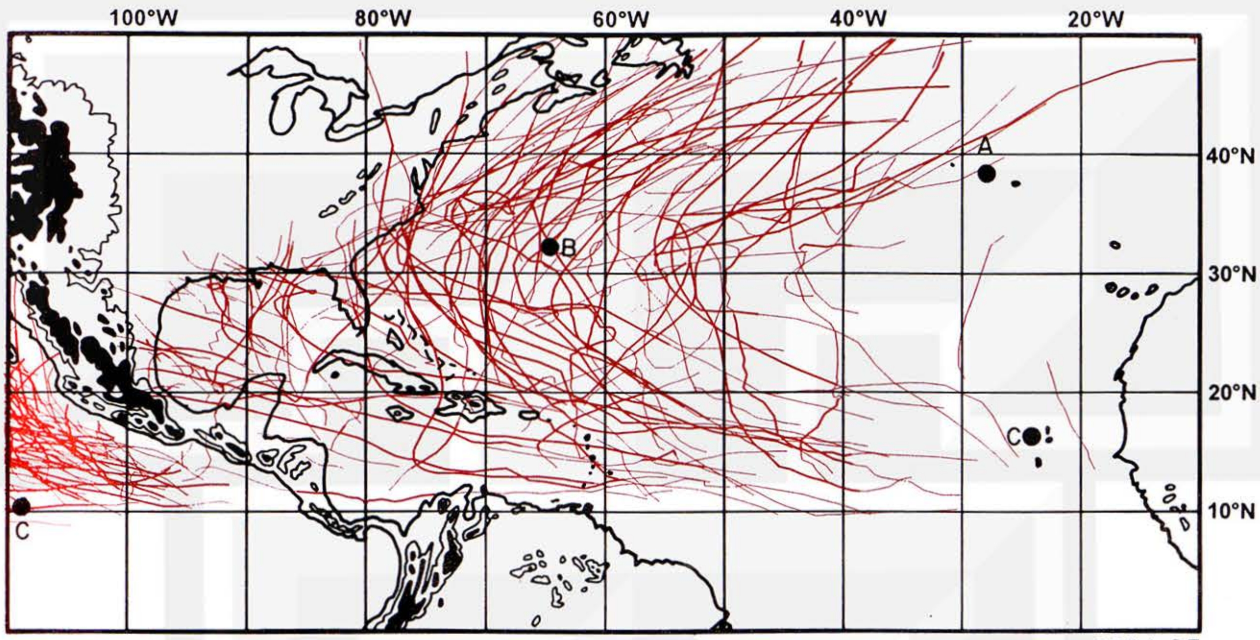

Fig. 5.21 1951-95

PPC La Niña (Top 10 Yrs) Area 4

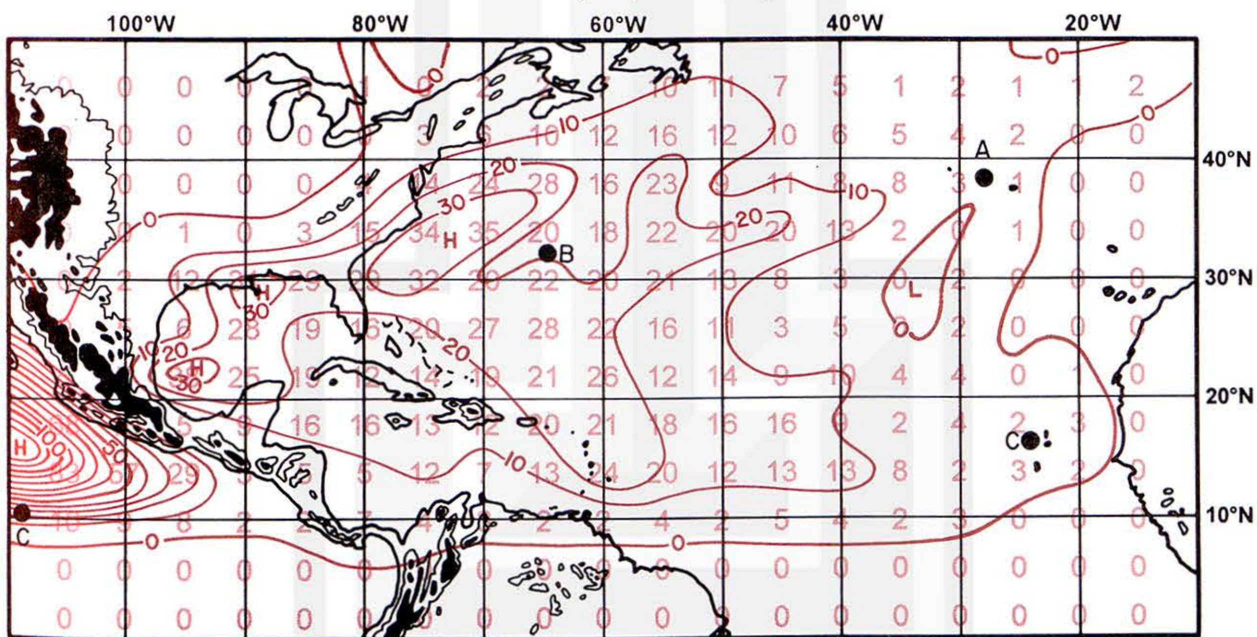

Fig. 5.22 1951-95

STORM PATHS El Niño (Top 10 Yrs) Area 5

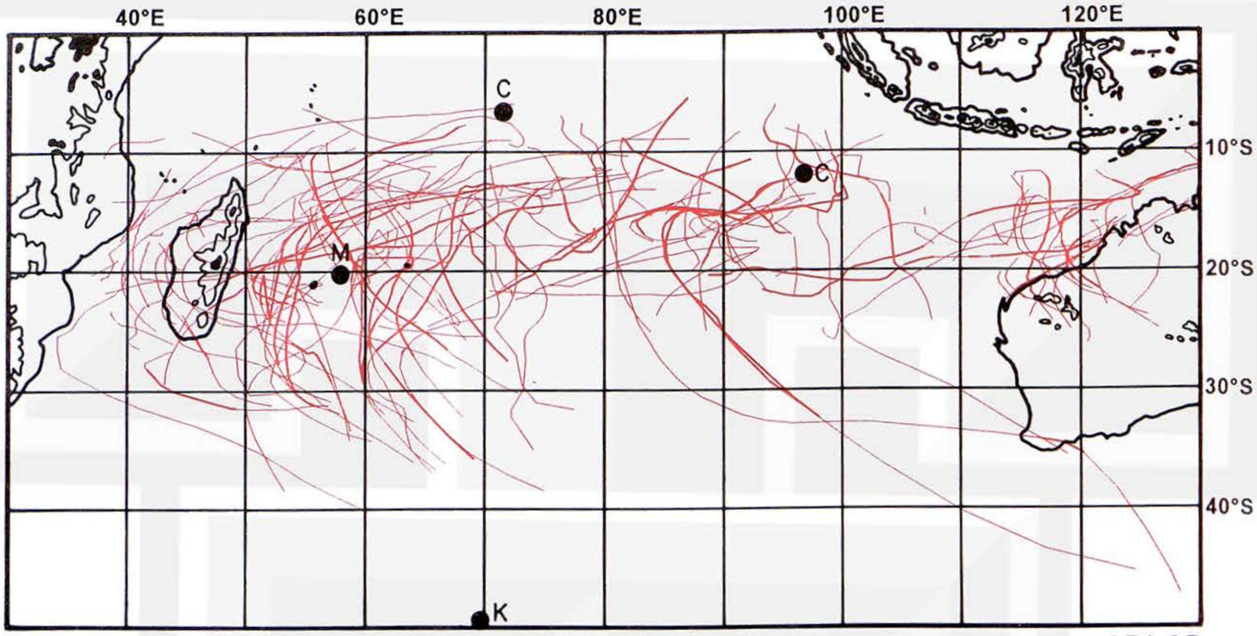

Fig. 5.23 1951-95

PPC El Niño (Top 10 Yrs) Area 5

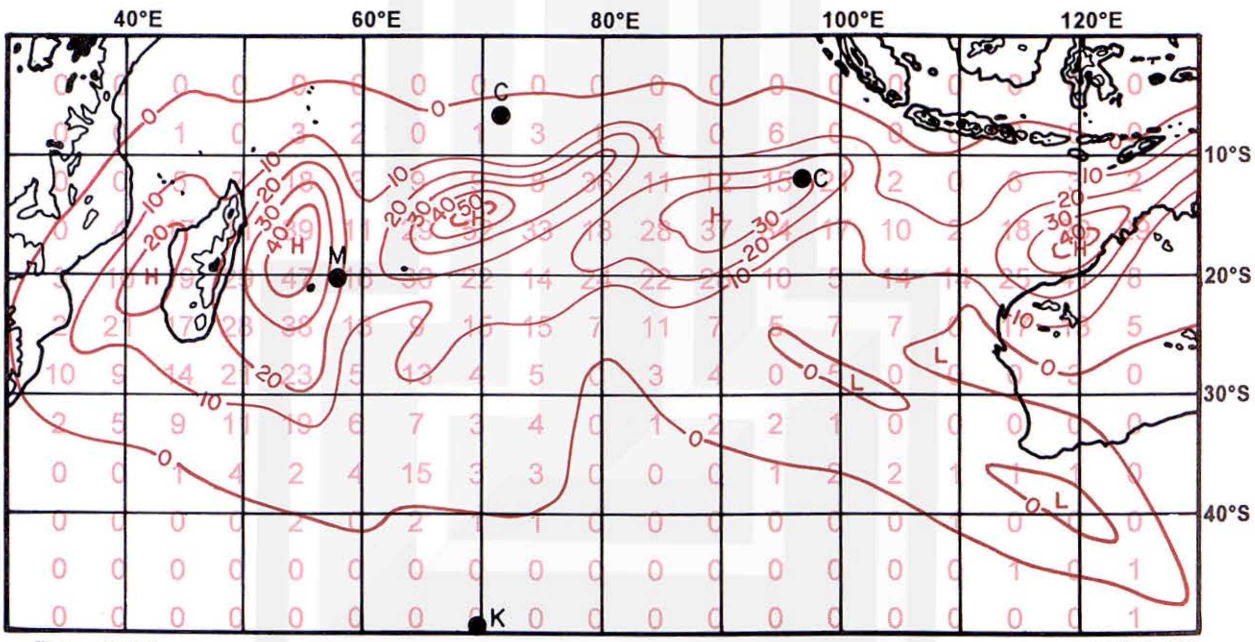

Fig. 5.24 1951-95

STORM PATHS La Niña (Top 10 Yrs) Area 5

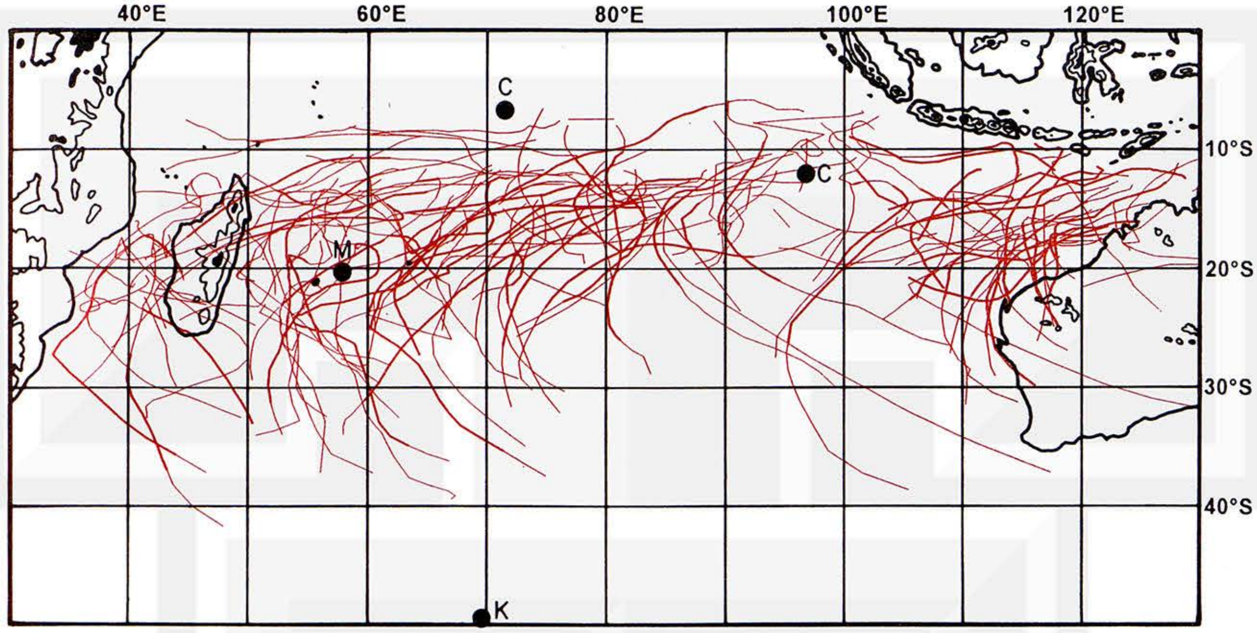

Fig. 5.25 1951-95

PPC La Niña (Top 10 Yrs) Area 5

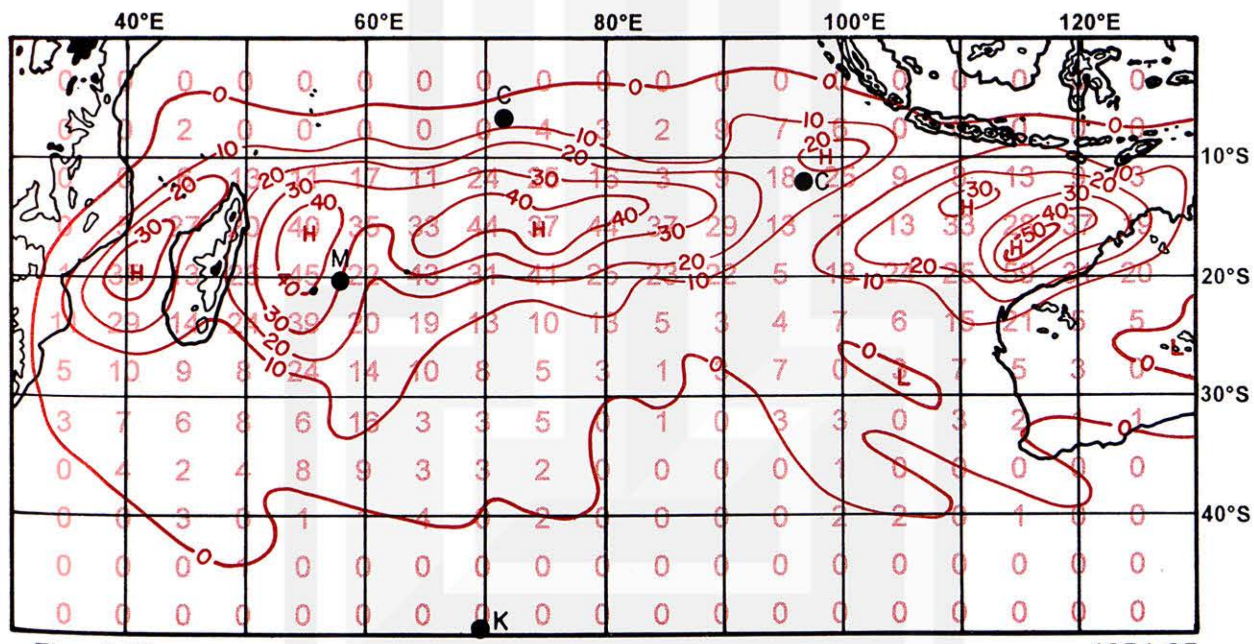

Fig. 5.26 1951-95

STORM PATHS El Niño (Top 10 Yrs) Area 6

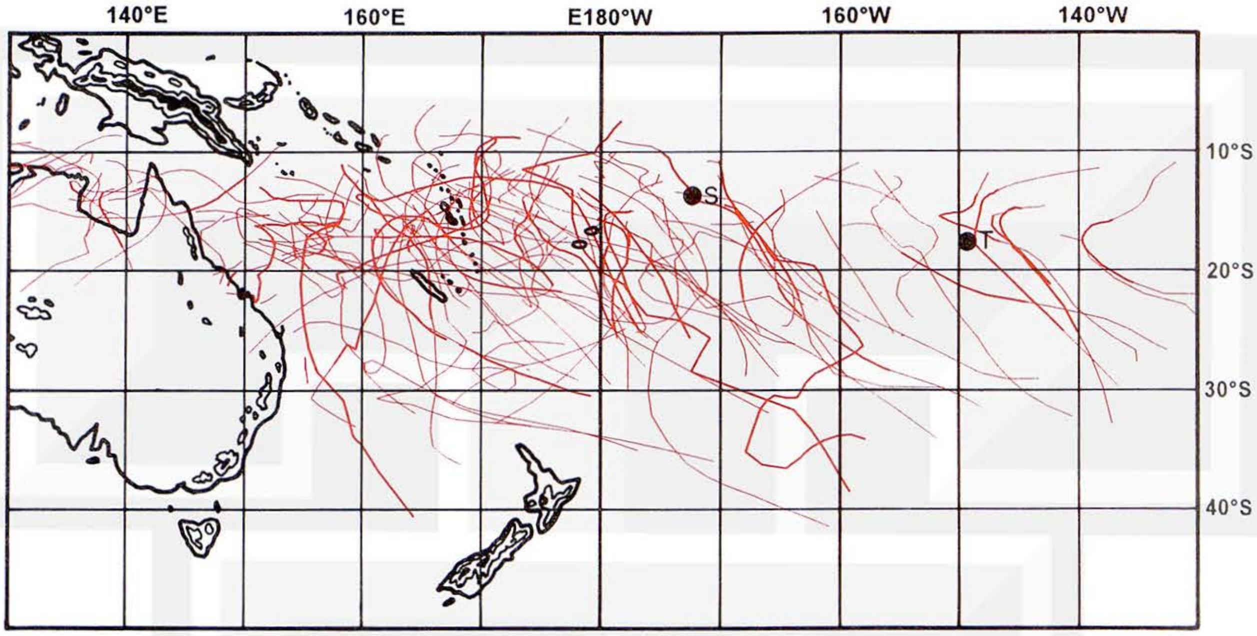

Fig. 5.27 1951-95

PPC El Niño (Top 10 Yrs) Area 6

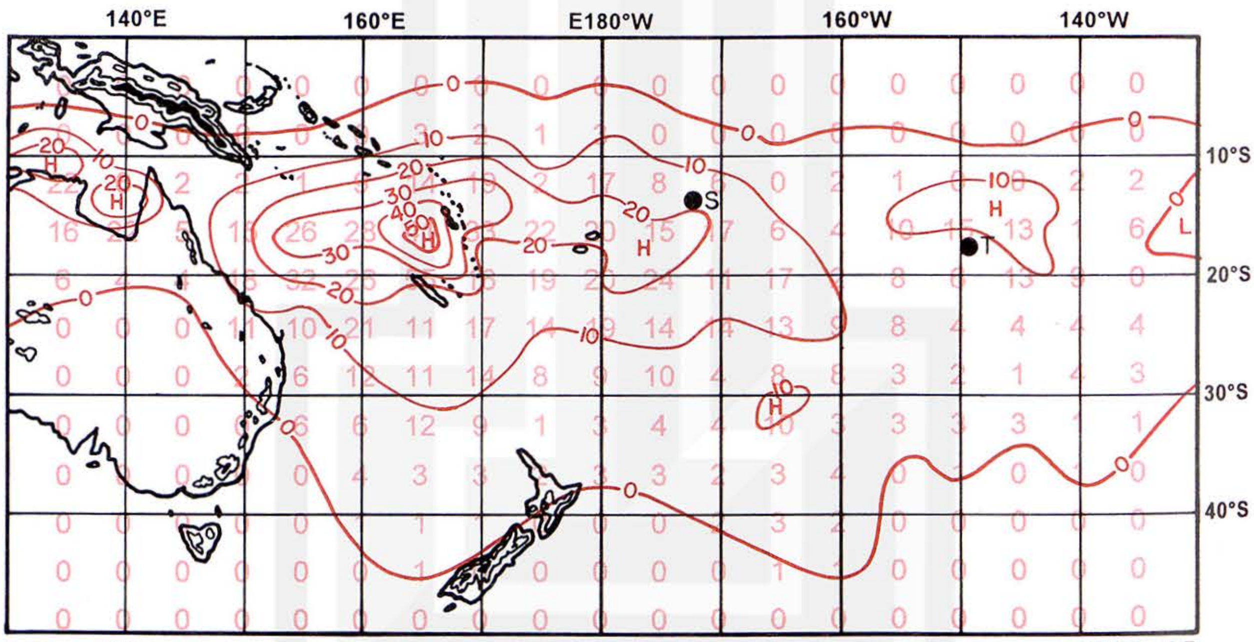

Fig. 5.28 1951-95

STORM PATHS La Niña (Top 10 Yrs) Area 6

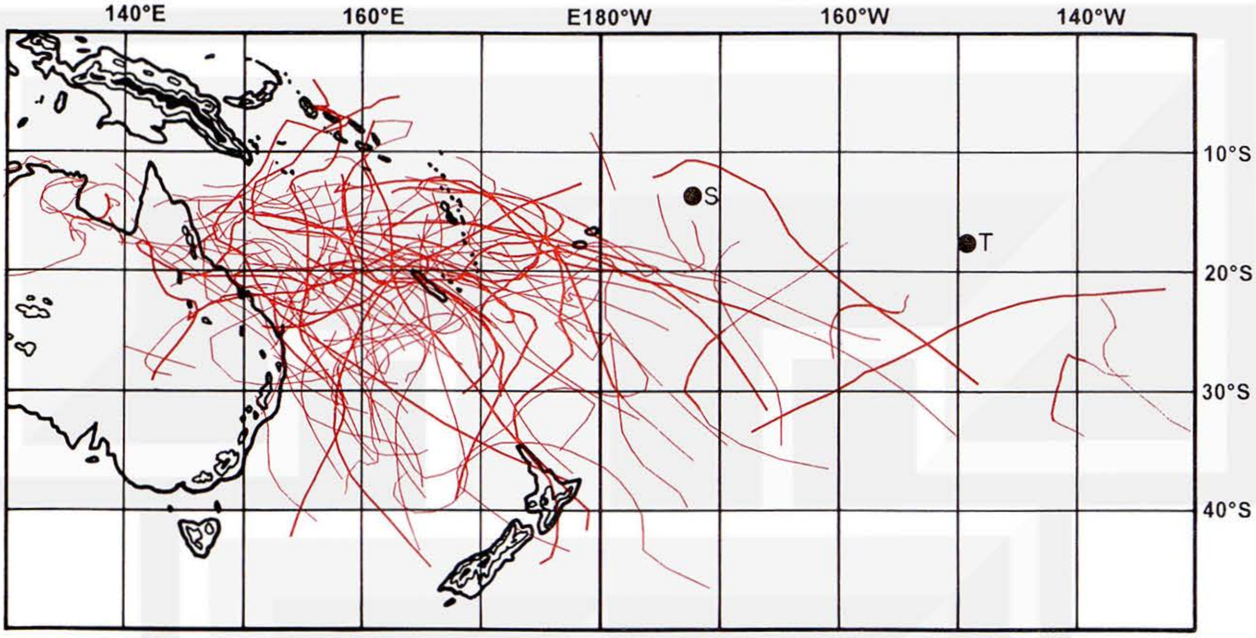

Fig. 5.29 1951-95

PPC La Niña (Top 10 Yrs) Area 6

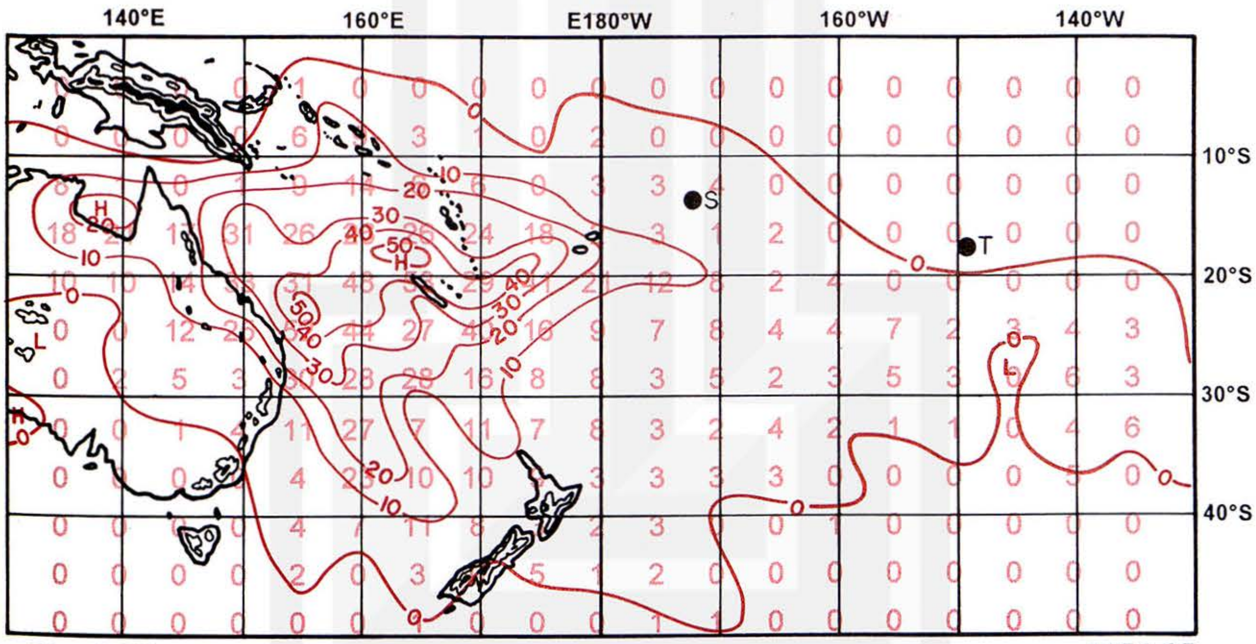

Fig. 5.30 1951-95

5.5 MHI Maps of Area 2 in El Niño and La Niña Years

STORM PATHS El Niño (Top 10 Yrs) Area 2

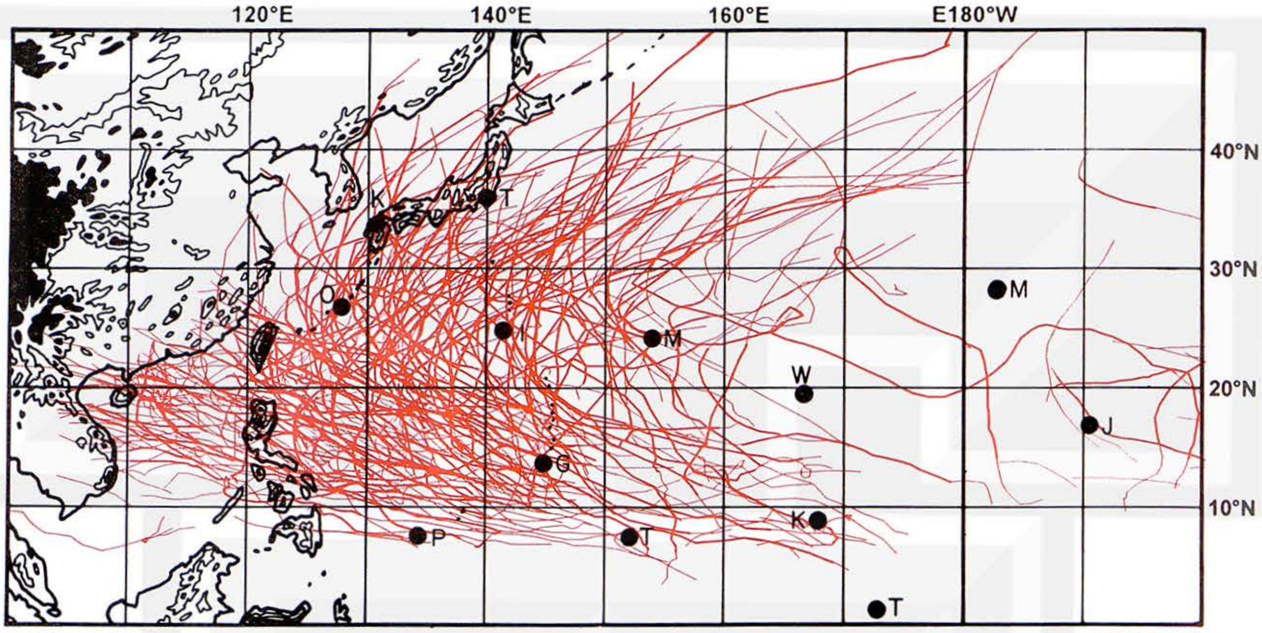

Fig. 5.31 1951-95

MHI El Niño (Top 10 Yrs) Area 2

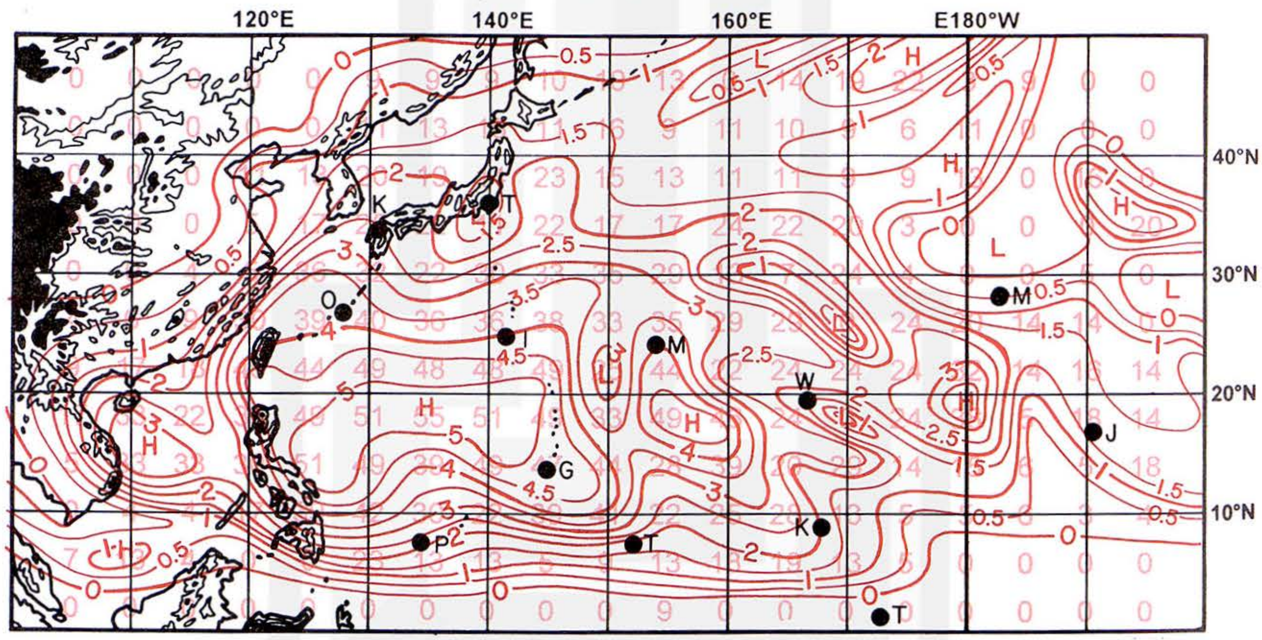

Fig. 5.32 1951-95

Maximum Hazard Index of Western Pacific Ocean (Area 2) in Top 10 El Niño Years.

STORM PATHS La Niña (Top 10 Yrs) Area 2

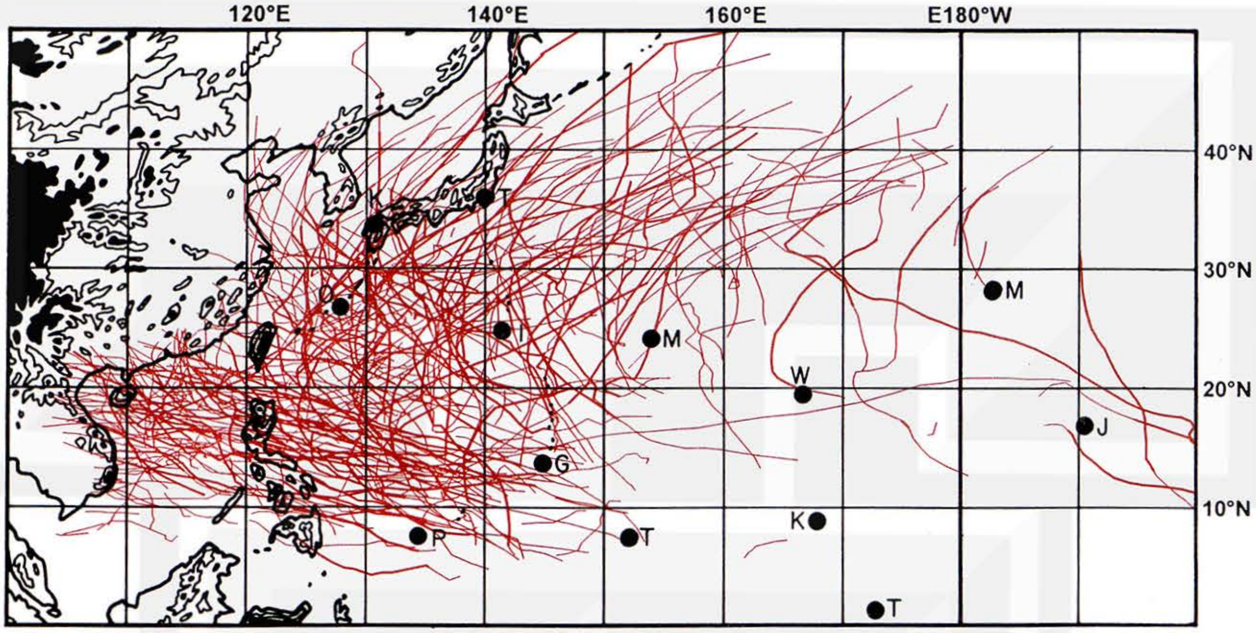

Fig. 5.33 1951-95

MHI La Niña (Top 10 Yrs) Area 2

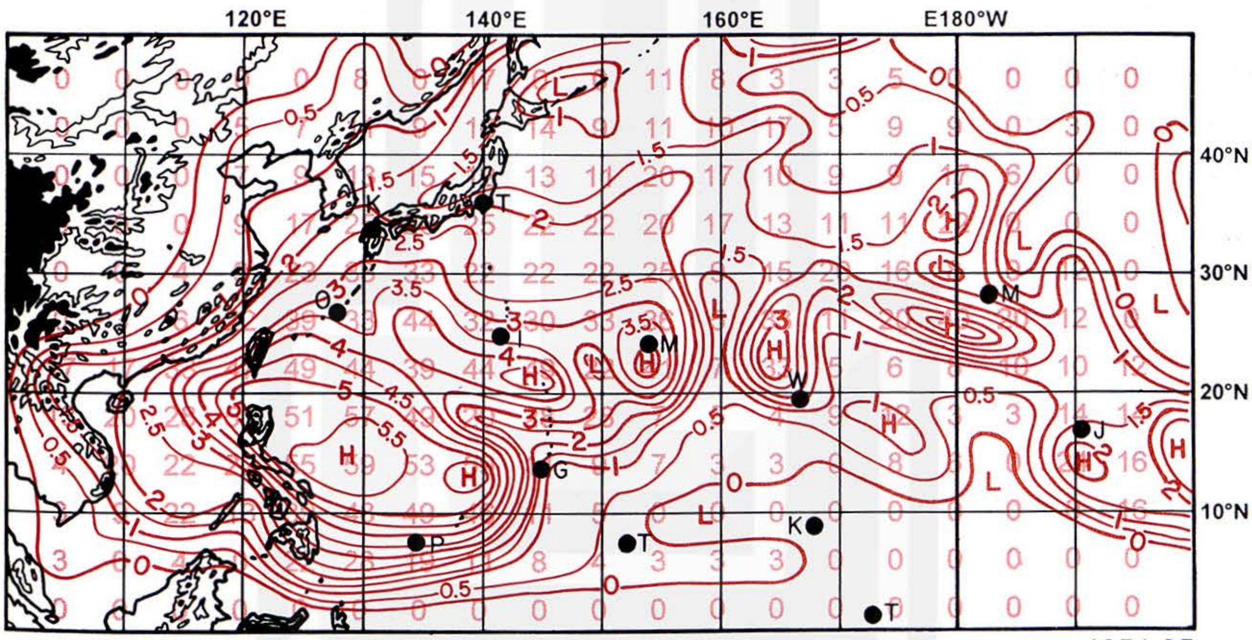

Fig. 5.34 1951-95

Maximum Hazard Index of Western Pacific Ocean (Area 2) in Top 10 La Niña Years.

APPENDIX

This research has been conducted in conjunction with others over a period sufficient to allow the collection of data for three additional storm years from both the northern and southern hemispheres since the end of the 45-year data base period, 1951-1995. Following are global storm path maps for the years 1996, 1997 and 1998 which, quite interestingly, have been years exhibiting periods of strong La Niña and a Super El Niño, the strongest of record.

Below, Table A.1 shows the storm-season SST anomalies for years 1996 through 1998 for each of the northern and southern hemispheres. The Super El Niño of '97-98 is shown by large positive anomalies in the 1997 northern hemisphere storm year and 1998 southern hemisphere storm year. If these storm years were included in the 45-year data base of this atlas they would rank #1 and #2, respectively in their Top 10 categories. Periods of La Niña are also reflected by the negative anomalies in the 1996 southern hemisphere storm year and 1998 northern hemisphere storm year which would similarly rank #5 and #7, respectively. As it is, the variance in storm activity corresponding to these periods and shown in the following maps closely mirrors the patterns shown in the Top 10 mappings of Chapter 5, thereby further supporting the findings.

Storm-Season SST Anomalies, 1996-1998

	1996	1997	1998
Northern Hemisphere	**-0.4°C**	**+2.6**	**-0.7**
Southern Hemisphere	**-0.7**	**-0.1**	**+2.0**

Table A.1

STORM PATHS 1996

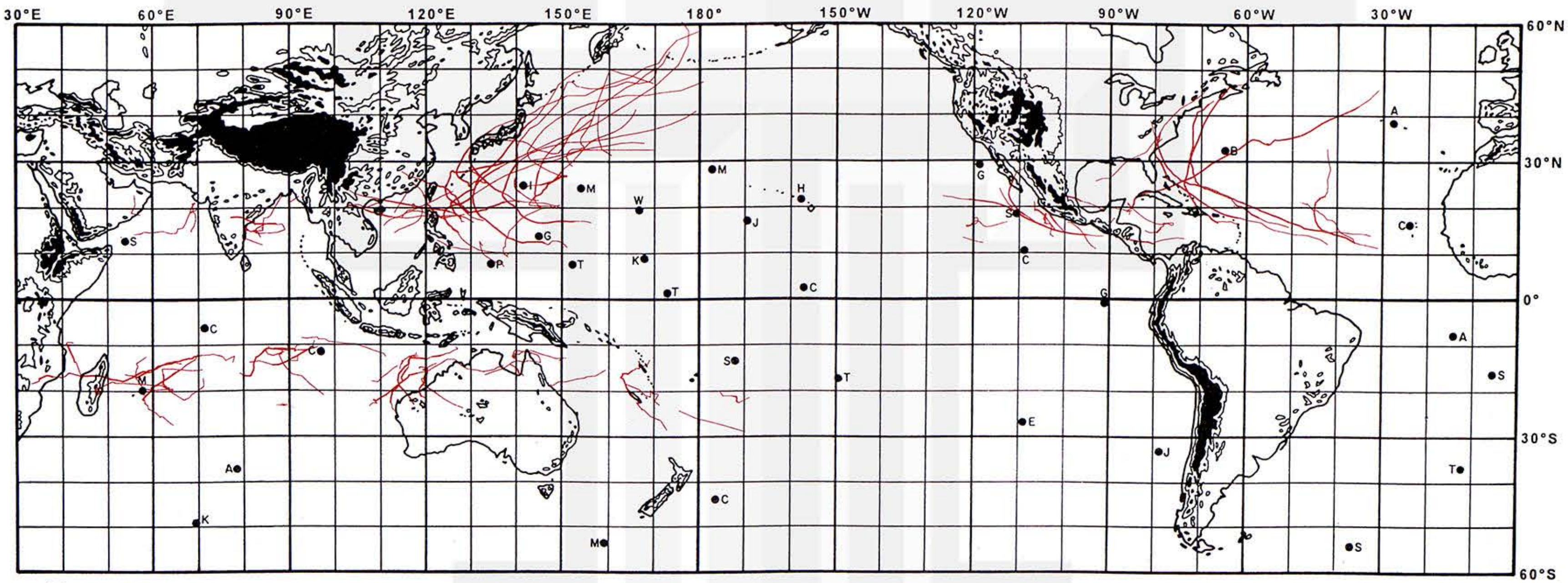

Fig. A.1

STORM PATHS 1997

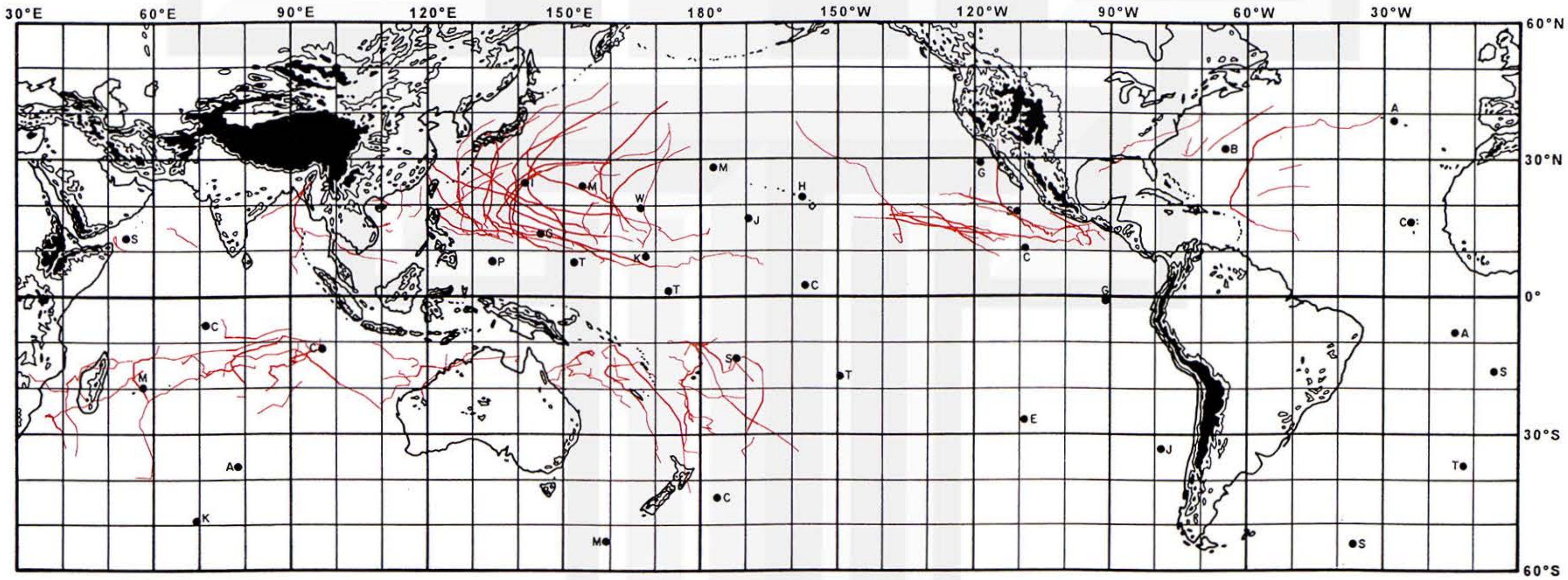

Fig. A.2

STORM PATHS 1998

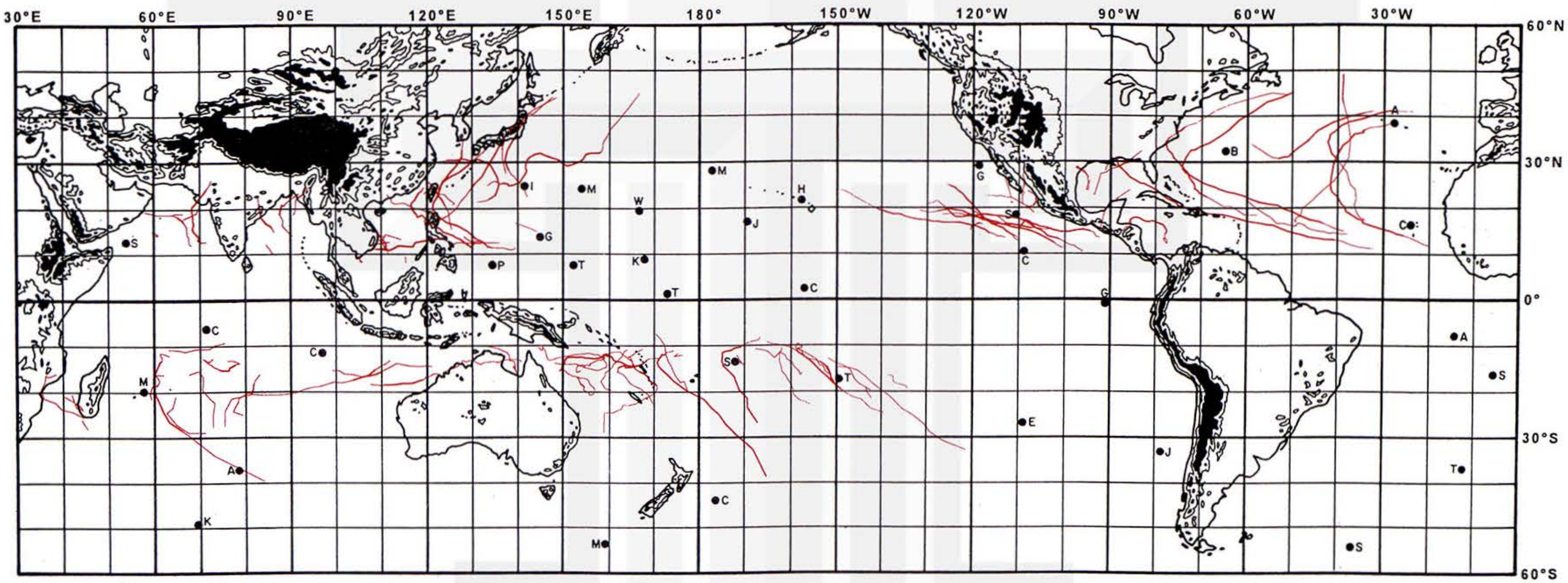

Fig. A.3

Percent Change of Typhoons in the Eastern Hemisphere

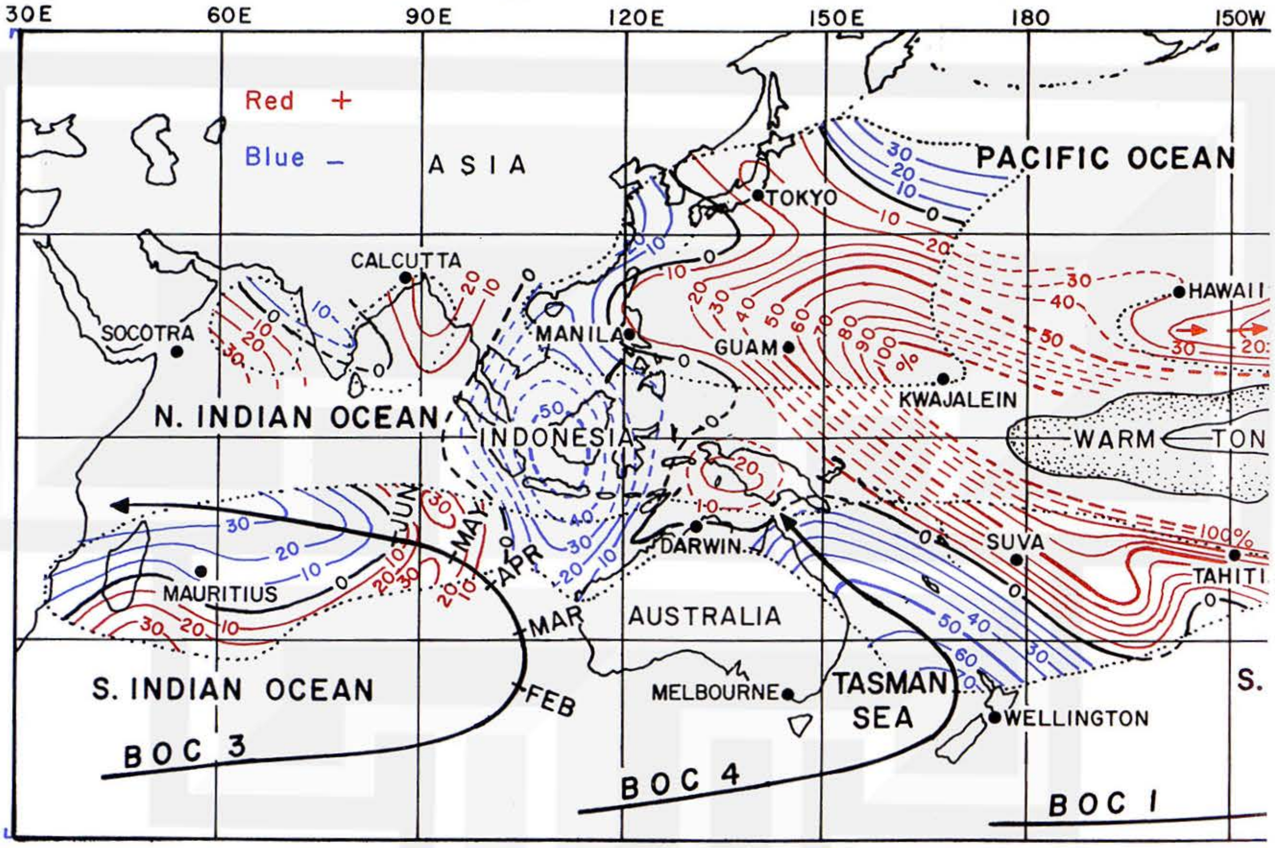

Fig. A.4 Percent change (+ in red and - in blue) of storm activity during El Niño versus La Niña. This change turned out to be much larger than anticipated. The percent change was computed by the simple formula,

$$\frac{E - \frac{1}{2}(E + L)}{\frac{1}{2}(E + L)} = \frac{E - L}{E + L}$$

where E and L are the Prorated Position Counts (PPC) in the Top 10 El Niño and Top 10 La Niña storm years, respectively, taken from the 45-year data base 1951-95. PPC is the number of 6-hourly storm positions within any area on the earth prorated to 100 years per 1° (111 km) square area. PPCs were computed at about 500 grid points in these Top 10 El Niño and Top 10 La Niña years. Both E and L can be applied to other parameters such as tornado frequency, rainfall amount, snow cover, drought index, and many more.

In December 1997, a tropical storm was born near Hawaii. The storm developed into hurricane Paka and moved west. Upon crossing the date line, the storm became typhoon Paka. On 17 December the eye moved west passing north of Anderson AFB in Guam where a record high, 236 mph (105.5 m/s) gust (F4.5) was measured. This rare storm was born in the +50% area, moved up through the 100% area, and hit Guam which is in the +52% area.

Percent Change of Hurricanes in the Western Hemisphere

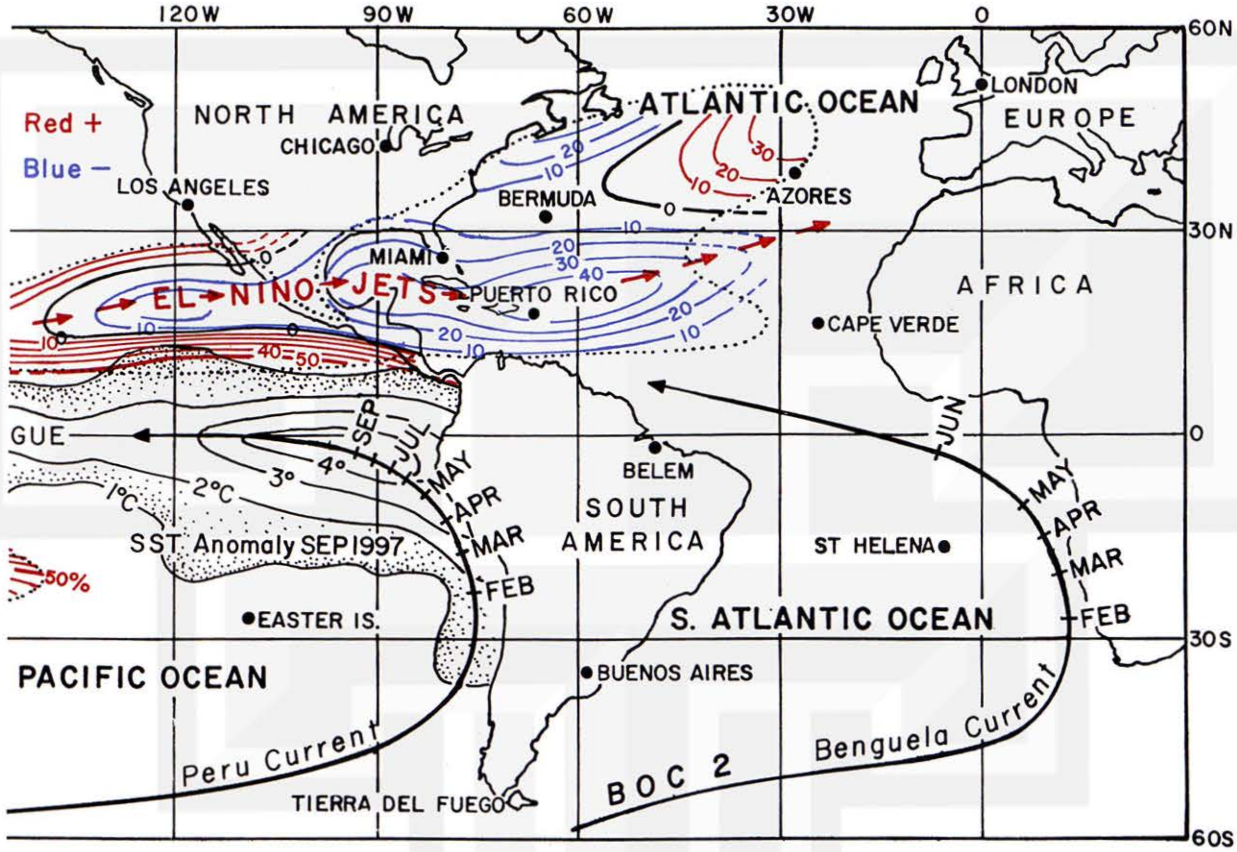

Also of interest is the low percent change in the Indonesia area, suggesting suppressed convection and drought. The percent change is also low in the Tasman Sea and South Indian Ocean, affected by BOC 3 and BOC 4, branch-off currents of the Antarctic Circumpolar Current. Why are they colder in El Niño years?

In the Western Hemisphere, the percent change of storms in El Niño years are mostly negative. Since incipient storms do not develop beneath a jet stream due to excessive vertical windshear, storms would be suppressed by the jet stream or jet streak which forms on the north side of the warm, equatorial sea surface.

Another unconfirmed evidence is the interaction of BOC 1 and BOC 2. In 1997, a weak La Niña was in the Atlantic while a strong El Niño was in progress in the Pacific. The fast movement of the SST peak from FEB to JUN in the Atlantic and the slower movement during the same months in the Pacific could be the important clue in solving the interaction of BOC 1 and 2.

This figure also appears as Figure 4.3 in Mystery of El Niño and Hurricanes, WRL Paper 249, a research that was performed concurrent with this and which discusses the mechanism of El Niño in greater detail.

GLOSSARY

Center Date
The date at the center of a storm year.
Northern Hemisphere: 01 September
Southern Hemisphere: 01 March

Daily Count
Count of storms in progress within a specific area on consecutive days in a statistical period.

EP Areas
Equatorial Pacific areas where the Japan Meteorological Agency has been updating long-term SST data. The term EP in this book denotes Equatorial Pacific Ocean. In the future, EI (Equatorial Indian Ocean), and EA (Equatorial Atlantic Ocean) areas may become available.

Hazard Index (HI)
The force of storm winds defined by the square of the windspeed ratio of an individual storm. Hazard Index of the weakest hurricane is 1.00 and that of a 180 kt Hurricane, 7.67.

Hurricane
Storm with maximum windspeed of standard definition equal to 65 knots (75 mph; 34 m/s) or greater.

Hurricane Hazard Index (HHI)
Wind-force hazard caused by storms which crossed the 1° equatorial latitude-longitude area centered at a grid point during the prorated 100-year period. This index increases with both intensity and count of storms. Unit of HHI is cumulative hazard indices per 1° Equatorial Lat-Lon area per 100 yrs.

Initial Path
Path of storms from the point of formation to the recurving point.

Intertropical Irrotational Zone (ITIZ)
A narrow storm-free zone located on both sides of the equator.

ITIZ Boundary
North and south limits of the storm-free zone (Intertropical Irrotational Zone) on either side of the equator. Both boundaries vary with the location of the Intertropical Convergence Zone (ITCZ) and local topography.

Maximum Hazard Index (MHI)
Hazard Index caused by the most intense storm which crossed the specific latitude-longitude box centered at a grid point during the statistical period. This index can't be prorated to 100-year period.

Monthly Count
Count of storm formations in consecutive months within a specific area and statistical period.

Position Count (PC)
Count of 6-hourly positions of storms within a statistical period, inside a latitude-longitude square or box area.

Prorated Position Count (PPC)
Position count prorated to a 100-year period and 1° equatorial latitude-longitude square area.

Recurved Path
Path of storms from the recurving point to the end point.

Seven Areas of Storms
Seven areas of aggregate storm activity over oceans around the world. They are: **1.** North Indian Ocean, **2.** West Pacific Ocean, **3.** East Pacific Ocean, **4.** North Atlantic Ocean, **5.** South Indian Ocean, **6.** South Pacific Ocean, and **7.** South Atlantic Ocean. No storm has been reported from South Atlantic Ocean.

SST
Sea-surface temperature of standard definition.

Storm
As applied here, all tropical cyclones attaining windspeeds of tropical storm or hurricane status.

Storm-Season Months
Six (6) consecutive months in which most of the storm activity in a storm year occurs.
Northern Hemisphere: June through November.
Southern Hemisphere: December through next May.

Storm-Season SST Anomaly
In order to obtain the highest correlation between SST anomaly and storm activity, the SST anomaly of a storm year is defined by the mean anomaly of the six storm-season months of the storm year.

Storm Year
A 12-month period extending equally on both sides of the storm season months.
Northern Hemisphere: March through next February.
Southern Hemisphere: September through next August.

Tropical Storm
Storm with maximum windspeed of standard definition between 35 and 64 knots (40 and 74 mph; 18 and 33 m/s).

Windspeed Ratio (WR)
Ratio of the windspeed of an individual storm divided by 65 kts, the lowest hurricane windspeed of standard definition. Windspeed ratio of the weakest hurricane is 1.00, and that of 180 kt Hurricane, 2.77.

History of the Wind Research Laboratory

1943-53 Unnamed Fujita Project, Kyushu Institute of Technology, Tobata City, Japan

BUDGET
$2,500
(11 Yrs)

Micro-network of 88% solar-eclipse weather
Survey of Hiroshima and Nagasaki bomb damage
Discovery of downdraft in 1947. (Costs: $100)
Pressure dip in typhoon Della
Analytical study of typhoons (ScD Thesis)

1953-60 Unnamed Fujita Project, University of Chicago (Fujita invited by Dr. Horace R. Byers)

$289,000
(8 Yrs)

Re-analysis of Thunderstorm Project data
"MESOANALYSIS" by Fujita and Tepper
Mesoanalysis of squall lines
Precipitation and cold-air production
Use of weather radar in mesoanalysis

1961-63 MRP, Mesometeorology Research Project, University of Chicago

$654,000
(3 Yrs)

Dawn of Mesometeorology
Mesometeorological Network in Oklahoma
Precise analysis of Tiros satellite photos
First aerial photo of rotating thunderstorm
Identification of mesocyclone radar echo

1964-87 SMRP, Satellite and Mesometeorology Research Project, University of Chicago

$7,531,000
(24 Yrs)

Aerial and ground survey of tornado damage
The Fujita Tornado Scale (F-scale)
Discovery of Downburst and Microburst
Overflight of tornadic thunderstorm by Lear Jet
First Color Movie of Planet Earth by Satellite

1988-99 WRL, Wind Research Laboratory, University of Chicago

$3,537,000
(12 Yrs)

Mini-swirls and microbursts in Andrew and Iniki
Identification of downbursts in Japanese typhoons
Mesoanalysis of typhoon damage in Japan
Mapping of cyclone paths in northern hemisphere
Mystery of El Niño and Hurricanes
World Atlas of Typhoons and Hurricanes